TAMPERE UNIVERSITY OF TECHNOLOGY

MIKKO SALMINEN

SHEAR BUCKLING RESISTANCE OF THIN METAL PLATE AT NON-UNIFORM ELEVATED TEMPERATURES

Licentiate Thesis

ABSTRACT

TAMPERE UNIVERSITY OF TECHNOLOGY
SALMINEN, MIKKO: Shear Buckling Resistance of Thin Metal Plate at Non-Uniform Elevated Temperatures
Licentiate Thesis, 107 pages, 25 appendix pages
October 2010
Major: Metal Structures
Examiners: Professor Markku Heinisuo (Tampere University of Technology), Professor Pentti Mäkeläinen (Helsinki University of Technology) and Professor Milan Veljkovic (Luleå University of Technology)
Keywords: Shear buckling, Elevated temperatures, Metal plate, Numerical analysis

Shear buckling of metal plates at elevated temperatures occurs in many applications when considering the resistance of metal structures. Such applications include webs of all-metal sandwich panels in fire, webs of hot gas ducts, webs of slim floor beams of buildings in fire, etc. This study presents a design method for calculating the shear buckling load of a rectangular simply supported metal plate when temperature distribution across the height of the plate is non-uniform. The behaviour of the web can be thought of as involving three stages. Only the shear buckling stage is considered in this study. The post-critical stage that involves tension field resistance and yielding of the flanges will be considered in forthcoming studies.

Simply supported rectangular plates made of carbon steel, aluminium and stainless steel are the basic cases examined in this study. They occur frequently in design. In cases where temperature across the plate is high and uniform, solutions and test results for shear resistance can be found in literature. This study proposes a calculation method for the cases, where temperature varies across the height of the plate linearly and non-linearly. Unfortunately, no test results are available for such cases.

The proposed method is based on the results of the finite element method and a search of solutions applying different averaging schemata, of which the most promising one is chosen. The basic idea is to use the equations and reduction factors provided in the Eurocodes. Only the reduction factor for elastic modulus is needed here. Calculations are performed for different types of plates at different temperature distributions. The FEM results are compared with the results from different calculation methods. The goal of the study is to find a practical method for reducing the elastic modulus of a plate with only a single value and then calculate the critical shear stress using Eurocode equations. The results of graphic design method correlate closely with those of the finite element analyses.

TIIVISTELMÄ

TAMPEREEN TEKNILLINEN YLIOPISTO
SALMINEN, MIKKO: Ohuen metallilevyn leikkauslommahduskestävyys korkeissa epätasaisissa lämpötiloissa
Lisensiaatintutkimus, 107 sivua, 25 liitesivua
Lokakuu 2010
Pääaine: Metallirakenteet
Tarkastajat: Professori Markku Heinisuo (Tampereen teknillinen yliopisto), Professori Pentti Mäkeläinen (Aalto-yliopisto) ja Professor Milan Veljkovic (Luleå University of Technology)
Avainsanat: Leikkauslommahdus, Korkeat lämpötilat, Metallilevy, Numeeriset analyysit

Metallilevyjen leikkauslommahdus korkeissa lämpötiloissa on ilmiö, joka esiintyy monissa sovellutuksissa kun käsitellään metallirakenteiden kestävyyttä. Metallikennojen ja hattupalkkien uumat tulipalossa sekä kuumien kaasukanavien uumat ovat esimerkkejä sovellutuksista. Tässä tutkimuksessa esitetään suunnittelumenetelmä vapaasti tuetun, suorakulmaisen metallilevyn leikkauslommahduskuorman laskemiseen siinä tapauksessa, kun lämpötilajakautuma ei ole vakio levyn korkeudella. Uuman käyttäytyminen kuorman kasvaessa voidaan jakaa kolmeen osaan. Ainoastaan leikkauslommahdusta käsitellään tässä työssä. Leikkauslommahduksen jälkeisiä vaiheita eli vetokentän kestävyyttä ja laippojen myötäämistä käsitellään seuraavissa tutkimuksissa.

Tässä tutkimuksessa käsitellään vapaasti tuettuja, suorakulmaisia, hiiliteräksestä, alumiinista ja ruostumattomasta teräksestä valmistettuja levyjä, jotka esiintyvät tyypillisesti rakenteiden suunnittelussa. Tapauksiin, joissa levyn lämpötila on korkea ja tasainen, löytyy laskentateorioita ja testituloksia kirjallisuudesta. Tässä työssä esitetään laskentamenetelmä tapauksiin, joissa lämpötila vaihtuu lineaarisesti ja epälineaarisesti levyn korkeudella. Valitettavasti testituloksia tällaisiin tapauksiin ei ole tarjolla.

Kehitetty laskentamenetelmä perustuu numeerisella laskennalla saatuihin tuloksiin ja erilaisiin keskiarvomenetelmiin. Ideana on käyttää eurokoodien yhtälöitä ja materiaaliominaisuuksien pienennyskertoimia. Tutkittaessa leikkauslommahdusta, ainoastaan kimmokertoimen pienennyskerrointa tarvitaan. Laskelmat tehdään erilaisille levyille erilaisilla lämpötilajakautumilla. Numeerisen laskennan tuloksia verrataan eri menetelmillä saatuihin tuloksiin. Tutkimuksen tavoitteena on löytää käytännöllinen menetelmä levyn kimmokertoimen pienentämiseen yhdellä arvolla ja sitten laskea leikkauslommahduskestävyys käyttäen eurokoodien yhtälöitä. Graafisen menetelmän tulokset korreloivat hyvin numeerisesta laskennasta saatujen tulosten kanssa.

PREFACE

This study was carried out in the Research Centre of Metal Structures at Tampere University of Technology between June 2009 and September 2010. The study was financially supported by the Research Centre of Metal Structures and Rautaruukki Oyj. The financiers are gratefully acknowledged. Emil Aaltonen Foundation is thanked for funding the participation for a short-course in Berlin.

First of all, I would like to thank my supervisor Professor Markku Heinisuo who has provided an excellent work and study environment. Without his consistent support, this thesis would never have been completed. The other examiners, Professor Pentti Mäkeläinen, Helsinki University of Technology, and Professor Milan Veljkovic, Luleå University of Technology are kindly acknowledged for their valuable comments and suggestions to improve the thesis.

I wish to express my thanks to all the staff members of the Research Centre of Metal Structures. It has been a pleasure to work in such an active and inspiring research group.

CSC – IT Center for Science Ltd is thanked for providing the software used in this study. Especially the assistance of Mr. Reijo Lindgren in constructing the FEM-models is gratefully acknowledged.

Mr. Jorma Tiainen is thanked for checking the language of this thesis.

Very special thanks go to the most important people of my life, Eeva and Eemil for their understanding and love during these golden years.

Tampere, October 2010

Mikko Salminen

CONTENTS

NOTATIONS

Roman characters

a	distance between stiffeners of the web
a_g	length of the gusset plate
c	width or depth of part of a cross-section
c_a, c_i	specific heat
E	elastic modulus
f_y	yield stress
h_g	height of the gusset plate
h_w	height of the web
k_E, $k_{E,\theta}$	reduction factor for elastic modulus
$k_{p0,2,\theta,web}$	reduction factor for design yield strength at average temperature of web
k_θ	reduction factor
k_τ	shear buckling coefficient
$k_{y,\theta,web}$	reduction factor for yield strength at average temperature of web
L	length
M_b	bending moment
R	resistance
T	temperature
T_a	steel temperature
T_{avg}	average plate temperature
T_{cold}	coldest plate temperature
T_f	temperature from method f
T_g, T_{gas}	gas temperature
T_{hot}	hottest plate temperature
T_{lf}	temperature of lower panel flange
T_{mid}	temperature in the middle of the height of plate
T_{stand}	gas temperature according to ISO fire curve
T_{test}	external temperature on exposed side of panel
T_{uf}	temperature of upper panel flange
t	time
t_{lf}	thickness of lower flange
t_w	thickness of web
u_x, u_y, u_z	displacements
$V_{b,Rd}$, V_{Rd}	shear force resistance at ambient temperature
$V_{bf,Rd}$	contribution of flanges to shear force resistance

$V_{bw,Rd}$	contribution of web to shear force resistance
V_{cr}	elastic shear buckling load
$V_{fi,t,Rd}$	shear resistance at elevated temperatures
V_{tf}, $V_{tension\ field}$, V_g	tension field resistance
V_u, $V_{u,D}$	ultimate shear force resistance
V_y	shear yield force
x, y, z	co-ordinates

Greek characters

α	thermal expansion coefficient
α_c	heat transfer coefficient
χ_w	shear buckling factor
ε	coefficient dependent on f_y
ε_m	surface emissivity
ϕ	factor related to method f
γ_{M0}	partial factor for resistance of cross-sections
γ_{M1}	partial factor related to instability of member
$\gamma_{M,fi}$	partial factor for relevant material property, for fire situation
η	factor for shear area
λ_w, $\bar{\lambda}_w$	slenderness parameter for web
ν	Poisson's ratio
θ_x, θ_y, θ_z	rotations
ρ, ρ_a	density
τ_{cr}	critical shear stress
$\tau_{cr,g}$	critical shear stress for the gusset plate
τ_u, $\tau_{u,D}$, $\tau_{u,D,design}$	ultimate shear stress
τ_y	shear yield stress

1. INTRODUCTION

1.1. Background

Fire safety of structures has become increasingly important in many respects. The safety of the people and property inside buildings when fire occurs is a major concern. The fire resistance of ships has also received much attention due to the observations made in connection with recent ship fires [Lois et al, 2004], [Colombi Jr., 2009]. The structures of other vehicles need to be designed fire resistant, too. For example, subway trains should be able to keep moving while on fire for at least two minutes so that they can reach the nearest station [Roh et al, 2009]. Elevated temperatures occur also in hot gas ducts and similar industrial structures.

The ultimate shear resistance of thin metal plate at non-uniform elevated temperatures is an important factor as regards the many applications mentioned above. Shear buckling resistance is the first phase of ultimate shear resistance studied here – the other phases are left for future studies. The solution to this basic problem can be used in a wide range of applications concerning real structures, for instance, to reduce the risks of structural failures at elevated temperatures.

Many structures are composed of thin plates of concrete, wood, metal, plastics and their mixtures. The main focus of this research is on metal (carbon steel, stainless steel and aluminium) structures, which appear in buildings, ships, trains, vehicles and many industrial products. It is believed that methods like those developed in this study can also be applied to plates made of other materials. Figure 1.1 illustrates an all-metal sandwich panel, hot gas duct walls and a composite welded slim floor beam (CWQ) including thin steel webs.

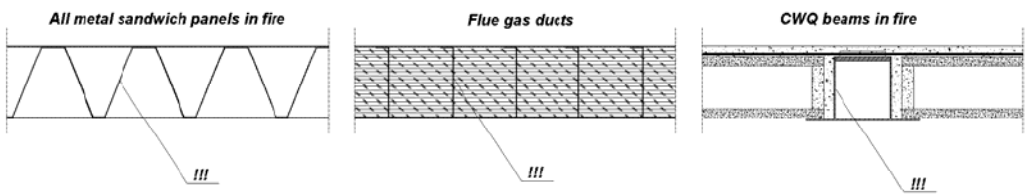

Figure 1.1. Plates under shear loading at elevated temperatures [Salminen et al, 2009].

The development of the linear theory of buckling of plates began with Saint-Venant, who presented the differential equation for the buckling of a plate loaded in its plane in 1870 [Saint-Venant, 1883]. The expression for the strain energy of a bent plate was developed by Bryan [Bryan, 1891]. Timoshenko applied the ideas of Rayleigh and Ritz to stability problems and was the first to solve the problem of a stiffened plate [Timoshenko, 1913], [Rayleigh, 1877], [Ritz, 1908].

The non-linear plate buckling problem is governed by the von Karman differential equations [von Karman, 1910]. Von Karman proposed the effective width idea for simply supported, uniformly axially loaded plates [von Karman et al, 1932].

The post-buckling phase was discussed by Rode as early as 1916. Rode adopted a tension field width of 50 times the thickness of the plate, which had not been verified by tests [Rode, 1916]. In the 1930's Wagner presented a pure tension field theory for aircraft structures with very thin web panels [Wagner, 1931]. However, post-buckling strength was not used directly in the design of plate girders in civil engineering. Elastic buckling remained the basis for their design until the 1960's.

In 1959, Basler and Thurlimann performed an extensive study on the post-buckling behaviour of plate girder web panels under shear loading [Basler, Thurlimann, 1959]. The American Institute of Steel Construction (AISC) was the first to include post-buckling shear strength in its specifications [AISC, 1963] as a result of the above study and another one by Basler [Basler, 1961].

Basler and Thurlimann's theory was followed by modified failure theories intended to achieve better correlation between theory and tests. Rockey and his co-workers proposed a theory, which assumed that flanges could develop plastic hinges after tension field action [Rockey et al, 1978]. This method was eventually also included in the British Standard [BS 5950, 1990]. In the Eurocodes, the shear resistance of slender plates is based on the rotated stress field theory as proposed by Höglund [Höglund, 1981].

Fire resistance of structures has drawn much more attention after the collapse of the World Trade Center towers. Shear resistance of plates at elevated temperatures has also been studied. Test results and theories are available for studies where temperature across the entire plate is uniform. Test results and finite element method (FEM) calculations on 18 steel-plate girders loaded predominantly in shear at elevated temperatures are presented in the reference [Vimonsatit, Tan, Qian, 2007]. The article by Tan and Qian deals with experimental and numerical investigation of a thermally restrained plate girder loaded in shear at elevated temperatures [Tan, Qian, 2007]. A theoretical model for predicting the failure load of a plate girder subjected to a specified constant elevated temperatures is presented in [Vimonsatit, Tan, Ting, 2007]. Kaitila

has also conducted various numerical buckling analyses of cold-formed steel members at elevated temperatures [Kaitila, 2002].

In many applications temperature is not uniform across the entire plate. Temperatures at opposite edges of a plate may vary when it is part of a larger structure such as in the cases shown in Figure 1.1. The article by Feng et al. presents the results of a numerical investigation into the axial strength of cold-formed thin-walled channel section under non-uniform elevated temperatures [Feng et al, 2003]. Lateral torsional buckling of steel I-beams at non-uniform elevated temperatures has been considered in the reference [Yin, Wang, 2003]. In both of the above articles, temperature distribution is constant in the longitudinal direction and non-uniform in the cross-section. No test results or theories on shear resistance at non-uniform elevated temperatures could be found. The safe solution is to always use the maximum temperature of the plate.

This study deals with the non-uniform temperature field in the basic case described next. It covers the scope of Eurocodes for carbon steel, stainless steel and aluminium structures: [EN 1993-1-1, 2005], [EN 1993-1-2, 2005], [EN 1993-1-4, 2006], [EN 1999-1-1, 2007], [EN 1999-1-2, 2007].

1.2. Goal and outline of study

The basic case to be solved involves a rectangular simply supported thin plate with different side ratios and temperature distributions. If a method for predicting shear resistance can be found and verified, the resistance of structures can be estimated during design without tests and with less risk than today.

The search method of this study involves testing potential averaging schemata to reduce the properties of the metal plate. The verification of FEM models is done by comparing the results from FEM to the test results presented in literature. Then, FEM models are used to search for a safe method to reduce the properties of the metal plate. This study concentrates merely on theoretical considerations – no mechanical loading tests are conducted. The temperature fields used in the studied cases are from literature and FEM calculations done as part of this study. All cases involve only the shear in the plane of the plate. No interactions with other stress components are taken into account.

The shear resistance of a plate consists of three phases both at ambient temperature and at elevated temperatures as the load increases [Vimonsatit et al, 2007] (Fig. 1.2): the

buckling phase, the post-buckling phase and yielding of supporting structures. This study is a part of a larger research project aimed at determining the ultimate shear resistance of a plate. It only deals with shear buckling.

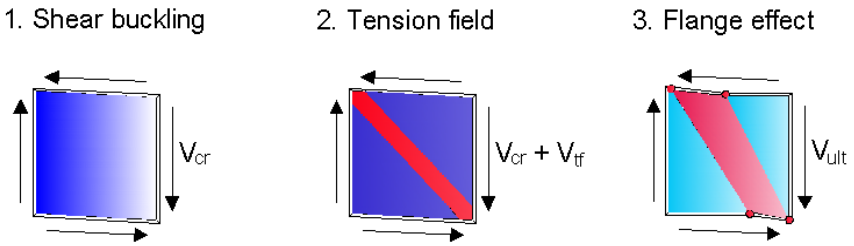

Figure 1.2. Three stages of plate before collapse as the load increases.

The goal of this part of the study is to develop an analytical design method to determine the shear buckling resistance of a metal plate in cases where temperature varies across the height of the plate linearly and non-linearly. In the longitudinal direction the temperature is assumed to be uniform. The design method is based on the equations and reduction factors given in Eurocodes [EN 1993-1-2, 2005] and [EN 1999-1-2, 2007]. In the case of shear buckling, only the reduction factor for elastic modulus is needed.

The main goal of this study is to find a practical method for reducing elastic modulus with only a single value to get safe and accurate results for design.

The content of this thesis is divided into eight chapters. The first chapter presents a brief background and motivation for the study as well as its goal.

The theoretical background for calculating shear resistance at ambient and elevated temperatures is presented in Chapters 2 and 3.

The fourth chapter shows the procedure and the results of the numerical calculations, which are used to verify the proposed design method.

The fifth chapter deals with averaging methods for reducing elastic modulus with a single value for the whole plate.

The results of FEM calculations and the comparison of the results of various methods are presented in Chapter 6. The results for aluminium and stainless steel are also shown.

Chapter 7 deals with an example problem. First, the temperature distributions of an all-metal sandwich panel are calculated by FEM based on the general heat transfer theory.

The numerical thermal analyses are compared to recent test results. Then the shear buckling resistance of the all-metal sandwich panel is calculated using FEM and the most promising method of Chapter 5. All the results are finally presented as a function of time using the standard temperature-time curve [EN 1991-1-2, 2002].

Chapter 8 summarises the results of the thesis and makes suggestions for further research.

2. SHEAR RESISTANCE OF WEB AT AMBIENT TEMPERATURE

As shown in Figure 1.2, the behaviour of a web under pure shear can be divided into three stages. The following equation expresses the relation between the stages:

$$V_{b,Rd} = V_{cr} + V_{tension\ field} + V_{bf,Rd} \quad (2.1)$$

where
- V_{cr} represents the elastic shear buckling load,
- $V_{tension\ field}$ represents the tension field resistance,
- $V_{bf,Rd}$ represents the yield of flanges at the ultimate collapse stage.

Only elastic shear buckling is considered in this study. However, Chapter 2.2 provides a short introduction to the tension field theory according to Dubas and Gehri [Dubas, Gehri, 1986], because when calculating shear resistance according to standard EN 1993-1-5 [EN 1993-1-5, 2005], it is impossible to determine what proportion of the shear force is contributed by elastic shear buckling and what proportion by the tension field effect if the web buckles. Only contributions from the web and the flanges are calculated separately. It should be noted that in EN 1993-1-5 tension field resistance is based on the rotated stress field theory of Höglund [Höglund, 1997], [Johansson et al, 2001].

2.1. Elastic shear buckling

The shear load that causes the web plate to buckle is given by:

$$V_{cr} = h_w\, t_w\, \tau_{cr} \quad (2.2)$$

where
- h_w is the height of the web,
- t_w is the thickness of the web,
- τ_{cr} is the critical shear stress.

Critical shear stress τ_{cr} can be determined from the classical stability theory for plates by Timoshenko [Timoshenko, 1936]:

$$\tau_{cr} = k_\tau \frac{\pi^2 E}{12 \cdot (1-\nu^2)} \cdot \left(\frac{t_w}{h_w}\right)^2 \tag{2.3}$$

where
- E is the elastic modulus of the plate,
- ν is the Poisson's ratio of the web material, and
- k_τ, the shear buckling coefficient, is obtained from:

$$k_\tau = 5{,}34 + 4 \cdot \left(\frac{h_w}{a}\right)^2 \quad \text{for } a \geq h_w, \tag{2.4}$$

$$k_\tau = 5{,}34 \cdot \left(\frac{h_w}{a}\right)^2 + 4 \quad \text{for } a \leq h_w, \tag{2.5}$$

where
- a is the distance between the stiffeners of the web.

The shear buckling coefficient as a function of ratio a/h_w is shown in Figure 2.1.

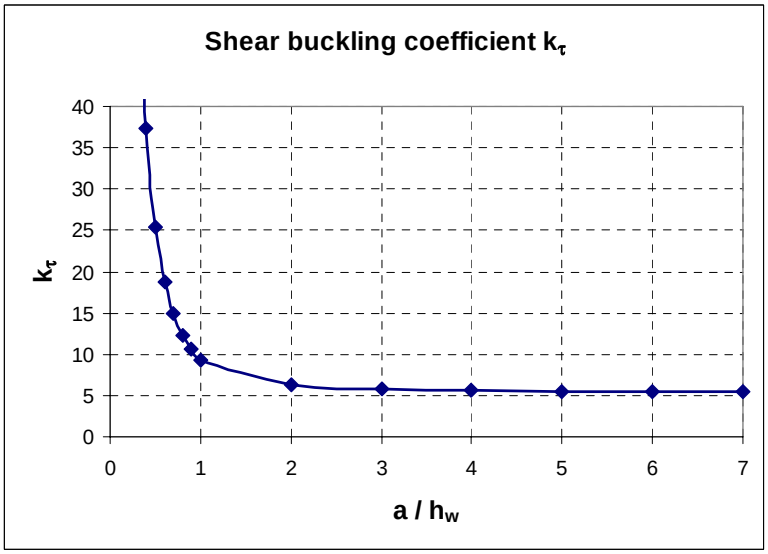

Figure 2.1. Shear buckling coefficient.

The material coefficients E and ν for carbon steel, stainless steel and aluminium at ambient temperatures according to Eurocodes [EN 1993-1-1, 2005], [EN 1993-1-4, 2006] and [EN 1999-1-1] are shown in Table 2.1.

Table 2.1. Material coefficients E and ν at ambient temperatures according to the Eurocodes.

	E [N/mm^2]	ν
Carbon steel	210 000	0,3
Stainless steel	200 000 195 000 220 000	0,3
Aluminium	70 000	0,3

EN 1993-1-4 [EN 1993-1-4, 2006] gives three values for the elastic modulus E of stainless steel in the depending on its grade as shown in Table 2.1. This study uses the value E = 200 000 N/mm^2 for stainless steel at ambient temperatures.

2.2. Tension field theory

When the web has reached critical shear strength, any increase in shear load will be carried by tensile membrane stresses in the tension band. In this study that is proved based on the tension field theory of Dubas and Gehri [Dubas, Gehri, 1986] illustrated in Figure 2.2.

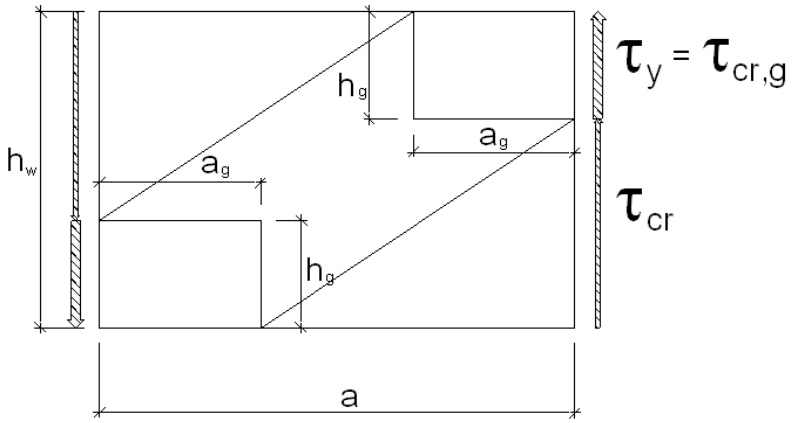

Figure 2.2. Tension field theory by Dubas and Gehri.

This theory supposes that the tension field develops at the gusset plate of a Pratt truss, as shown in the previous figure. The gusset plate is supposed to be a rectangle with the same aspect ratio as the web plate so that $\frac{a_g}{h_g} = \frac{a}{h_w}$, notations as in Figure 2.2.

The tension field develops between the two gusset plates. The gusset plates are assumed to act as plates under pure shear with a buckling coefficient k_τ equal to that of the web, i.e. in general hinged boundary conditions.

The dimension h_g results from the assumption, similar to the von Karman hypothesis [von Karman et al, 1932] for plates in compression, that the critical buckling strength for the gusset plate $\tau_{cr,g}$ equals the shear yield stress of the web plate τ_y:

$$\tau_y = \frac{f_y}{\sqrt{3}} \tag{2.6}$$

This means that the critical shear stresses for the gusset plate and the whole web are now:

$$\tau_{cr,g} = k_\tau \frac{\pi^2 E}{12 \cdot (1-\nu^2)} \cdot \left(\frac{t_w}{h_g}\right)^2 = \tau_y, \tag{2.7}$$

$$\tau_{cr} = k_\tau \frac{\pi^2 E}{12 \cdot (1-\nu^2)} \cdot \left(\frac{t_w}{h_w}\right)^2 \tag{2.8}$$

By combining equations (2.7) and (2.8) we obtain the size of the gusset plate:

$$k_\tau \frac{\pi^2 E}{12 \cdot (1-\nu^2)} = \tau_y \left(\frac{h_g}{t_w}\right)^2 = \tau_{cr} \left(\frac{h_w}{t_w}\right)^2 \quad \Rightarrow \tag{2.9}$$

$$h_g = h_w \sqrt{\frac{\tau_{cr}}{\tau_y}} \tag{2.10}$$

$$a_g = a \sqrt{\frac{\tau_{cr}}{\tau_y}} \tag{2.11}$$

The yield in shear for the gusset is composed of the "gusset contribution" V_g (= $V_{tension\ field}$) and the critical shear stress for the whole web. That leads to the following equation:

$$h_g\, t_w\, \tau_y = V_g + h_g\, t_w\, \tau_{cr} \Rightarrow V_g = h_g\, t_w\, \tau_y - h_g\, t_w\, \tau_{cr} = h_g\, t_w\, (\tau_y - \tau_{cr}) \tag{2.12}$$

The ultimate shear load $V_{u,D}$ (where D represents Dubas) of the web is:

$$V_{u,D} = h_w\, t_w\, \tau_{cr} + V_g \tag{2.13}$$

It can also be presented in the following form:

$$V_{u,D} = h_w\, t_w\, \tau_{cr} + h_g\, t_w\, (\tau_y - \tau_{cr}) = h_w\, t_w\, \tau_{cr} + h_w \sqrt{\frac{\tau_{cr}}{\tau_y}}\; t_w\, (\tau_y - \tau_{cr}) \qquad (2.14)$$

$$= h_w\, t_w \left[\tau_{cr} + \sqrt{\tau_{cr}\tau_y} \left(\tau_y - \tau_{cr} \right) \right]$$

The ultimate stress is:

$$\tau_{u,D} = \frac{V_{u,D}}{h_w t_w} = \sqrt{\tau_{cr}\tau_y} \left[1 + \left(\sqrt{\frac{\tau_{cr}}{\tau_y}} - \frac{\tau_{cr}}{\tau_y} \right) \right] \leq \tau_y \qquad (2.15)$$

The first term corresponds to the ultimate strength from the von Karman assumption. The second one is an enhancement factor with a maximum value of 1,25 corresponding to $\tau_{cr} / \tau_y = 0{,}25$. Figure 2.3 shows the enhancement factor as a function of the ratio τ_{cr} / τ_y. The gusset conditions are less favourable for end panels, and it is, therefore, reasonable to reduce the ultimate stress. Dubas proposed the following design formula where the enhancement factor is ignored and a factor of 0,9 is used:

$$\tau_{u,D,design} = 0{,}9 \sqrt{\tau_{cr}\tau_y} \leq \tau_y \qquad (2.16)$$

Equation (2.16) correlate closely with the test results as shown in Figure 2.4 and is suitable for design.

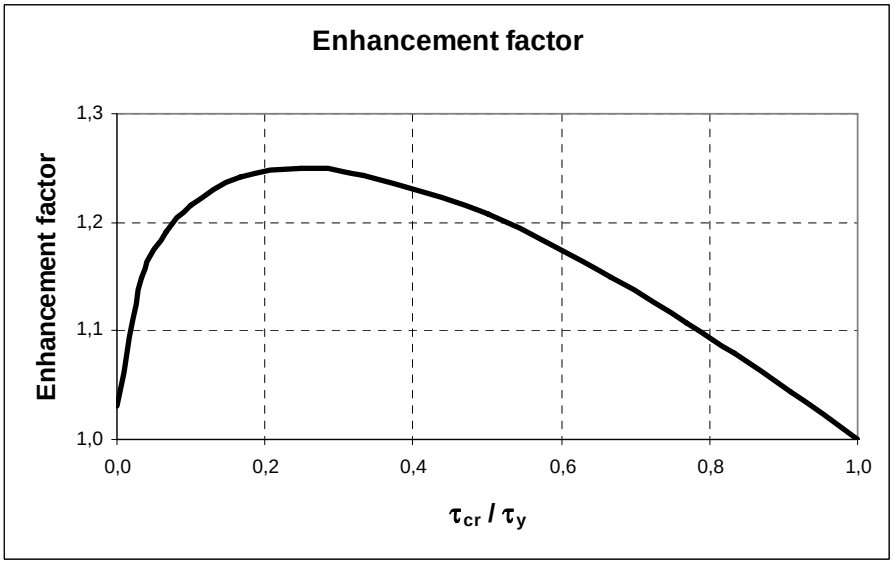

Figure 2.3. Enhancement factor of Equation 2.15.

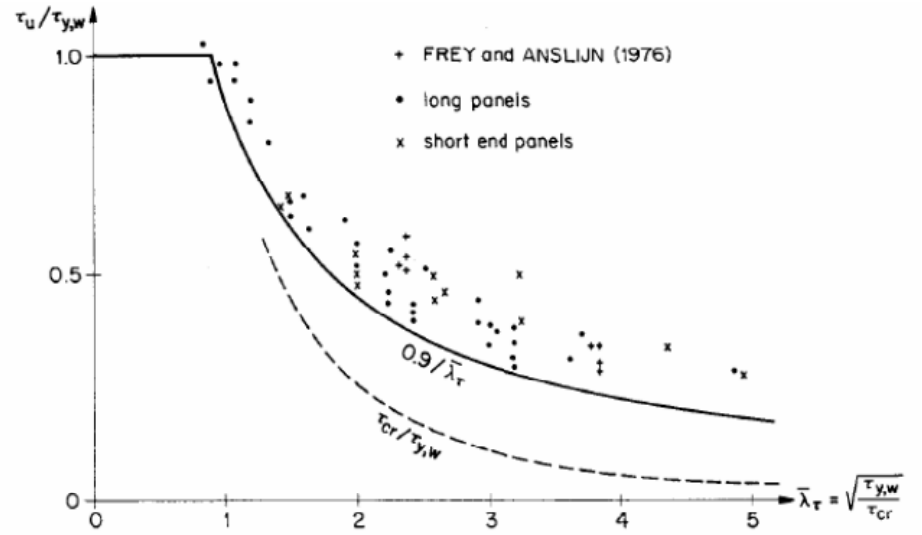

Figure 2.4. Comparison of design formula (Eq. 2.16) and test results [Dubas, Gehri, 1986].

Comparison of the method presented in EN 1993-1-5 [EN 1993-1-5, 2005] and the presented tension field theory is done in Chapter 2.3.

2.3. Shear resistance of web according to the Eurocodes

This chapter only deals with the shear resistance of plates made of carbon steel. Standard EN 1993-1-1 [EN 1993-1-1, 2005] states that the shear buckling resistance of webs without intermediate stiffeners should be calculated according to EN 1993-1-5 [EN 1993-1-5, 2005], if

$$\frac{h_w}{t_w} > 72\frac{\varepsilon}{\eta} \tag{2.17}$$

where

- $\varepsilon = \sqrt{\frac{235}{f_y}}$, (2.18)
- η = 1,2 when T $\leq$ 400 °C and steel grade is not higher than S460. In all other cases η = 1,0 [EN 1993-1-5, 2005], [Finnish National Annex to SFS-EN 1993-1-5, 2008].

It should be noted that in EN 1993-1-5 [EN 1993-1-5, 2005] the height of the web h_w is defined as the clear web depth between flanges.

EN 1993-1-5 [EN 1993-1-5, 2005] gives the slenderness parameter $\bar{\lambda}_w$:

$$\bar{\lambda}_w = 0{,}76\sqrt{\frac{f_y}{\tau_{cr}}} \tag{2.19}$$

The slenderness parameter $\bar{\lambda}_w$ can also be written similarly as for compressed plates:

$$\bar{\lambda}_w = \sqrt{\frac{\tau_y}{\tau_{cr}}} = 0{,}76\sqrt{\frac{f_y}{\tau_{cr}}} = \sqrt{\frac{f_y}{\sqrt{3}\tau_{cr}}} \tag{2.20}$$

The following example illustrates when shear buckling should be considered according to EN 1993-1-1 [EN 1993-1-1, 2005] and when according to classical formulas (Equations (2.2)–(2.5)).

Consider a plate with the following properties:

$$\begin{aligned} &E = 210\,000 \text{ N/mm}^2 \\ &\nu = 0{,}3 \\ &f_y = 355 \text{ N/mm}^2 \Rightarrow \tau_y = \frac{f_y}{\sqrt{3}} = 204{,}96 \text{ N/mm}^2 \end{aligned} \tag{2.21}$$

According to EN 1993-1-1 [EN 1993-1-1, 2005] (Eq. 2.17), shear buckling should be considered in the following cases:

$$\frac{h_w}{t_w} > 58{,}6 \quad \text{for } \eta=1{,}0 \tag{2.22}$$

$$\frac{h_w}{t_w} > 48{,}8 \quad \text{for } \eta=1{,}2 \tag{2.23}$$

Theoretically shear buckling may occur when $\tau_{cr} < \tau_y$. Equation (2.3) can then be expressed as:

$$\frac{h_w}{t_w} > \sqrt{\frac{\sqrt{3}k_\tau \pi^2 E}{12(1-\nu^2) f_y}} \tag{2.24}$$

The ratio $\frac{h_w}{t_w}$ reaches its minimum value when the shear buckling coefficient k_τ reaches its minimum value 5,34 (a is infinite). Then, by using the defined properties we obtain the following condition for shear buckling:

$$\frac{h_w}{t_w} > 70{,}3 \tag{2.25}$$

If the ratio h_w / a = 1, the shear buckling coefficient k_τ = 9,34, then the shear buckling may occur when:

$$\frac{h_w}{t_w} > 93{,}0 \tag{2.26}$$

Figure 2.5 shows when shear buckling may occur theoretically and according to EN 1993-1-5 [EN 1993-1-5, 2005] when using the properties defined earlier in this example. The theoretical values of Equation (2.24) are calculated with two different distances between the stiffeners (a = h_w and a = ∞).

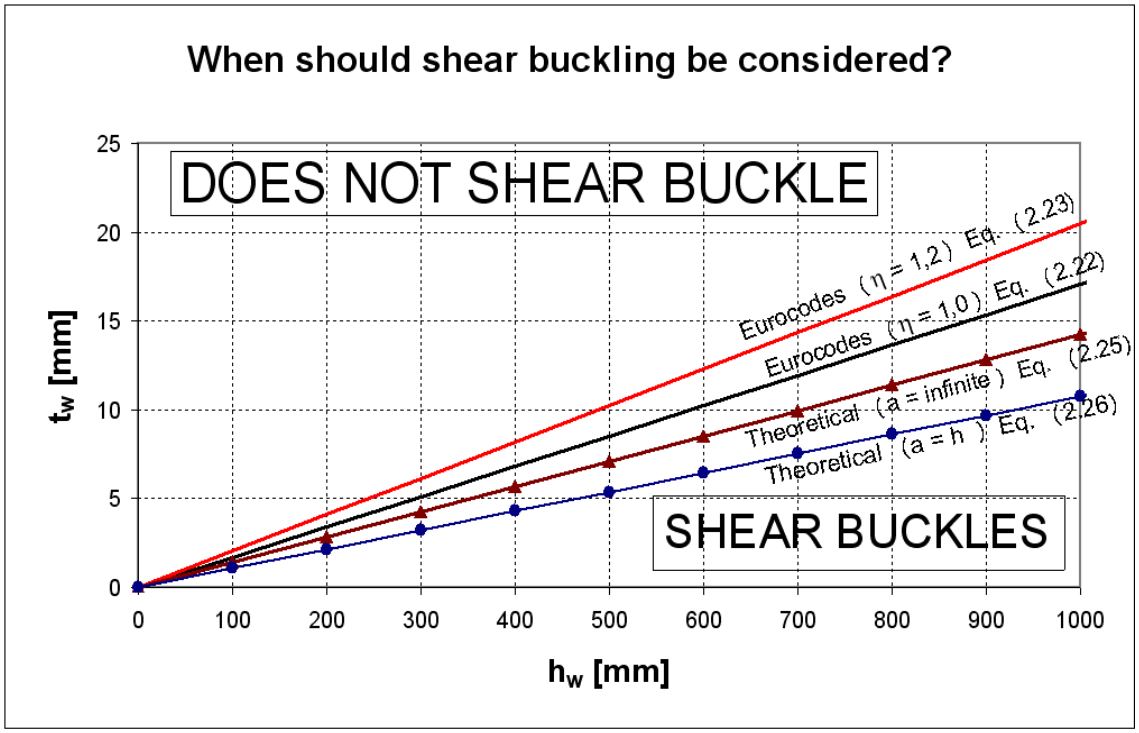

Figure 2.5. Shear buckling of the example plate.

It is obvious from Figure 2.5 that the distance between the stiffeners has no effect on shear buckling in the EN 1993-1-1 [EN 1993-1-1, 2005] condition. It can also be said that Equation 2.17 of EN 1993-1-1 is clearly conservative compared to Equation 2.24. According to EN 1993-1-5 [EN 1993-1-5, 2005] (Eq. 2.23), shear buckling at ambient conditions should be considered in this case with about 40 % thicker plates than when using the theoretical Equation (2.25).

Furthermore, when using the slenderness parameter $\bar{\lambda}_w$ (Eq. 2.20), EN 1993-1-5 suggests that shear buckling may occur when $\bar{\lambda}_w > \frac{58,6}{70,3} = 0,83$ (see Equations (2.22) and (2.25)). The same value for slenderness parameter appears also in Table 2.2 and Figure 2.7. [EN 1993-1-5, 2005]. The values for shear buckling resistance and ultimate shear resistance according to EN 1993-1-5 are somewhat reduced to allow for scatter in test results as a result of initial imperfections and plastic buckling as shown in Figure 2.6. [Höglund, 1997]. It has been long accepted that the existence of initial imperfections in thin-walled structures can reduce their buckling resistance. [Alinia et al, 2009].

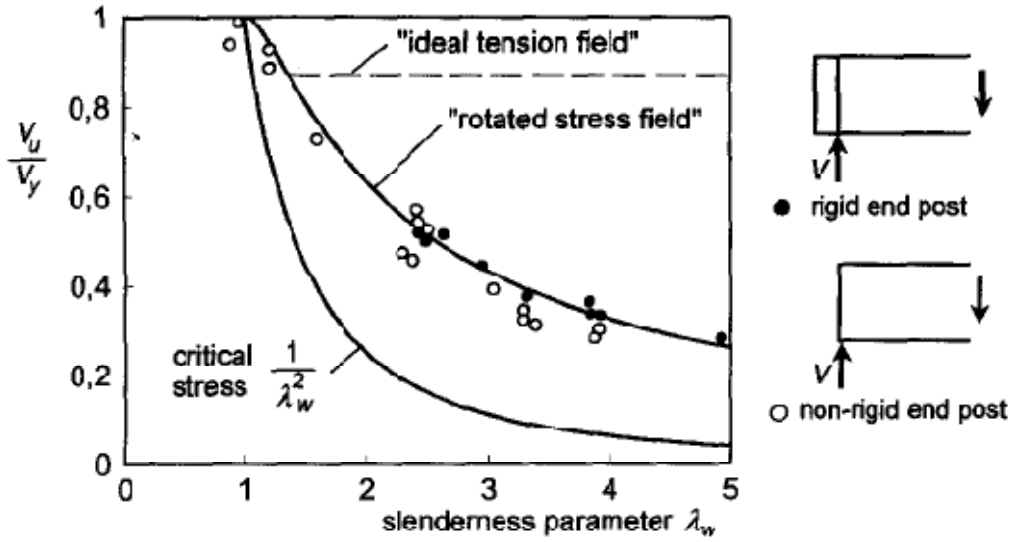

Figure 2.6. Shear force resistance according to tension field theories and tests [Höglund, 1997].

In this study, all the considered plates are assumed to be so thin that they buckle before yielding. Therefore, the design resistance of the web for shear is calculated according to standard EN 1993-1-5 [EN 1993-1-5, 2005] as follows:

$$V_{b,Rd} = V_{bw,Rd} + V_{bf,Rd} \leq \frac{\eta f_y h_w t}{\sqrt{3}\gamma_{M1}} \tag{2.27}$$

where

- $V_{bw,Rd} = \frac{\chi_w f_y h_w t}{\sqrt{3}\gamma_{M1}}$, the contribution of the web,
- $V_{bf,Rd}$ is the contribution from the flanges (ignored in this study),

• χ_w is the factor for the contribution of the web shown in Table 2.2 and Figure 2.7, and
• γ_{M1} = 1,00 [EN 1993-1-1, 2005].

Table 2.2. Contribution from the web χ_w for shear resistance [EN 1993-1-5, 2005]

	Rigid end post	Non-rigid end post
$\bar{\lambda}_w < 0{,}83/\eta$	η	η
$0{,}83/\eta \le \bar{\lambda}_w < 1{,}08$	$0{,}83/\bar{\lambda}_w$	$0{,}83/\bar{\lambda}_w$
$\bar{\lambda}_w \ge 1{,}08$	$1{,}37/(0{,}7+\bar{\lambda}_w)$	$0{,}83/\bar{\lambda}_w$

This study only considers plates with non-rigid end posts.

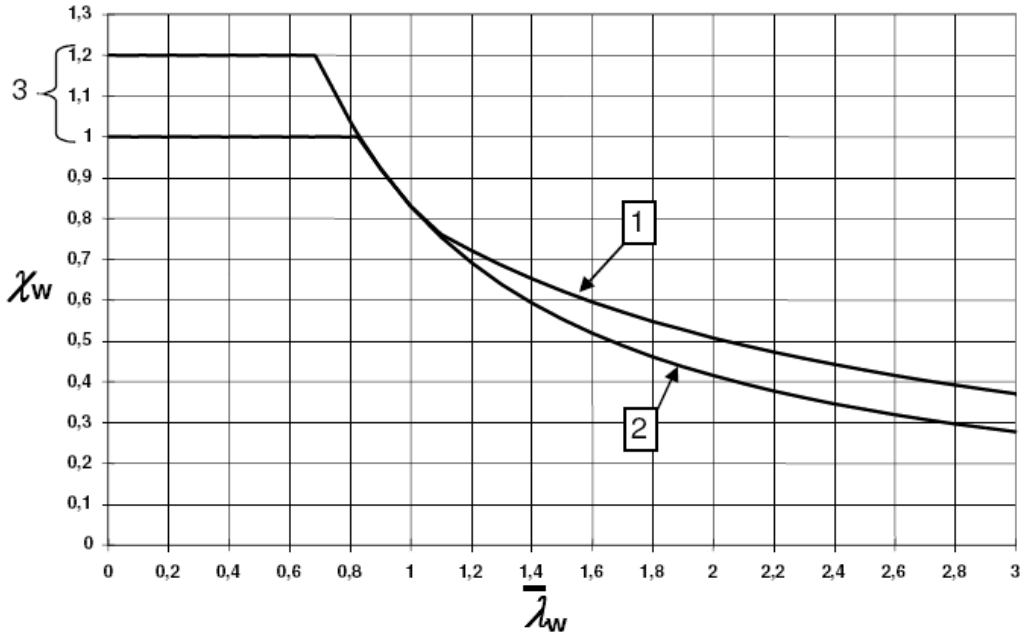

1 Rigid end post
2 Non-rigid end post
3 Range of recommended η

Figure 2.7. Shear buckling factor χ_w [EN 1993-1-5, 2005].

Critical shear stress τ_{cr} is calculated according to the informative Annex A of EN 1993-1-5 [EN 1993-1-5, 2005]. In this study webs have no vertical stiffeners, so the EN 1993-1-5 equations for the shear buckling coefficient and critical shear stress are the same as with the classical theory shown in Equations (2.2)–(2.5).

Figure 2.8 presents a comparison of theoretical shear buckling stress and ultimate shear stress according to EN 1993-1-5 [EN 1993-1-5, 2005] (for non-rigid end post, flanges

ignored) and the tension field theory by Dubas and Höglund [Höglund, 1997], [Dubas, Gehri, 1986]. All shown stresses are presented as a function of the slenderness parameter λ_w.

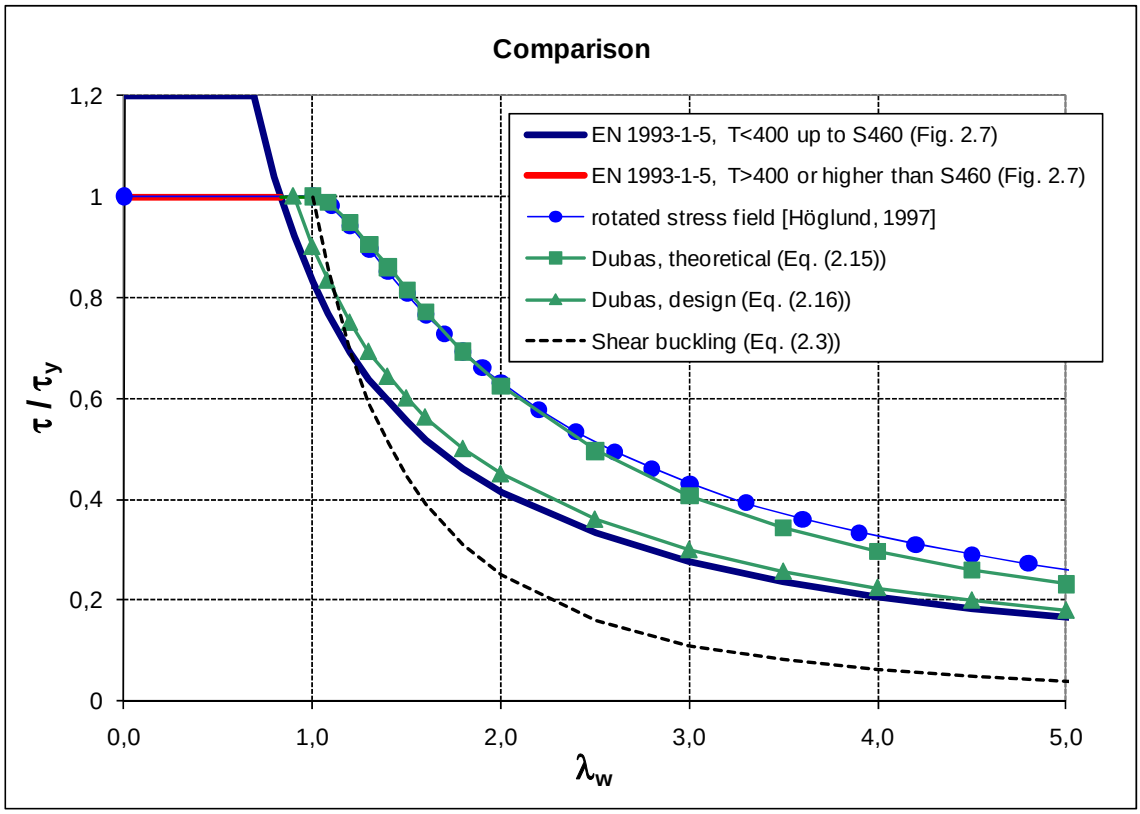

Figure 2.8. Shear buckling and ultimate shear resistances.

From Figure 2.8 it can be seen that the tension field theories of Dubas and Höglund yield much the same results. The difference between the design formula of Dubas and the EN 1993-1-5 [EN 1993-1-5, 2005] curve is based on the difference between the factor 0,9 (see Eq. 2.16) and the factor 0,83 (see Table 2.2).

From Figure 2.8 it can also be concluded that the post-buckling phase is a highly significant factor in ultimate shear resistance especially in the case of slender webs. This is illustrated also in Figure 2.9 which shows the ratio of theoretical shear buckling stress τ_{cr} (Eqs. (2.2) - (2.5)) to Eurocode web resistance $\tau_{bw,Rd}$ (Eq. (2.27)) when temperature is just over 400 ^{o}C meaning that η=1. The effect of the flanges are neglected and the end-post is assumed to be non-rigid.

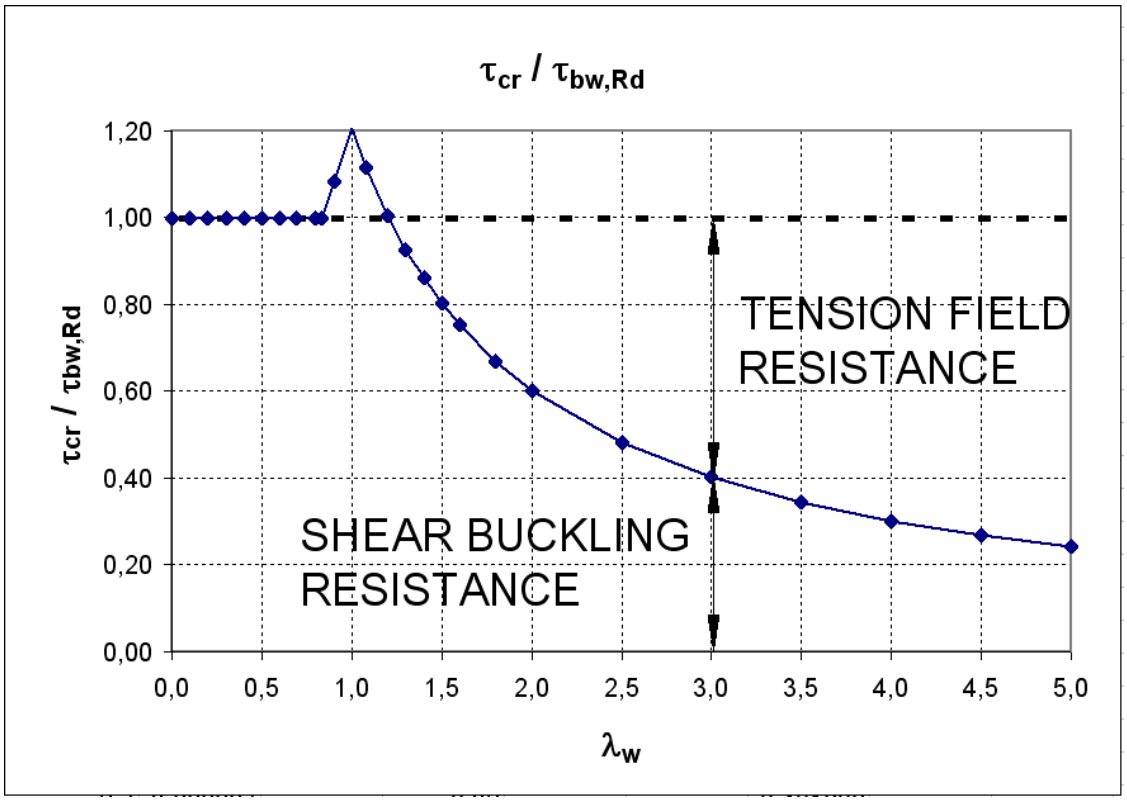

Figure 2.9. Contribution of post buckling resistance to the ultimate shear resistance (effect of the flanges neglected).

Figure 2.9 shows, for example, that at web slenderness λ_w = 3, theoretical shear buckling resistance is about 40 % of the ultimate shear resistance of the web according to EN 1993-1-5 [EN 1993-1-5, 2005]. The curve reaches values higher than 1 when relative slenderness λ_w is between 0,83 and 1,20. However, it can be seen from Figure 2.9 that when the relative slenderness of the web λ_w increases, say above 2,5, tension field resistance is larger than shear buckling resistance. Tension field resistance will hopefully be the subject of the further studies.

3. SHEAR RESISTANCE OF WEB AT ELEVATED TEMPERATURES

The shear resistance of a web at elevated temperatures can be determined by modifying the Eurocode equations with the reduction factors suggested in them to reduce elastic modulus and yield strength. Figure 3.1 shows the reduction factors for effective yield strength, elastic modulus and design strength of class 4 members of carbon steel as a function of steel temperature T_a according to EN 1993-1-2 [EN 1993-1-2, 2005]. Stainless steel and aluminium will be considered later.

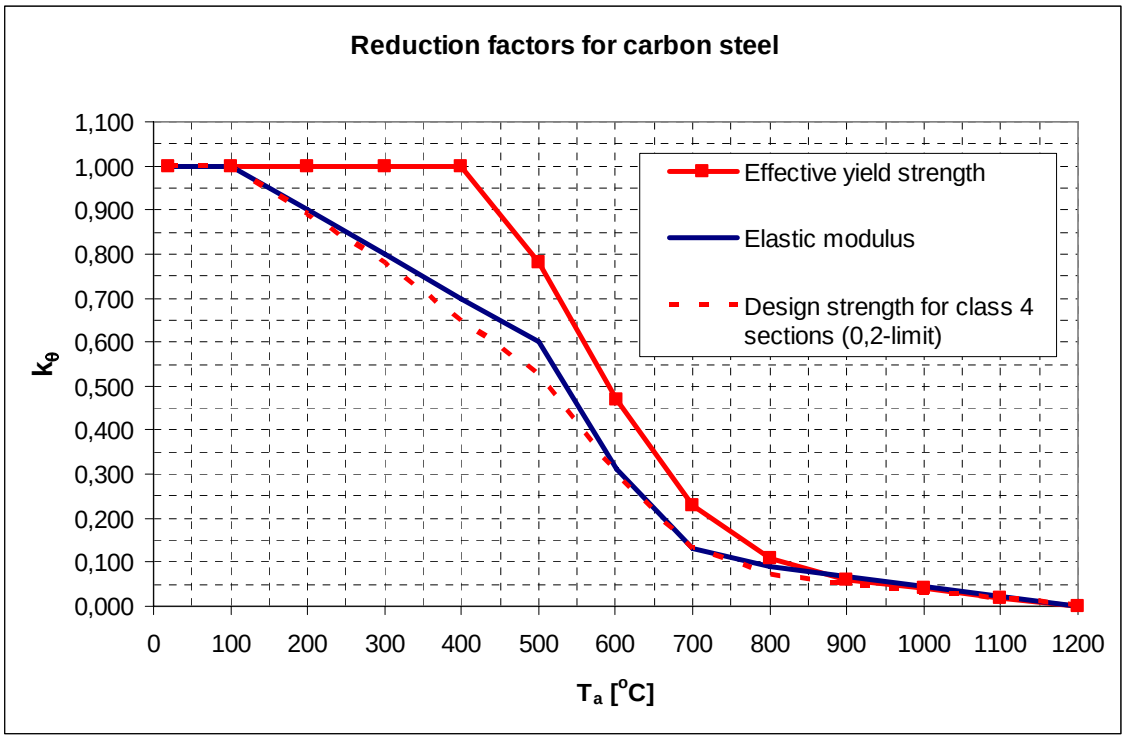

Figure 3.1. Reduction factors for carbon steel according to EN 1993-1-2 [EN 1993-1-2, 2005].

According to EN 1993-1-2 [EN 1993-1-2, 2005], the design shear resistance $V_{fi,t,Rd}$ of class 1, 2 and 3 cross-sections at elevated temperatures can be derived from the following equation:

$$V_{fi,t,Rd} = k_{y,\theta,web} V_{Rd}[\gamma_{M0}/\gamma_{M,fi}] \quad (3.1)$$

where
- $k_{y,\theta,web}$ is the reduction factor for yield strength at the average temperature of the web (see Fig. 3.1),
- V_{Rd} is design shear resistance at ambient temperature,
- $\gamma_{M0} = \gamma_{M,fi} = 1{,}00$ [EN 1993-1-1, 2005], [EN 1993-1-2, 2005].

The design yield strength of class 4 cross-sections should be used as the 0,2 per cent proof strength according to informative Annex E of EN 1993-1-2 [EN 1993-1-2, 2005]. Shear resistance at elevated temperatures is then calculated as follows:

$$V_{fi,t,Rd} = k_{p0,2,\theta,web} V_{Rd}[\gamma_{M,0}/\gamma_{M,fi}] \quad (3.2)$$

where
- $k_{p0,2,\theta,web}$ is the reduction factor for design yield strength at the average temperature of the web,
- V_{Rd} is design shear resistance at ambient temperature,
- $\gamma_{M0} = \gamma_{M,fi} = 1{,}00$ [EN 1993-1-1, 2005], [EN 1993-1-2, 2005].

According to EN 1993-1-1 [EN 1993-1-1, 2005], the web of a bended beam is a class 4 cross-section when $c/t > 124\varepsilon$. At ambient temperature the example plate shown on pages 19–21 ($f_y = 355$ N/mm^2, $c \approx h_w$) is a class 4 cross-section when:

$$\frac{h_w}{t_w} > 100{,}9 \quad (3.3)$$

Classification of cross-sections at elevated temperatures is done with the reduced factor ε [EN 1993-1-2, 2005]:

$$\varepsilon = 0{,}85\sqrt{\frac{235}{f_y}} \quad (3.4)$$

In the example case, the condition (Eq. 2.17) becomes:

$$\frac{h_w}{t_w} > 85{,}8\,. \quad (3.5)$$

As can be seen from Equations (3.1) and (3.2), shear resistance at elevated temperatures can be calculated according to EN 1993-1-2 [EN 1993-1-2, 2005] when temperature distribution is not constant. Reduction of shear resistance at elevated temperatures is done by using the average temperature of the web and the factor $k_{y,\theta,web}$ or $k_{p0,2,\theta,web}$ depending on the class of the web. For the purposes of this study all plates are assumed to slender enough to qualify as class 4 cross-sections.

In the following, two different cases as regards temperature distribution are presented:

- Uniform temperature across the height of the web,
- Varying temperature across the height of the web.

3.1. Uniform temperature across the web height

Test results are available for this case. The reference [Vimonsatit, Tan, Qian, 2007] presents test results and FEM calculations for 18 steel-plate girders loaded predominantly in shear at elevated temperatures. The article by Tan and Qian deals with experimental and numerical investigation of thermally restrained plate girders loaded in shear at elevated temperatures. Tan and Qian observed that ultimate shear capacity decreased significantly under a thermal restraint effect [Tan, Qian, 2007]. That is why only the results of the reference [Vimonsatit, Tan, Qian, 2007] are considered in this study.

Table 3.1 presents the properties of the webs of girders loaded primarily in shear at ambient and elevated temperatures. From Table 3.1 it can be determined that according to EN 1993-1-1 [EN 1993-1-1, 2005] shear buckling may occur in test panels TG3, TG4 and TG5 ($h_w/t_w > 72\ \varepsilon/\eta$) at ambient temperature as shown in Equation (2.17). All test panels were loaded at ambient temperature and the elevated temperatures of 400, 550–565 and 700 ^oC, except for test panel TG1, which was loaded only at ambient temperature and 400 ^oC. The distributions of temperature across the height of the web were very close to uniform.

Table 3.1. Properties of tested web girders from the reference [Vimonsatit, Tan, Qian, 2007].

	Web details						
Test panel	a [mm]	h_w [mm]	t_w [mm]	h_w/t_w	λ_w	E [GPa]	f_y [MPa]
TG1	139	139	6,1	22,8 = 27,5 ε/η	0,25	197	342
TG2	181	181	8	22,6 = 26,9 ε/η	0,24	205	332
TG3	305	305	2	152,5 = 168,8 ε/η	1,51	200	287,8
TG4	305	305	2,7	113,0 = 112,5 ε/η	1,01	200	232,8
TG5	305	305	1,5	203,3 = 241,6 ε/η	2,17	200	332

All specimens were designed so that the tested panels would fail primarily due to shear force. Figure 3.2 gives an example of a test girder configuration while Figure 3.3 shows the typical points where deformations were measured. Line LVDTs (linear variable differential transducers) were used at the centre of web panels to determine when shear buckling had occurred [Vimonsatit, Tan, Qian, 2007].

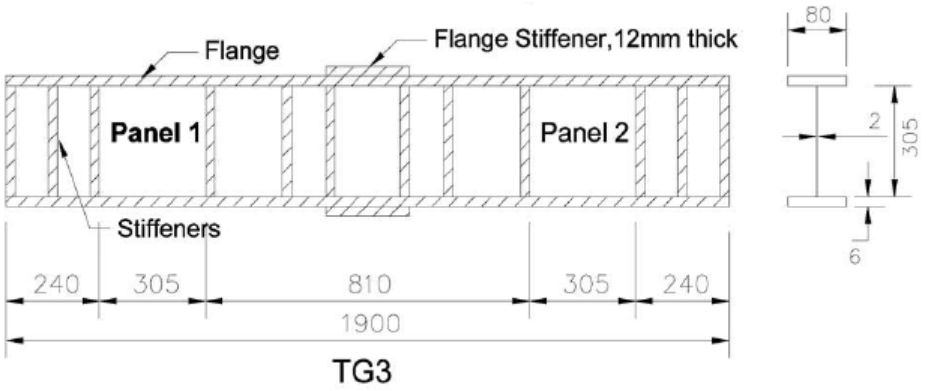

Figure 3.2. Test girder configuration with test panel TG3 [Vimonsatit, Tan, Qian, 2007].

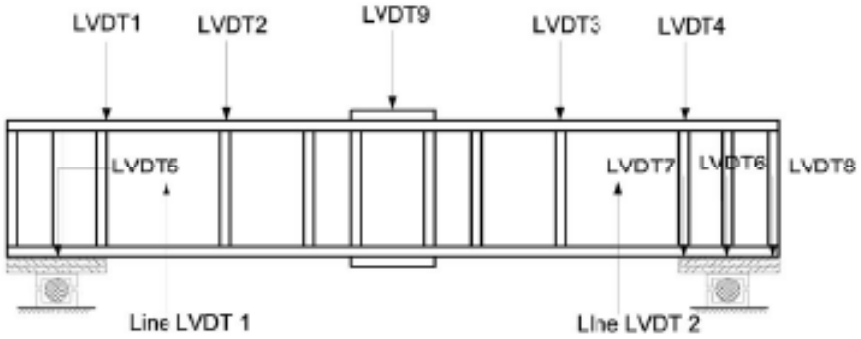

Figure 3.3. Supports and typical points where deformations were measured [Vimonsatit, Tan, Qian, 2007].

Table 3.2 compares the shear buckling loads of the tests to Eurocode shear buckling resistances. The Eurocode resistances were calculated using Equations (2.2) - (2.5). Elastic modulus (and yield strength of TG1 and TG2) was reduced according to EN 1993-1-2 [EN 1993-1-2, 2005] as in the reference [Vimonsatit, Tan, Qian, 2007]. FEM analysis in the reference article [Vimonsatit, Tan, Qian, 2007] were conducted for isolated panels, which included flanges. Test panels TG1 and TG2 were so thick that they did not buckle at all and they failed due to yielding. Their critical stress is calculated using formula $V_{cr} = \tau_y h_w t_w$. The reference [Vimonsatit, Tan, Qian, 2007] does

not compare its results to the Eurocodes. It should be noted that there were some problems with test panel TG4 during the execution of the tests.

Table 3.2. Critical shear forces of the reference [Vimonsatit, Tan, Qian, 2007] and this study.

Paper [Vimonsatit et al, 2007]					This study	
Test	T [^{o}C]	$V_{cr,test}$ [kN]	$V_{cr,analytical}$ [kN]	$V_{cr,FEM}$ [kN]	$V_{cr,calculated}$ [kN]	$V_{cr,test}$ / $V_{cr,calculated}$
TG1-1	20	172,2	174	170	167,4	1,03
TG1-2	550	79,85	100,6	95	104,6	0,76
TG2-1	20	270,3	288,4	280	277,6	0,97
TG2-2	400	260	288,4	280	277,6	0,94
TG2-3	550	183,6	178,8	180	173,5	1,06
TG2-4	700	62,4	66,34	62	63,8	0,98
TG3-1	20	53,35	44,36	45	44,3	1,20
TG3-2	400	30,08	31,05	30	31,0	0,97
TG3-3	565	19,87	18,23	19,2	18,2	1,09
TG3-4	690	7,05	5,77	6,4	6,6	1,07
TG4-1	20	101,4	113,6	102	109,0	0,93
TG4-2	400	58,9	85,23	84	76,3	0,77
TG4-3	550	24,54	50,43	39	49,6	0,49
TG4-4	700	10,59	14,53	15	14,2	0,75
TG5-1	20	21,05	19,18	18	18,7	1,13
TG5-2	400	17,63	13,43	18	13,1	1,35
TG5-3	550	13	11,51	10	8,5	1,53
TG5-4	700	4,5	2,49	3	2,4	1,88

From Table 3.2 it can be seen that some of the analytically calculated critical shear forces according to the reference [Vimonsatit, Tan, Qian, 2007] and according to this study differ a little. The reason is unclear. In the following, all comparisons are based on the values calculated analytically in this study. In this study, no FEM calculation was done for this case.

In the tests shear buckling was indicated by a sudden increase in out-of plane deflection. At elevated temperatures the steel material stress-strain relationship becomes highly non-linear causing out-of plane deflection to develop rather smoothly [Vimonsatit, Tan, Qian, 2007]. The exact shear buckling load is therefore hard to define at elevated temperatures. That can be seen from Figure 3.4 where out-of-plane deflection is presented as a function of shear load for the TG4 series at elevated temperatures. More prominent buckling was also reported at ambient than at elevated temperatures. An example is shown in Figure 3.5.

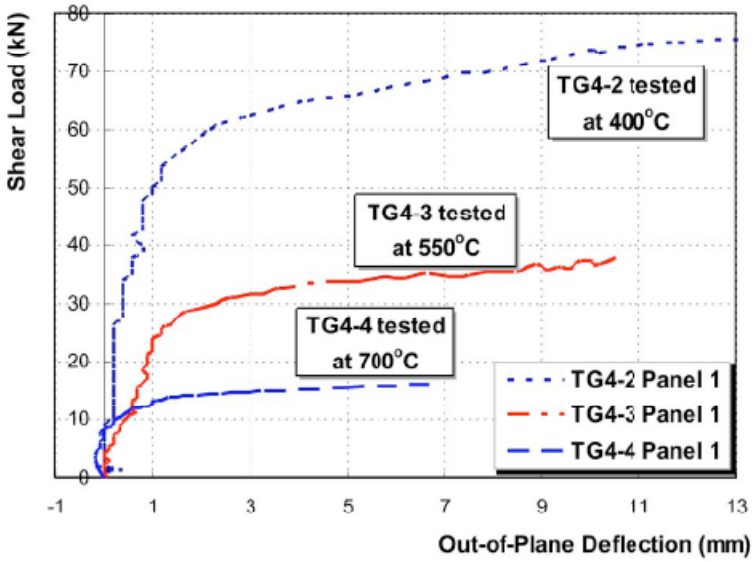

Figure 3.4. Shear load versus out-of-plane deflection for TG4 series [Vimonsatit, Tan, Qian, 2007].

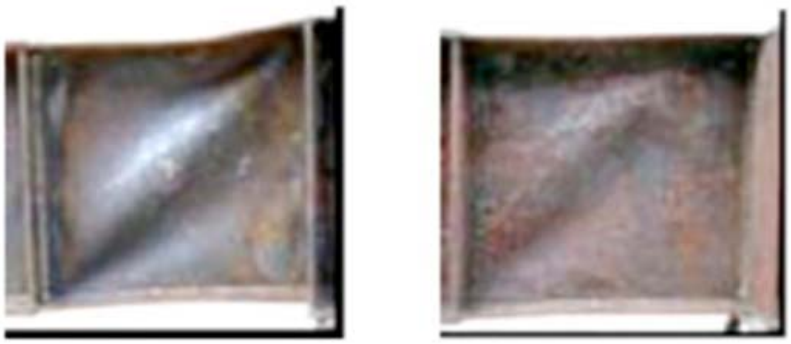

Figure 3.5. Failure modes of panel TG3 at 20 °C (at left) and 700 °C (at right) [Vimonsatit, Tan, Qian, 2007].

Figure 3.6 only deals with panels that buckled (TG3, TG4 and TG5). The vertical axis shows the ratio of the shear buckling load of the test to the calculated shear buckling load while the horizontal axis shows the temperature. If the ratio is higher than 1, the calculated result is on the safe side.

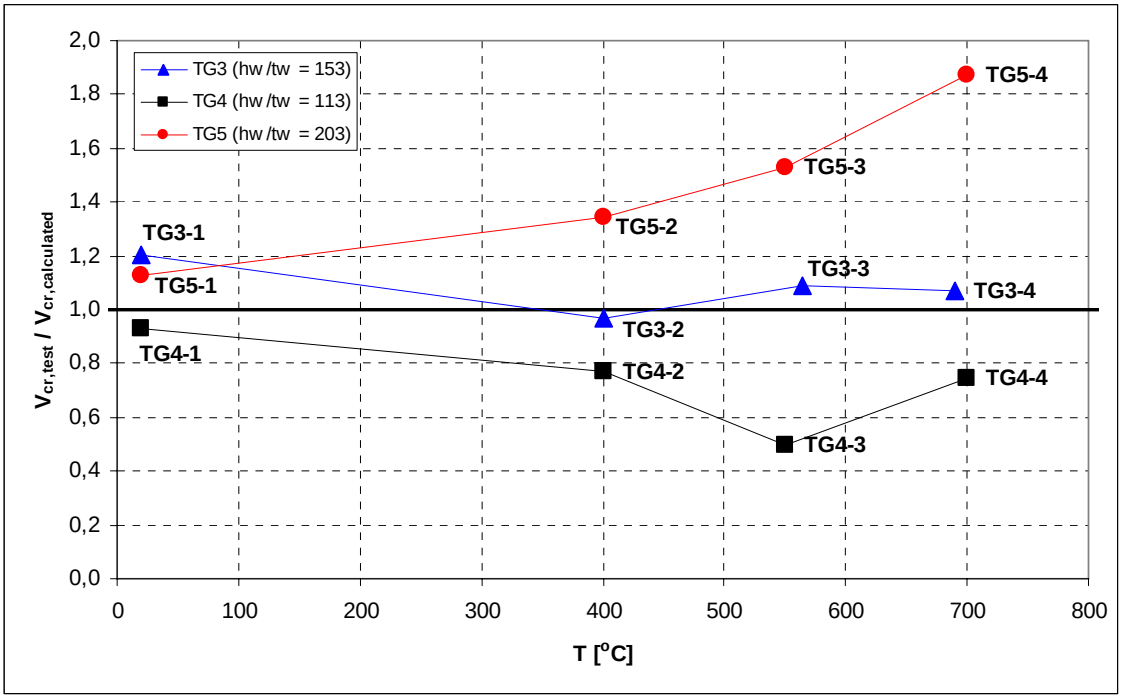

Figure 3.6. Ratio $V_{cr,test}$ / $V_{cr,calculated}$ for test panels that buckled.

It appears from Figure 3.6 that the results for test series TG4 are not on the safe side, perhaps due to the reported problems in the tests. In the case of test series TG3, the test and calculated values correlate quite well. With test series TG5 (very slender web, h_w/t_w = 203), the reported values are much higher than the calculated ones.

Figure 3.7 gives the $V_{cr,test}$ / $V_{cr,calculated}$ values for all tested cases at elevated temperatures as a function of web slenderness λ_w (Eq. 2.19). Web slenderness was calculated separately for each temperature using reduced values for elastic modulus E and yield strength f_y.

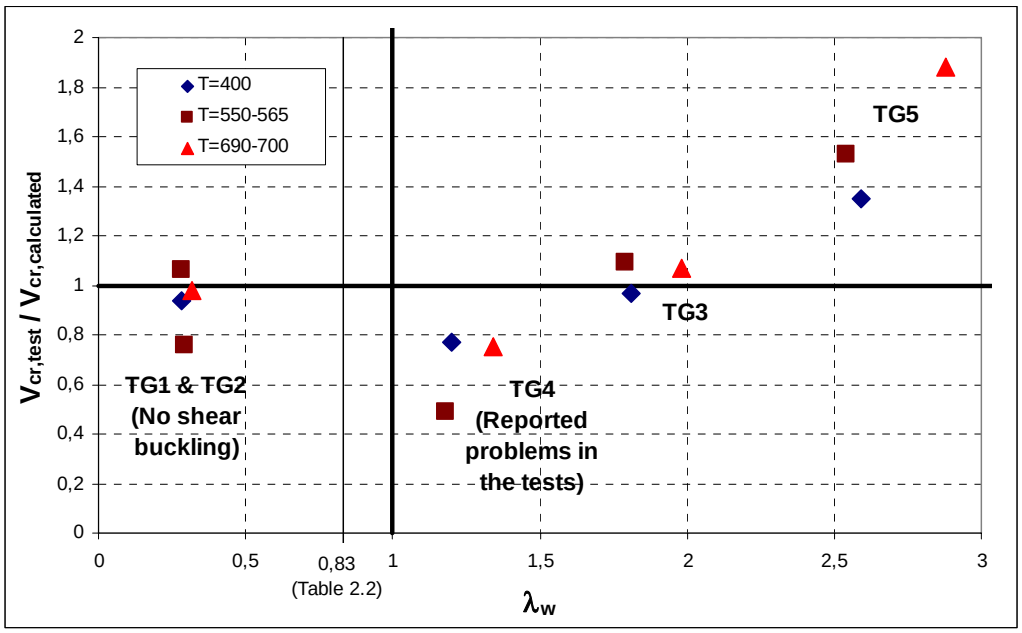

Figure 3.7. Ratio $V_{cr,test}$ / $V_{cr,calculated}$ for all panels tested at elevated temperatures.

Considering only webs that buckled and ignoring the results of test series TG4, only one result out of six (TG3, T = 400 °C) is a little bit on the unsafe side ($V_{cr,test}$ / $V_{cr,calculated}$ = 0,97).

Table 3.3 presents the ultimate shear forces of the tests, FEM analysis and the calculations with the analytical method [Vimonsatit, Tan, Ting, 2007]. In this study the ultimate shear resistance of tested panels was calculated by two different strategies:

• Strategy 1, EN 1993-1-2 [EN 1993-1-2, 2005] as such:
→ First the shear resistance of the web at ambient temperature was calculated according to EN 1993-1-5 [EN 1993-1-5, 2005] followed by reduction at elevated temperatures using Equation (3.1) or Equation (3.2).

• Strategy 2, EN 1993-1-5 with reduction factors:
→ First the elastic modulus and yield strength of the web and flanges are reduced according to EN 1993-1-2 [EN 1993-1-2, 2002] followed by calculation of the ultimate shear resistance of the web according to EN 1993-1-5 (Eq. 2.27). In this strategy the calculation is the same as at ambient temperature, but with reduced material properties.

Four cases were considered in order to observe the effect of the flanges and the rigidity of the end posts (see Fig. 2.7) according to EN 1993-1-5 [EN 1993-1-5, 2002].

In Table 3.3 four cases are considered based on both strategies:

- Wn → Only web, non-rigid end post,
- WR → Only web, rigid end post,
- Fn → Web and flanges, non-rigid end post,
- FR → Web and flanges, rigid end post.

The calculated ultimate shear resistances, enclosed by thicker lines in Table 3.3, are used in the comparisons. Test series TG3, TG4 and TG5 seem to have rigid end-posts based on the reference article [Vimonsatit, Tan, Qian, 2007].

Table 3.3. Ultimate shear forces according to reference [Vimonsatit, Tan, Qian, 2007] and the Eurocodes.

Paper [Vimonsatit et al, 2007]					This study							
					1. EN 1993-1-2 directly				2. EN 1993-1-5 with reduction factors			
Test panel	T [°C]	$V_{ult,test}$ [kN]	$V_{ult,anal.}$ [kN]	$V_{ult,FEM}$ [kN]	Wn V_{Rd} [kN]	WR V_{Rd} [kN]	Fn V_{Rd} [kN]	FR V_{Rd} [kN]	Wn V_{Rd} [kN]	WR V_{Rd} [kN]	Fn V_{Rd} [kN]	FR V_{Rd} [kN]
TG1-1	20	193,5	192,19	190	201	201	201	201	201	201	201	201
TG1-2	550	97,3	111,09	100	126	126	126	126	105	105	105	105
TG2-1	20	343,8	345,65	322	333	333	333	333	333	333	333	333
TG2-2	400	324,3	345,65	314	333	333	333	333	333	333	333	333
TG2-3	550	234,6	214,3	198	208	208	208	208	174	174	174	174
TG2-4	700	74,2	79,5	72,6	77	77	77	77	64	64	64	64
TG3-1	20	79,85	85,7	88	56	63	61	68	56	63	61	68
TG3-2	400	67,63	65,2	66	36	41	40	44	47	55	53	61
TG3-3	565	34,34	37,13	38,4	21	24	23	26	21	26	25	30
TG3-4	690	17,15	15,7	16,4	8	9	9	10	5	7	8	10
TG4-1	20	111,8	113,64	112	91	91	92	92	91	91	92	92
TG4-2	400	77,1	85,89	86	91	91	92	92	76	80	79	82
TG4-3	550	37,75	51,86	52,1	57	57	58	58	38	43	42	46
TG4-4	700	15,94	18,19	18	21	21	21	21	8	10	9	12
TG5-1	20	59,6	69,28	70	34	42	41	49	34	42	41	49
TG5-2	400	46,4	53,17	53,4	22	27	27	32	28	37	36	44
TG5-3	550	28,6	32,39	32,5	14	17	17	20	14	19	19	24
TG5-4	700	10,16	11,48	11,7	4	5	5	6	3	4	5	6

Based on Table 3.3 it can be said that in the case of a slender web (TG3, TG4 and TG5), the chosen strategy, the contribution from the flanges and the rigidity of the end posts have an impact on calculated resistances. The following graphs provide a comparison between the test results and the calculated results using two different strategies. Figure 3.8 presents webs that did not buckle while Figure 3.9 shows webs that buckled.

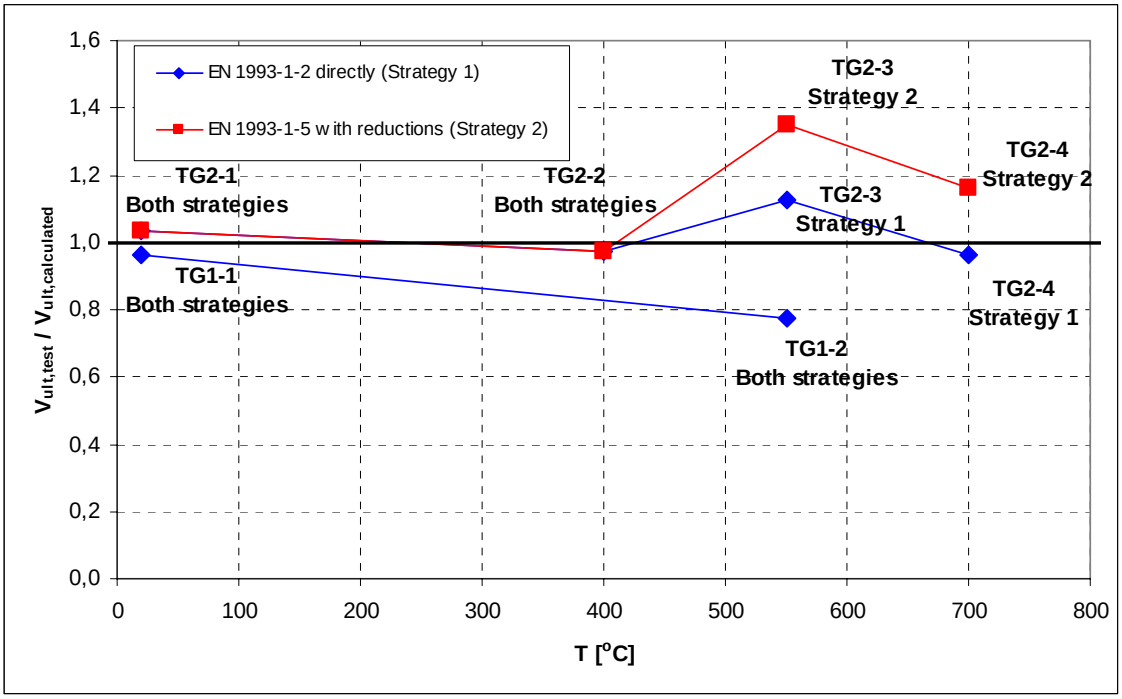

Figure 3.8. Comparison of tested and calculated ultimate shear resistances of stocky webs.

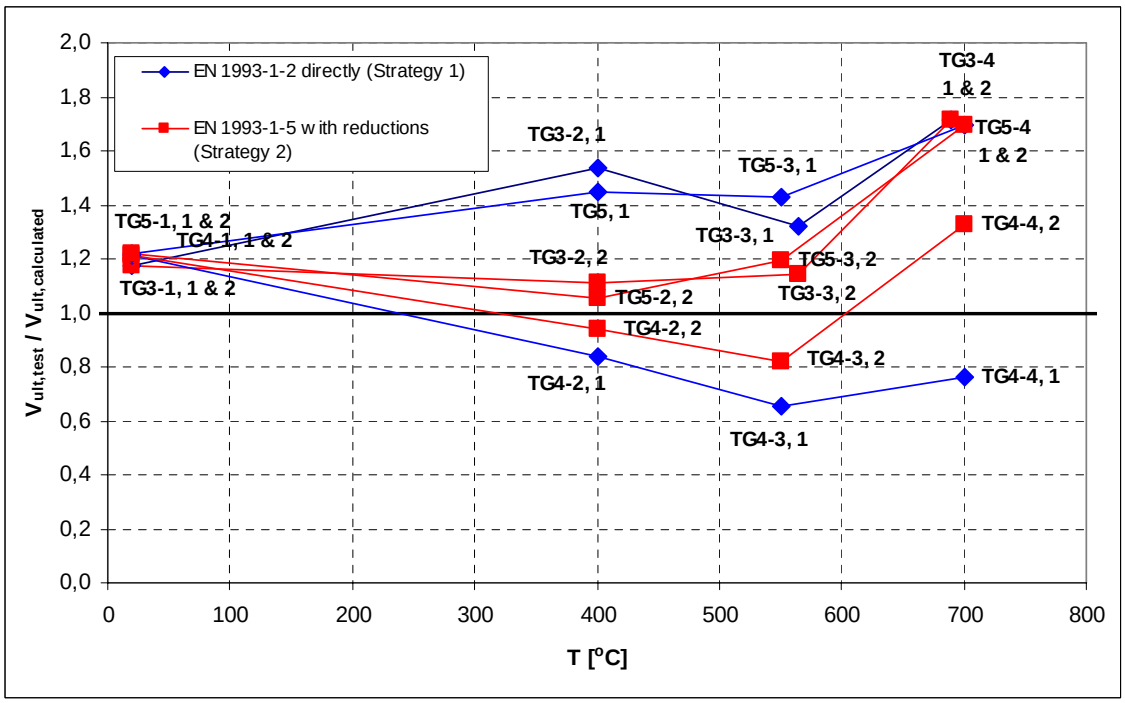

Figure 3.9. Comparison of tested and calculated ultimate shear resistances of slender webs.

As concerns the stocky webs (Fig. 3.8), it can be said that the calculated results dependended on the used strategy in two cases (TG2-3 and TG2-4). In these cases the resistances calculated by strategy 1 were closer to the tested resistances, but the result from test TG2-4 is slightly on the unsafe side. In the case of the slender webs (Fig. 3.9),

if we ignore the results of test series TG4, all the results are on the safe side. It can be said, that strategy 2 yields better results for slender webs than strategy 1 based on the test results. The calculated results for slender webs are clearly more conservative at 690–700 ^{o}C (especially with strategy 2) than at ambient and other elevated temperatures.

3.2. Non-uniform temperature across the web height

The problem in this case is the defining of the right temperature and the reduction factors for elastic modulus and yield strength (not part of this study). It is extremely difficult to search for a solution for two reduction factors at the same time, which is why the task is divided into two stages. It is obvious that the design shear stress consists of two components: τ_{cr} and τ_y. It is also apparent that the critical shear stress depends only on elastic modulus. So the strategy for the search is as follows:

- Firstly, search the reduction factor of elastic modulus by applying the eigenvalue solution (this study),
- Then, search the reduction factor of yield strength by applying the non-linear solution (forthcoming studies).

Due to the lack of the test results, the eigenvalue solutions (shear buckling) and the non-linear solutions (tension field effect) are used as controls in the search for design methods.

The temperature across the web height may vary in many different ways. The temperature distributions used in this study were derived from the fire test results on a typical slim floor hat beam [Teräsnormikortti N:o 21/2009, 2009] and a thermal analysis of an all- metal sandwich panel by FEM based on the general heat transfer theory.

The dimensions of the considered hat beams and gas temperatures in the fire tests at different times are shown in Figure 3.10. The temperatures used in the tests followed the ISO fire curve. Figure 3.11 presents the temperature distributions for the beam web in the case of four elevated temperatures and three thicknesses of the lower flange t_{lf}. The temperature distributions of the hat beams are shown as a function of relative height co-ordinate y/h_w

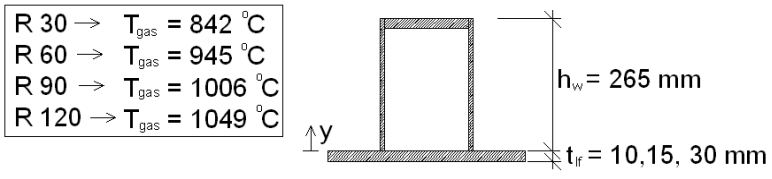

Figure 3.10. Hat beam dimensions and gas temperatures.

The hat beams were embedded in concrete slabs to simulate an actual slim floor construction.

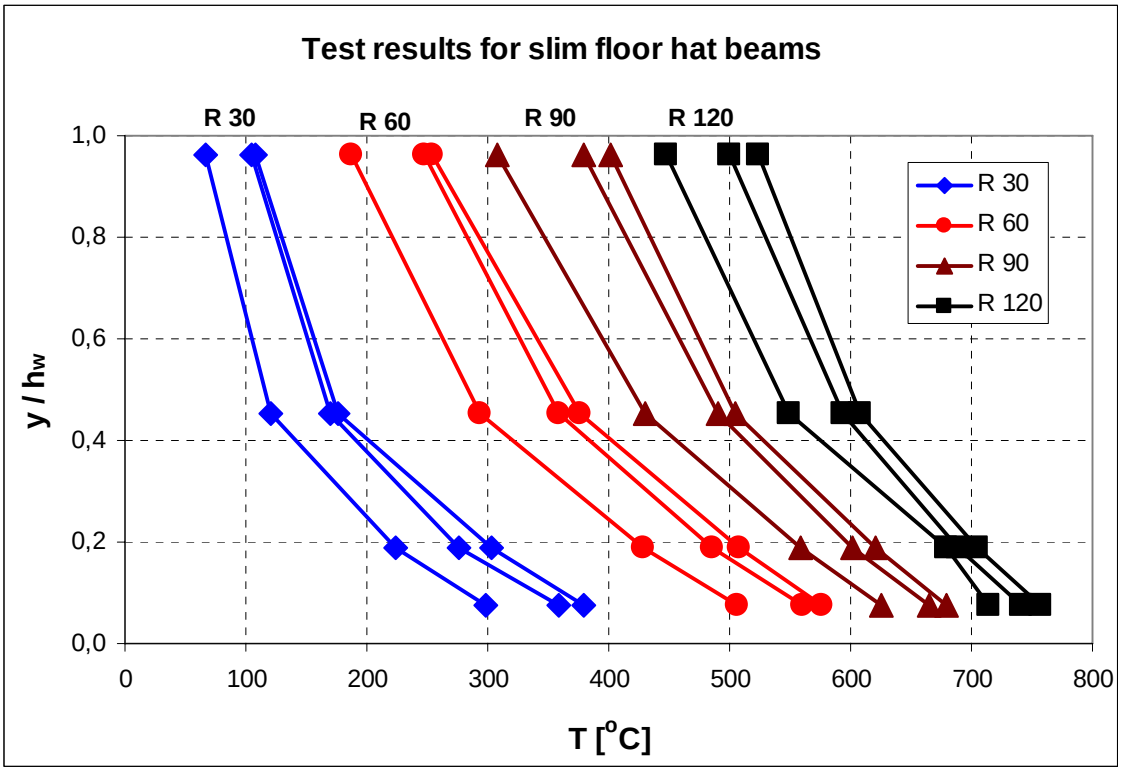

Figure 3.11. Measured temperature distributions in webs of slim floor hat beams from the reference [Teräsnormikortti 21/2009, 2009].

The all-metal sandwich panel considered in Chapter 7 has no insulation inside. Thermal and mechanical FEM calculations on a similar panel with insulation can be found from the reference [Ala-Outinen et al, 2006].

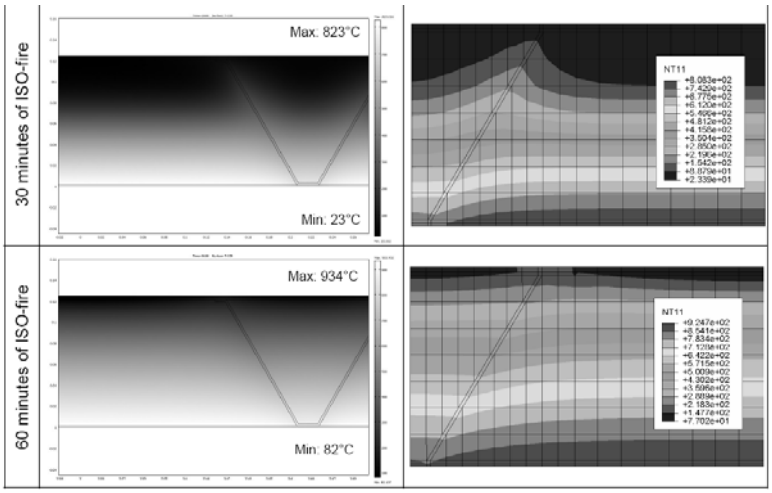

Figure 3.12. Temperature distributions across insulated sandwich panel [Ala-Outinen et al, 2006].

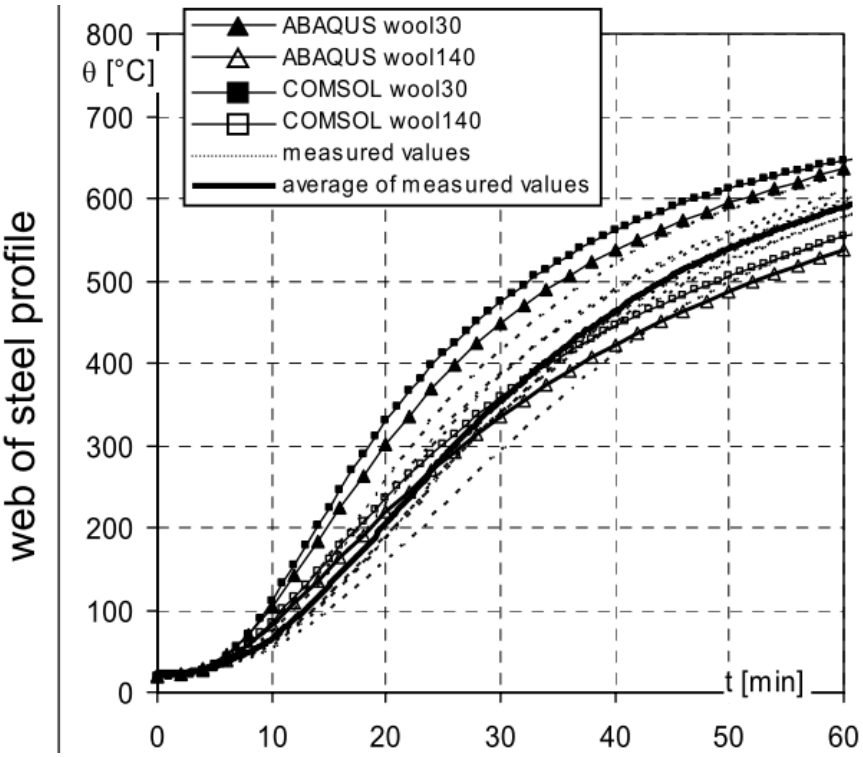

Figure 3.13. Temperatures of the web of the sandwich panel [Ala-Outinen et al, 2006].

From Figure 3.13 it can be seen that there is scattering between temperatures from the test and FEM calculations. The FEM software *COMSOL* [COMSOL, 2008] gives higher temperatures in this case than *ABAQUS* [ABAQUS, 2007]. Two different wools were applied in the analyses, because there was no material model for the blowing rock wool used in the tests [Ala-Outinen et al, 2006].

4. FEM ANALYSIS OF SHEAR BUCKLING

Eigenvalue solutions were used as controls in the search for design methods. Eigenvalues were calculated for six different plates at ambient temperature and at 18 different non-uniform elevated temperatures. The plates were made of carbon steel, aluminium and stainless steel. The procedure was the same with all materials. Chapters 4.1 and 4.2 describe the procedure in the case of carbon steel while Chapter 4.3 points out the differences between aluminium and stainless steel.

4.1. Modelling

Critical shear stresses were calculated using *ABAQUS* [ABAQUS, 2007] FEM software to conduct a buckling analysis. A linear buckling analysis takes into account the stiffening effects caused by nonlinear strain terms. The stiffnesses due to stresses and materials define an eigenvalue problem where the eigenvalue is a load factor that, when multiplied by the actual load, gives the critical load in a linear context. Four node reduced integration quadrilateral shell elements (S4R) were used for modelling the plates. The following properties were used at ambient temperature:

- $E = 210\ 000\ N/mm^2$
- $\nu = 0{,}3$
- $t_w = 6$ and 10 mm
- $h_w = 1000$ mm
- a = 1000, 2000 and 3000 mm

At elevated temperatures the elastic modulus was reduced according to EN 1993-1-2 [EN 1993-1-2, 2005] (Fig. 3.1). The Poisson's ratio ν is supposed to be 0,3 also at elevated temperatures.

The plates were supported at all edges in the perpendicular direction against the web plane, and the rigid body motion was supported as shown in Figure 4.1 and Table 4.1. Shear force was applied as a uniform stress of 1 $kN/(t_w\ h_w)$ acting on the edges of the plate. In each case the size of the used elements was 20 x 20 mm^2. Depending on the size of the plate, 50–150 elements were used in the horizontal direction and 50 in the vertical direction. Applied shear stress and the used element mesh are shown in Figure

4.2. The modelling of the 1000 x 1000 x 10 mm^3 is shown in more detail in Appendix A.

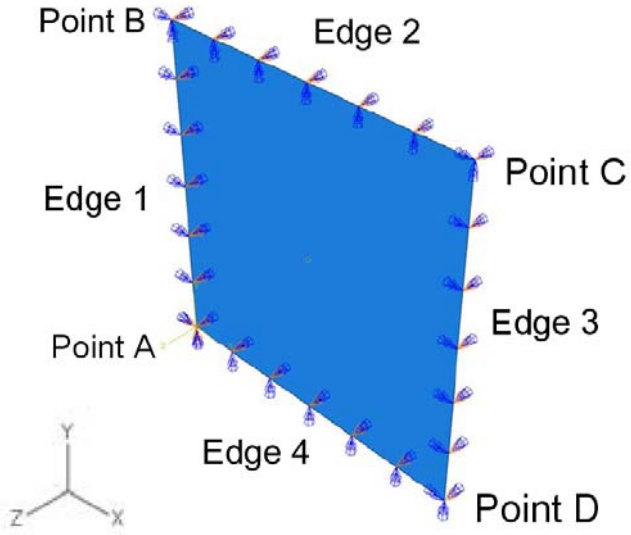

Figure 4.1. Boundary conditions of the 1000 x 1000 mm^2 plate.

Table 4.1. Boundary conditions used for the plate.

Location	u_x	u_y	u_z	θ_x	θ_y	θ_z
Point A	Fixed	Fixed	Fixed	Fixed	Fixed	Fixed
Points B, C and D	Free	Free	Fixed	Fixed	Fixed	Fixed
Edges 1 and 3	Free	Free	Fixed	Fixed	Free	Fixed
Edges 2 and 4	Free	Free	Fixed	Free	Fixed	Fixed

Same kinds of boundary conditions have also been used in other studies concerning shear buckling and post-buckling of plates [Yoo, Lee, 2006], [Alinia et al, 2009].

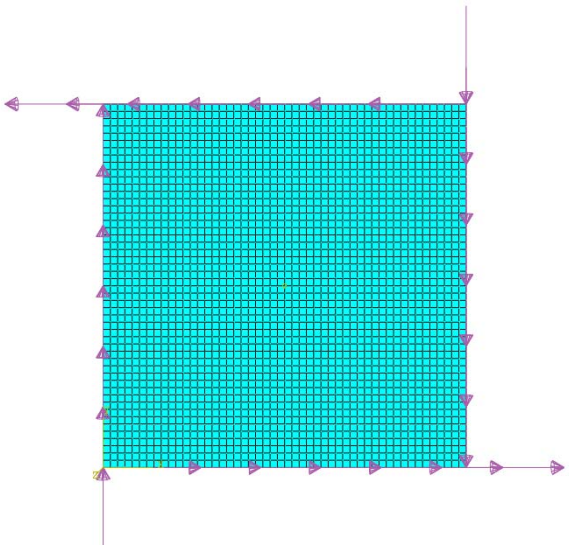

Figure 4.2. Applied loading and mesh of the 1000 x 1000 mm^2 plate.

Calculations were first done at uniform temperature fields including ambient temperature to compare the results to classical theory (Equations (2.2) - (2.5)) and to get a reference value for the elevated temperatures.

The temperature distributions used in the calculations were derived from the fire tests [Teräsnormikortti 21/2009, 2009] and FEM calculations [Kaitila, 2002] shown in Chapter 3.2. Temperature distributions for all-metal sandwich panel are calculated in Chapter 7 using FEM.

Temperature over the length of the plate is constant. Temperature distributions across the plate height are: 100–300, 100–500, 100–700, 100–900, 200–500, 300–600, 400–700, 500–800 and 600–900 degrees Celsius. All distributions are considered linear and non-linear (3rd order polynomial) so that the hottest temperature occurs at the lower edge of the plate as shown in Figure 4.3 and Equations (4.1) and (4.2). Figure 4.4 shows all used temperature distributions.

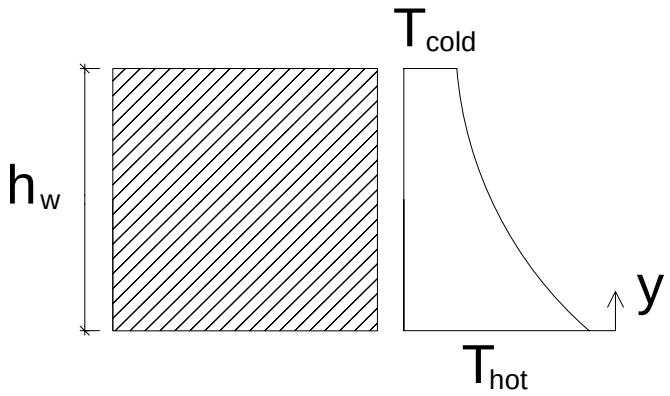

Figure 4.3. Temperature distributions.

Linear distribution: $$T(y) = T_{cold} + (1 - \frac{y}{h_w})(T_{hot} - T_{cold}) \quad (4.1)$$

Non-linear distribution: $$T(y) = T_{cold} + (1 - \frac{y}{h_w})^3 (T_{hot} - T_{cold}) \quad (4.2)$$

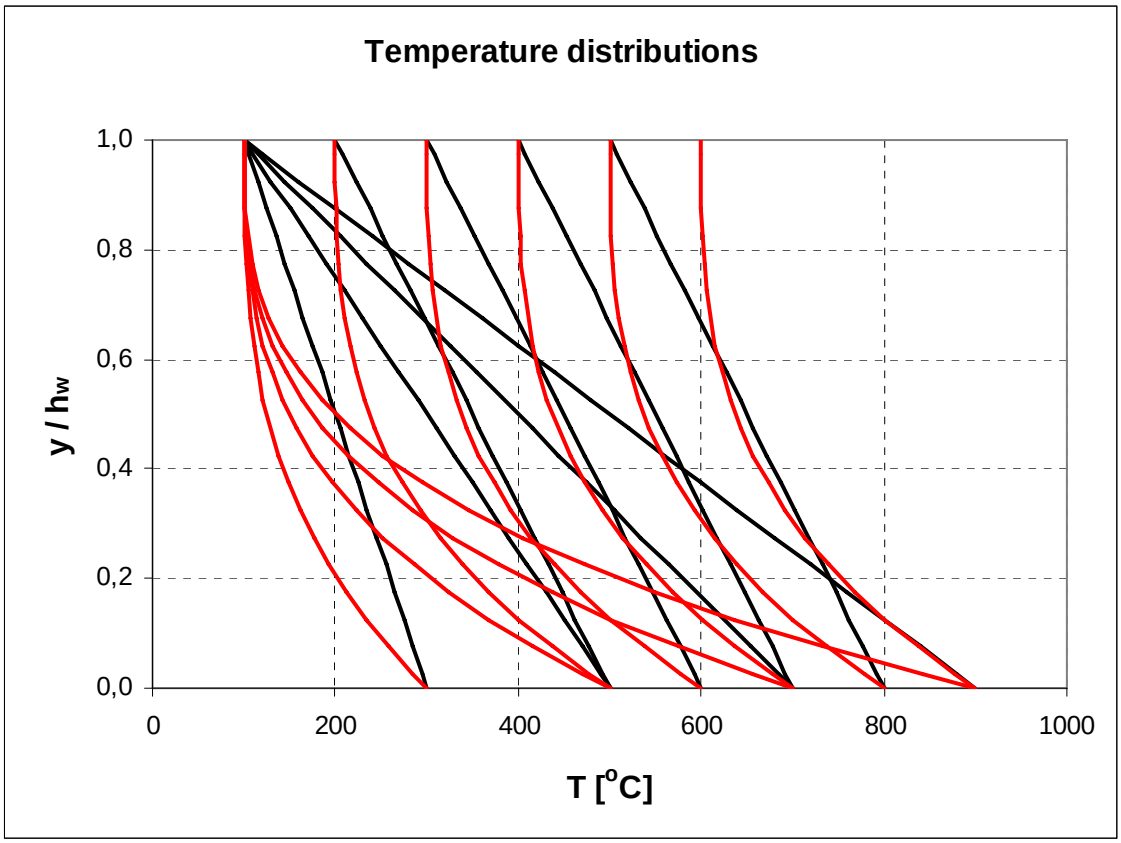

Figure 4.4. Temperature distributions used in FEM calculations.

4.2. Results

Table 4.2 presents the critical shear forces according to classical formulas (Equations (2.2) - (2.5)) and FEM calculations at ambient temperature.

Table 4.2. Ambient temperature results.

Plate [mm^3]	$V_{cr,theoretical}$ [kN]	$V_{cr,FEM}$ [kN]	$V_{cr,theoretical}$ / $V_{cr,FEM}$
1000 x 1000 x 10	1772,7	1771,3	1,00
1000 x 1000 x 6	382,9	383,1	1,00
1000 x 2000 x 10	1203,3	1243,9	0,97
1000 x 2000 x 6	259,9	268,9	0,97
1000 x 3000 x 10	1097,9	1109,8	0,99
1000 x 3000 x 6	237,1	239,9	0,99

The differences between the results from FEM calculations and classical formulas at ambient temperature are in every case less than 3,5 %. From this point on, all calculated

resistances at elevated temperatures are compared to the corresponding ambient temperature results from FEM calculations.

Table 4.3 shows the reduction factors $k_{E,FEM} = V_{cr,FEM,elevated} / V_{cr,FEM,ambient}$ calculated from uniform temperature distributions in comparison to EN 1993-1-2 [EN 1993-1-2, 2005] reduction factors for elastic modulus.

Table 4.3. Calculated reduction factors for uniform elevated temperatures.

Plate [mm^3]	100 °C	200 °C	300 °C	400 °C	500 °C	600 °C	700 °C
1000 x 1000 x 10	1,000	0,900	0,800	0,700	0,600	0,310	0,130
1000 x 1000 x 6	1,000	0,900	0,800	0,700	0,600	0,310	0,130
1000 x 2000 x 10	1,000	0,900	0,800	0,700	0,600	0,310	0,130
1000 x 2000 x 6	1,000	0,900	0,800	0,700	0,600	0,310	0,130
1000 x 3000 x 10	1,000	0,900	0,800	0,700	0,600	0,310	0,130
1000 x 3000 x 6	1,000	0,900	0,800	0,700	0,600	0,310	0,130
EN 1993-1-2	1,000	0,900	0,800	0,700	0,600	0,310	0,130

The reduction factors from uniform temperature distributions are used to validate the FEM model. The table shows that the reduction factors from FEM and EN 1993-1-2 are exactly the same.

Table 4.4 shows the calculated reduction factors for linear temperature distributions and Table 4.5 for non-linear distributions. The minimum values for each distribution are written in bold.

Table 4.4. Calculated reduction factors for linear temperature distributions.

Plate [mm^3]	100-300 °C	100-500 °C	100-700 °C	100-900 °C	200-500 °C	300-600 °C	400-700 °C	500-800 °C	600-900 °C
1000 x 1000 x 10	**0,897**	**0,788**	**0,567**	0,290	**0,743**	**0,605**	**0,376**	**0,193**	**0,114**
1000 x 1000 x 6	**0,897**	**0,788**	**0,567**	**0,287**	**0,743**	**0,605**	**0,376**	**0,193**	**0,114**
1000 x 2000 x 10	0,898	0,789	0,580	0,318	0,744	0,608	0,387	0,200	**0,114**
1000 x 2000 x 6	0,898	0,789	0,580	0,318	0,744	0,608	0,387	0,200	**0,114**
1000 x 3000 x 10	0,898	0,791	0,587	0,329	0,744	0,610	0,392	0,204	0,116
1000 x 3000 x 6	0,898	0,791	0,587	0,329	0,744	0,610	0,392	0,204	0,116
Min.	**0,897**	**0,788**	**0,567**	**0,287**	**0,743**	**0,605**	**0,376**	**0,193**	**0,114**

Table 4.5. Calculated reduction factors for non-linear temperature distributions.

Plate [mm^3]	100-300 °C	100-500 °C	100-700 °C	100-900 °C	200-500 °C	300-600 °C	400-700 °C	500-800 °C	600-900 °C
1000 x 1000 x 10	**0,953**	**0,901**	**0,809**	**0,638**	**0,827**	**0,715**	**0,561**	**0,351**	**0,182**
1000 x 1000 x 6	**0,953**	**0,901**	0,810	0,639	**0,827**	**0,715**	**0,561**	**0,351**	**0,182**
1000 x 2000 x 10	0,955	0,904	0,820	0,661	0,829	0,719	0,567	0,363	0,188
1000 x 2000 x 6	0,955	0,904	0,820	0,662	0,829	0,719	0,567	0,363	0,188
1000 x 3000 x 10	0,954	0,904	0,825	0,672	0,829	0,720	0,571	0,368	0,190
1000 x 3000 x 6	0,954	0,904	0,826	0,673	0,829	0,720	0,571	0,368	0,190
Min.	**0,953**	**0,901**	**0,809**	**0,638**	**0,827**	**0,715**	**0,561**	**0,351**	**0,182**

Reduction factors were calculated for all six plates with 18 different temperature distributions. In all cases the square 1000 x 1000 mm^2 plate yielded the minimum value.

The lowest buckling modes for the 1000 x 1000 x 10 mm^3 plate at ambient and at three elevated temperatures are illustrated in Figure 4.5. The hottest temperature occurs at the lower edge of the plate in each case.

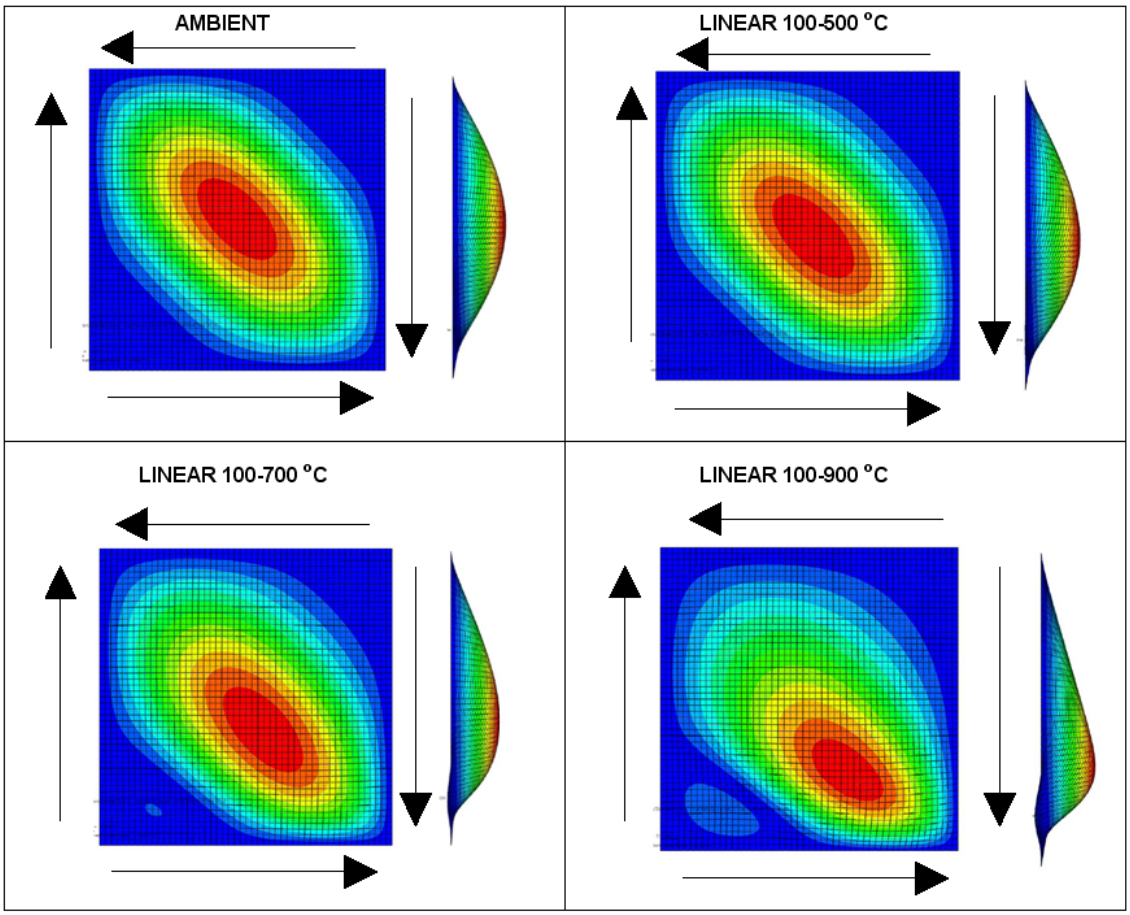

Figure 4.5. Buckling modes of the 1000 x 1000 x 10 mm^3 plate at ambient and elevated temperatures.

The buckling modes indicate that when temperature rises at the lower edge of the plate, buckling occurs lower due to greater reduction in elastic modulus.

4.3. Aluminium and stainless steel

The FEM model used for carbon steel plates was also applied to aluminium and stainless steel plates. An ambient temperature value of E = 70 000 N/mm^2 was used for aluminium [EN 1999-1-1, 2007] and E = 200 000 N/mm^2 [EN 1993-1-4, 2006] for stainless steel. The reductions in elastic modulus were done according to EN 1999-1-2 [EN 1999-1-2, 2007] for aluminium and according to EN 1993-1-2 [EN 1993-1-2, 2005] for stainless steel as shown in Figure 4.6. It should be noted that in the case of aluminium and stainless steel reductions in yield strength depend on the material grade, but only one curve is given for elastic modulus.

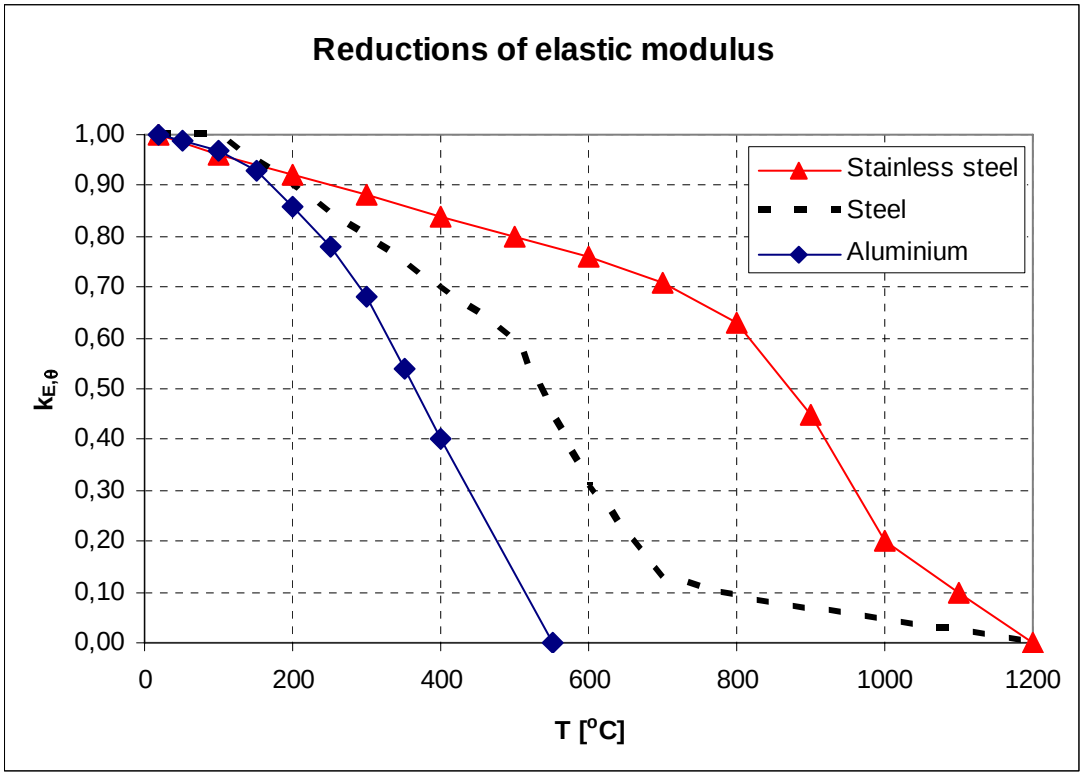

Figure 4.6. Reductions of elastic modulus of carbon steel, aluminium and stainless steel [EN 1993-1-2, 2005], [EN 1999-1-2, 2007].

It can be seen from Figure 4.6 that the reductions in elastic modulus at elevated temperatures are totally different for these three materials. Therefore, different temperature distributions were used for aluminium and stainless steel than for carbon steel. For aluminium the used temperature distributions were: 100–200, 100–300, 100–400, 100–500, 150–300, 200–350, 250–400, 300–450 and 350–400 °C. For stainless steel they were: 100–400, 100–600, 100–800, 100–1000, 200–600, 300–700, 400–800, 500–900, 600–1000 °C.

The calculated values for carbon steel (Tables 4.4 and 4.5) show that the 1000 x 1000 mm^2 plate yielded the minimum values for the reduction factor in each case. They also indicate that the difference between the reduction factors of 1000 x 1000 x 10 mm^3 and 1000 x 1000 x 6 mm^3 plates is very small. Therefore, only the 1000 x 1000 x 10 mm^3 plate was considered in the FEM analysis of aluminium and stainless steel plates.

The calculated elastic modulus reduction factors for aluminium and stainless steel are shown in Tables 4.6 and 4.7.

Table 4.6. Calculated reduction factors for aluminium.

Distribution	100-200 °C	100-300 °C	100-400 °C	100-500 °C	150-300 °C	200-350 °C	250-400 °C	300-450 °C	350-500 °C
Linear	0,932	0,853	0,731	0,544	0,820	0,721	0,595	0,453	0,306
Non-linear	0,959	0,927	0,877	0,797	0,886	0,803	0,702	0,574	0,427

Table 4.7. Calculated reduction factors for stainless steel.

Distribution	100-400 °C	100-600 °C	100-800 °C	100-1000 °C	200-600 °C	300-700 °C	400-800 °C	500-900 °C	600-1000 °C
Linear	0,899	0,857	0,810	0,708	0,838	0,797	0,750	0,678	0,539
Non-linear	0,933	0,913	0,892	0,854	0,883	0,843	0,800	0,750	0,674

Figure 4.7 presents all calculated reduction factors as a function of the hottest temperature of the plate.

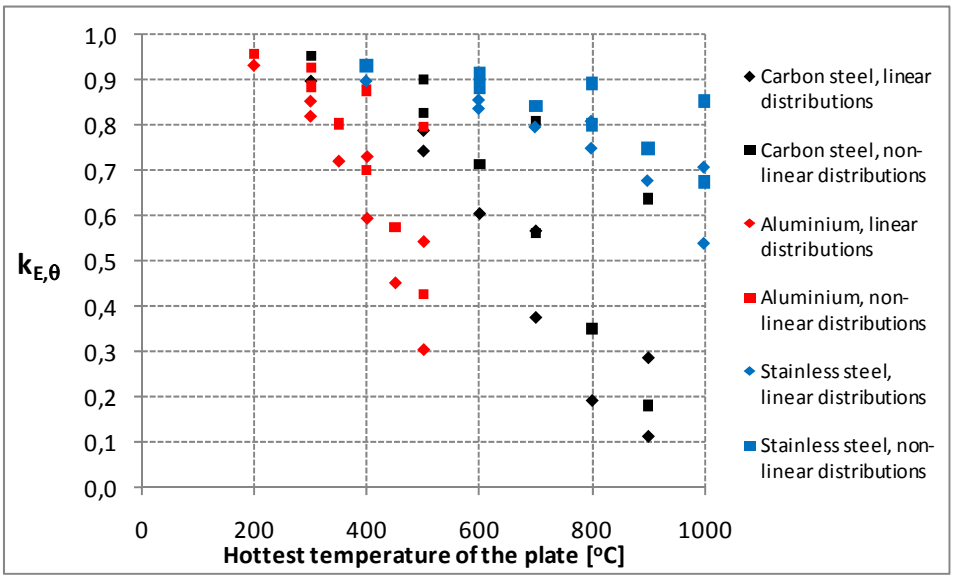

Figure 4.7. All calculated reduction factors.

Based on Figure 4.7 it can be concluded that for stainless steel the reduction factors are greatest and for aluminium smallest if the hottest temperature of the plate is the same. Same conclusion can be drawn from Figure 4.6. It can also be said that the effect of the distribution (linear or 3rd order polynomial) has significant effect on the reduction factor with all considered materials.

5. REDUCTION MODELS FOR NON-UNIFORM TEMPERATURE DISTRIBUTIONS

As mentioned before, the purpose of this study was to develop a hand-calculation method for predicting the shear buckling load of metal plates at elevated temperatures in cases where temperature distribution is non-uniform in the height of the plate. The method should be easy to apply and reliable. Since the shear buckling load depends only on the elastic modulus E (not on yield strength f_y) of the plate material, the idea is to reduce E with a single value and use it with classical formulas (Eqs. (2.2)–(2.5)). This chapter illustrates different strategies for defining that single reduction factor for an entire plate.

The FEM calculations for 18 different temperature distributions in Chapter 4 are used to validate the proposed method. Six different methods (a-f) are presented in the following. A comparison of all the methods and the results from FEM calculations are presented in Chapter 6. Methods a-d and f are applicable for carbon steel, aluminium and stainless steel. Method e is suitable only for carbon steel. In all methods the ranges for temperatures are 20-1200 ^{o}C in the case of carbon- and stainless steel and 20-550 ^{o}C in the case of aluminium [EN 1993-2,2005], [EN 1999-1-2, 2007]. In all considered methods it is also required that the temperature at the middle of the height of the plate is between the temperatures at lower and upper edge of the plate.

5.1. Methods a–d

Methods a-d are very simply to use. In method a the reduction in elastic modulus is based only on the temperature of the plate in the middle of its height. With methods b, c and d the hottest and coldest temperatures of the plate are also used in calculating the reduction factor. The plate temperatures needed for these methods are shown in Figure 5.1.

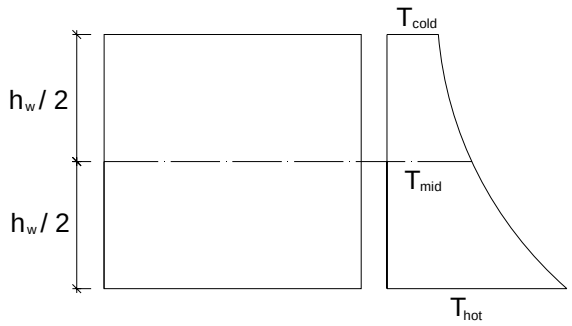

Figure 5.1. Plate temperatures needed for methods a–d [Salminen et al, 2009].

The reduction factors for methods a–d are calculated as follows:

Method a: $$k_{E,\theta,a} = k_{E,\theta}(T_{mid}) \tag{5.1}$$

Method b: $$k_{E,\theta,b} = \frac{k_{E,\theta}(T_{cold}) + k_{E,\theta}(T_{mid}) + k_{E,\theta}(T_{hot})}{3} \tag{5.2}$$

Method c: $$k_{E,\theta,c} = \frac{k_{E,\theta}(T_{cold}) + 1{,}1 \cdot k_{E,\theta}(T_{mid}) + 1{,}2 \cdot k_{E,\theta}(T_{hot})}{3{,}3} \tag{5.3}$$

Method d: $$k_{E,\theta,d} = \sqrt[3]{k_{E,\theta}(T_{cold}) \cdot k_{E,\theta}(T_{mid}) \cdot k_{E,\theta}(T_{hot})} \tag{5.4}$$

5.2. Method e

The idea behind method e is to leave the hottest part (T>500 ^{o}C) out of the calculations and use the temperature at the middle of the "cold" part. This means that the height of the web is also reduced with this method. Therefore, it is slightly more complicated to use than the previous ones. The strategy is illustrated in Figure 5.2.

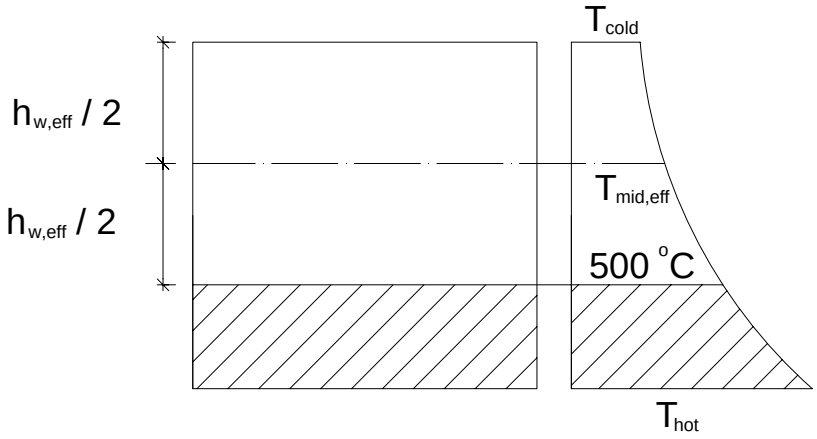

Figure 5.2. Method e [Salminen et al, 2009].

The reduction factor according to method e is then calculated as follows:

Method e: $$k_{E,\theta,e} = \frac{h_{w,eff}}{h_w} \cdot k_{E,\theta}(T_{mid,eff}) \quad (5.5)$$

If the maximum temperature of the web is less than 500 °C, then method e becomes like method a. When the minimum temperature of the web is more than 500 °C, the reduction factor becomes zero. Another problem with this method is that the shape of the effective plate is not the same as the shape of the original plate. It means that theoretically the shear buckling coefficient k_τ changes. That has not been considered in the calculations.

5.3. Method f

Method f provides a graphic way to solve the problem. It is based on the reduction factor curve for elastic modulus given in EN 1993-1-2 [EN 1993-1-2, 2005]. The temperatures needed with this method are shown in Figure 5.3. In deviation from methods a–e, the average temperature of the plate is also needed.

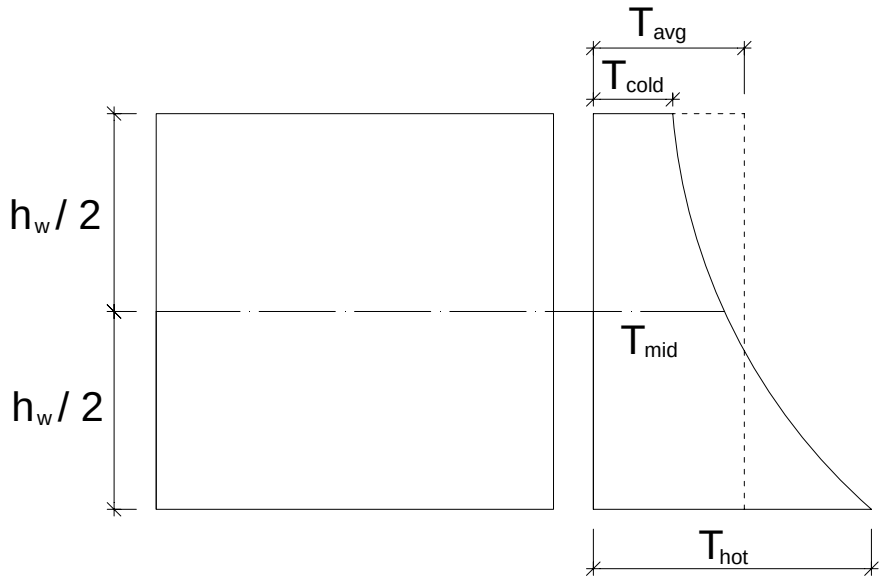

Figure 5.3. Temperatures needed for method f [Salminen et al, 2009].

The idea of this method is to draw a line between points $\begin{pmatrix} T_{mid} \\ k_{E,\theta}(T_{hot}) \end{pmatrix}$ and $\begin{pmatrix} 2 \cdot T_{avg} - T_{cold} \\ k_{E,\theta}(T_{cold}) \end{pmatrix}$ in a drawing displaying the EN 1993-1-2 [EN 1993-1-2, 2005] reduction curve. The intersection of the drawn line and the reduction curve shows the temperature and the reduction factor to be used. The use of method f is illustrated in Figure 5.4.

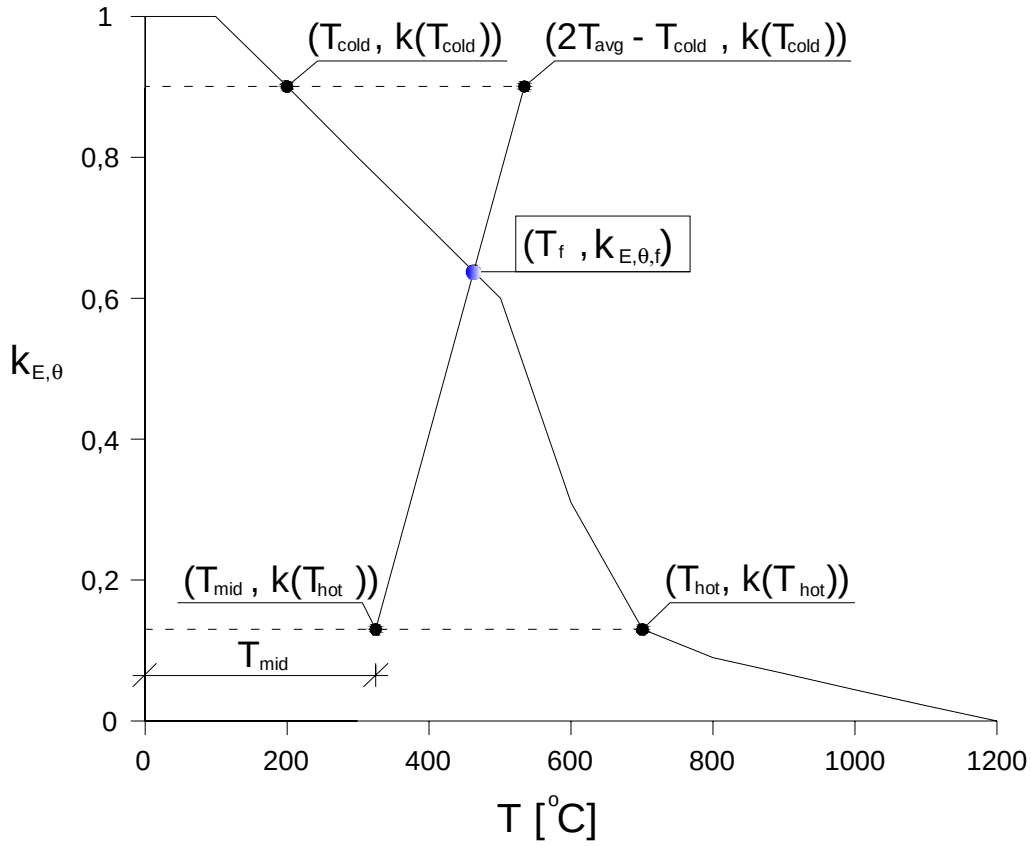

Figure 5.4. Method f [Salminen et al, 2009].

If the drawn line is vertical, this method yields the same result as method a, but here the slope of the line depends on temperature distribution.

Figure 5.5 shows five different temperature distributions. In all of them T_{cold} is 200 °C and T_{hot} is 700 °C. The location and the slope of the line depend on temperature distribution as illustrated in Figure 5.6.

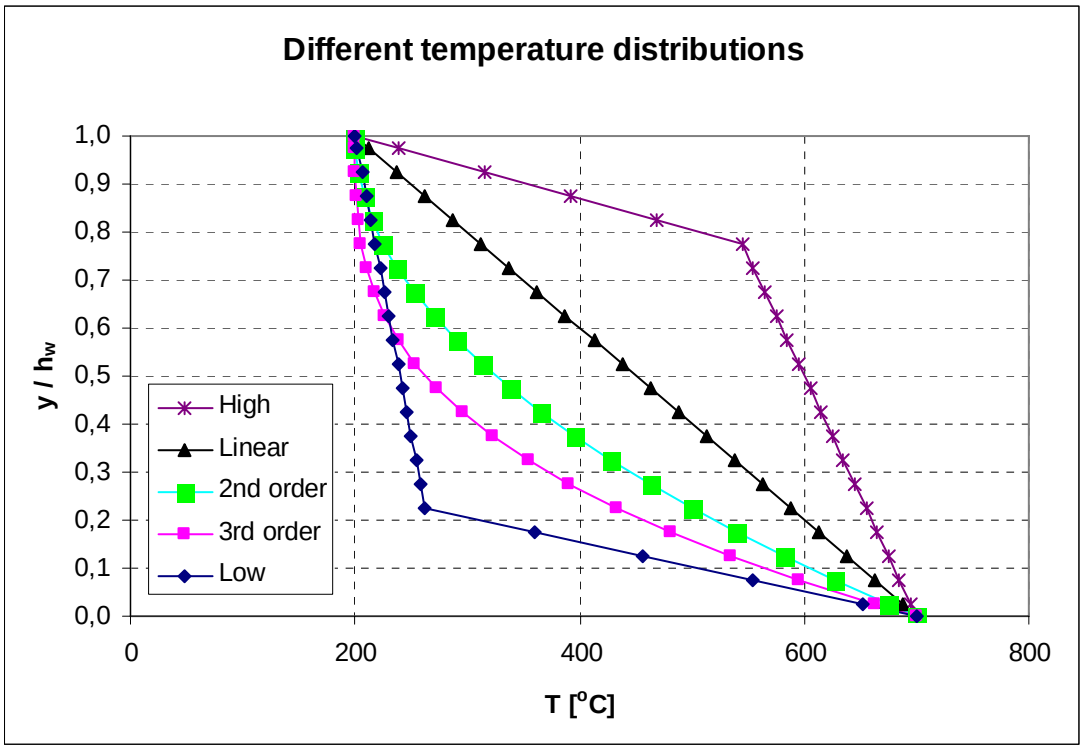

Figure 5.5. Different temperature distributions.

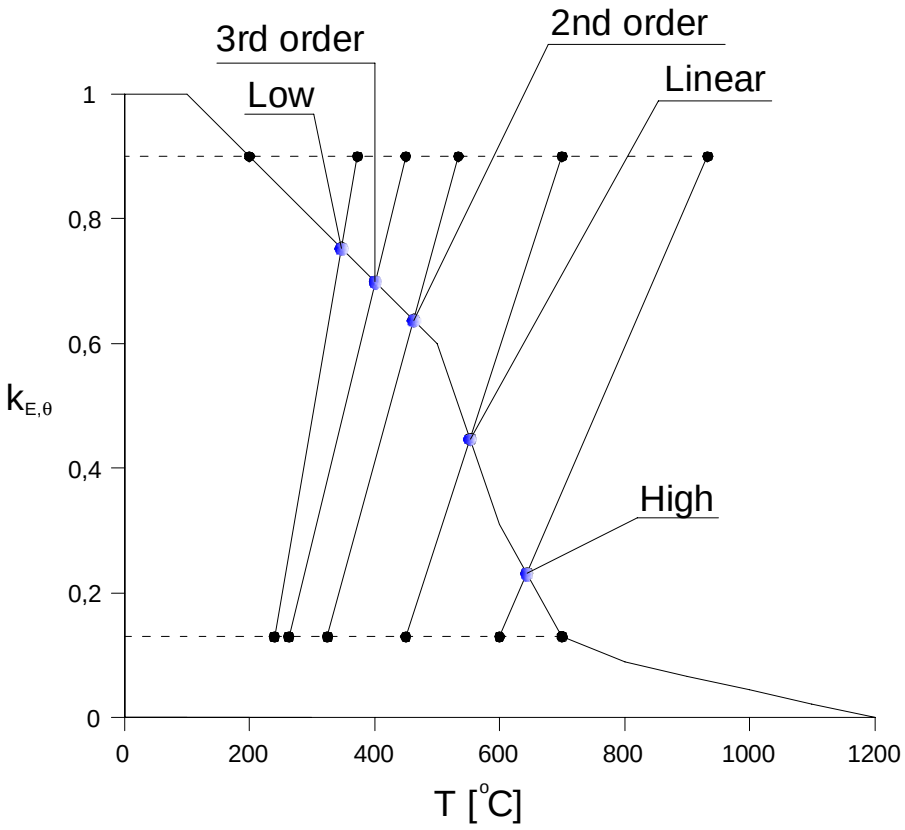

Figure 5.6. Effect of temperature distribution in method f.

Method f can also be presented analytically as a formula by calculating the intersections of the elastic modulus reduction-factor curve and the line shown in Figure 5.4. Since the reduction-factor curve is defined in parts, an iterative process is needed, which may consist of a few steps. However, the method is easy to apply, for example, in spreadsheet computation. Figure 5.7 shows an analytical solution to the calculation of temperature T_f, which can be used for the whole plate. A reduction factor $k_{E,\theta,f}$ for elastic modulus can then be chosen based on the calculated temperature T_f. Temperature is calculated instead of the reduction factor because it may be possible to use the same temperature to reduce yield strength when studying tension field resistance in the future.

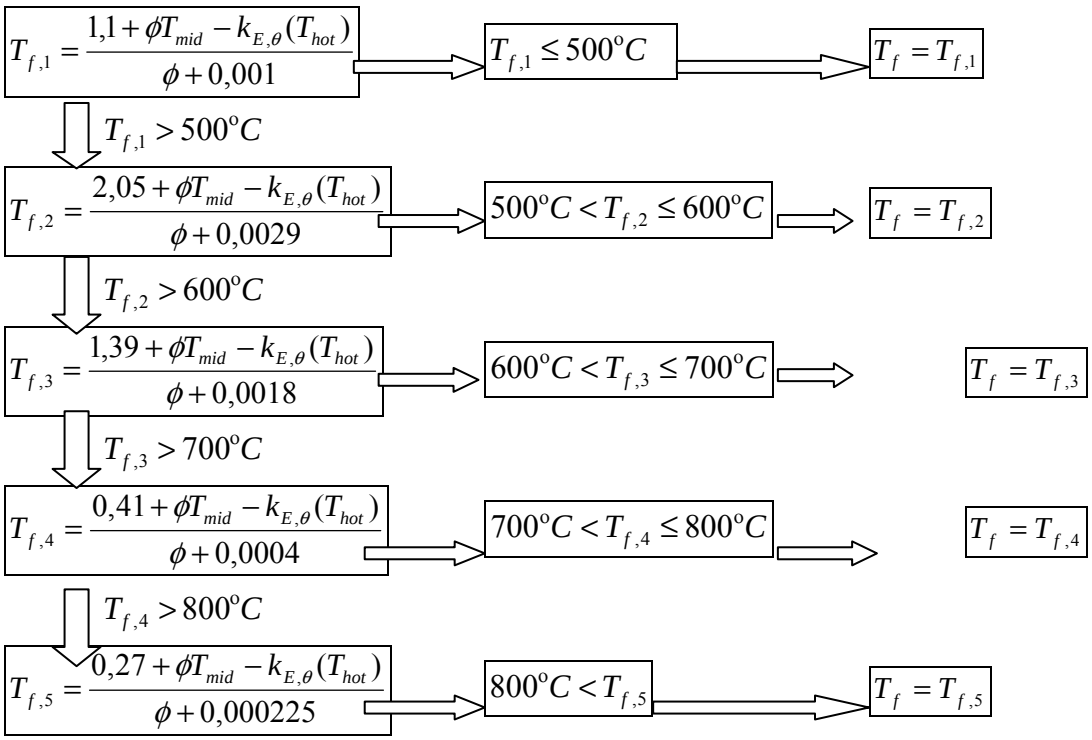

where $\phi = \dfrac{\Delta k_{E,\theta}}{2T_{avg} - T_{cold} - T_{mid}}$,

$\Delta k_{E,\theta} = k_{E,\theta}(T_{cold}) - k_{E,\theta}(T_{hot})$,

$k_{E,\theta}(T_{cold})$ and $k_{E,\theta}(T_{hot})$ are reduction factors according to EN 1993-1-2 [EN 1993-1-2, 2005],

T_{hot}, T_{cold}, T_{mid} and T_{avg} are shown in Figure 5.3.

Figure 5.7. Analytical presentation of method f.

6. COMPARISON OF RESULTS FROM METHODS A–F AND FEM CALCULATIONS

The results from methods a-f were compared to those of FEM calculations with 18 different temperature distributions (9 linear and 9 third order polynomial). This chapter presents and compares the results from FEM calculations ($V_{cr,elevated}/V_{cr,ambient}$) and the reduction factors calculated according to each method.

In the case of carbon steel, FEM calculations were performed six times for each temperature distribution (three different lengths and two thicknesses of the plate). The minimum value for the reduction factor was used. In each case the square plate yielded the minimum value. For aluminium and stainless steel only the 1000 x 1000 x 10 mm^3 plate was considered.

6.1. Carbon steel

Calculation of the reduction factors for the linear temperature distribution 100–900 ^oC (4th distribution in Table 6.1) by each presented method (Chapter 5) is shown below:

FEM: $k_{E,\theta,FEM,min} = 0,287$ (see Table 4.4)

Values needed in the calculations:

$T_{cold} = 100\ ^oC$, $T_{mid} = 500\ ^oC$, $T_{avg} = 500\ ^oC$ and $T_{hot} = 900\ ^oC$

$k_{E,\theta}(100\ ^oC) = 1,000$; $k_{E,\theta}(300\ ^oC) = 0,800$; $k_{E,\theta}(500\ ^oC) = 0,600$ and

$k_{E,\theta}(900\ ^oC) = 0,0675$

Method a: $k_{E,\theta,a} = k_{E,\theta}(T_{mid}) = \underline{0,600}$

Method b: $$k_{E,\theta,b} = \frac{k_{E,\theta}(T_{cold}) + k_{E,\theta}(T_{mid}) + k_{E,\theta}(T_{hot})}{3} = \frac{1 + 0,6 + 0,0675}{3} = \underline{0,556}$$

Method c: $$k_{E,\theta,c} = \frac{k_{E,\theta}(T_{cold}) + 1,1 \cdot k_{E,\theta}(T_{mid}) + 1,2 \cdot k_{E,\theta}(T_{hot})}{3,3}$$

$$k_{E,\theta,c} = \frac{1 + 1,1 \cdot 0,6 + 1,2 \cdot 0,0675}{3,3} = \underline{0,528}$$

Method d: $k_{E,\theta,d} = \sqrt[3]{k_{E,\theta}(T_{cold}) \cdot k_{E,\theta}(T_{mid}) \cdot k_{E,\theta}(T_{hot})} = \sqrt[3]{1 \cdot 0{,}6 \cdot 0{,}0675} = \underline{0{,}343}$

In method e, also the height of the plate is reduced and the temperature $T_{mid,eff}$ is taken from the middle of the effective height as shown in Figure 6.1 (see also Chapter 5.2).

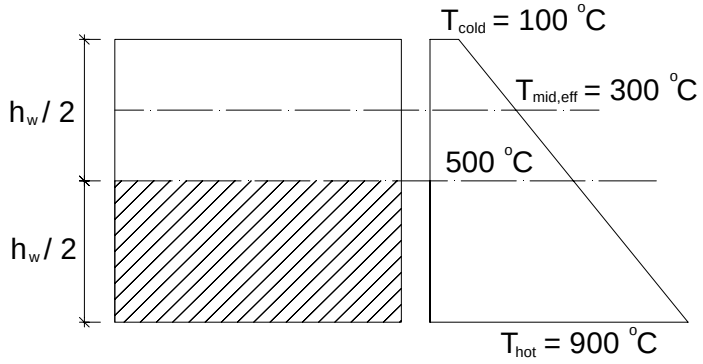

Figure 6.1. Method e and linear temperature distribution 100–900 °C.

Method e: $k_{E,\theta,e} = \frac{h_{w,eff}}{h_w} \cdot k_{E,\theta}(T_{mid,eff}) = 0{,}5 \cdot 0{,}8 = \underline{0{,}400}$

In method f, the reduction factor is defined graphically as shown in Figure 6.2. See also Chapter 5.3 for further details.

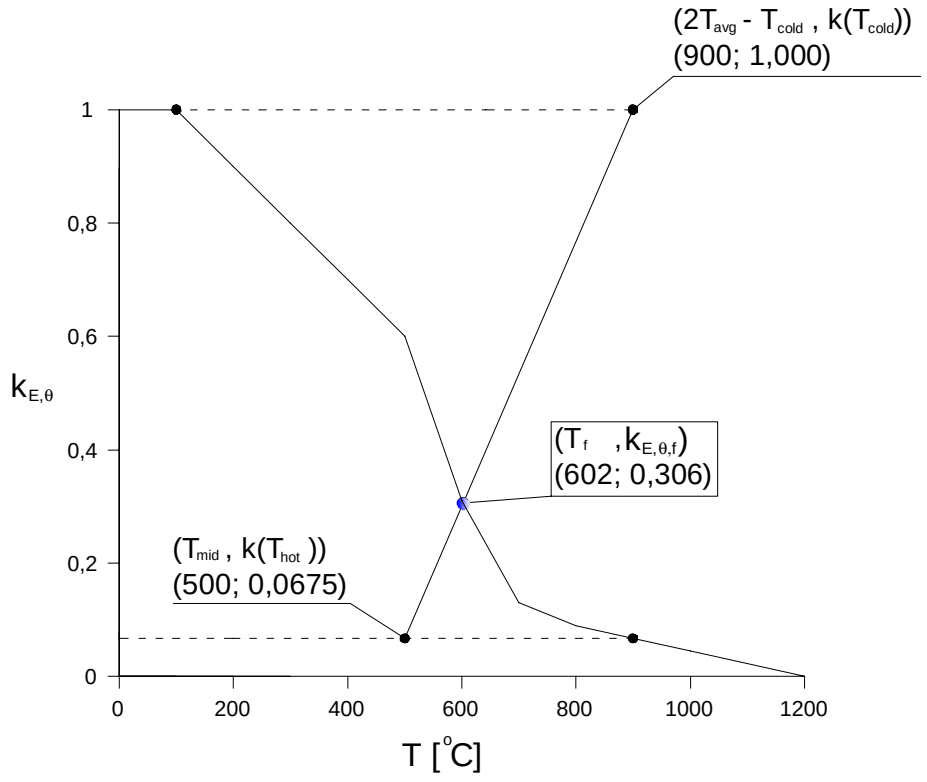

Figure 6.2. Method f and linear temperature distribution 100–900 °C.

All calculated reduction factors for carbon steel are shown in Table 6.1. The last column shows the reduction factor calculated using the reduction of design strength $k_{0.2p,\theta}$ (see Fig. 3.1) and the average temperature of the plate (EN 1993-1-2 [EN 1993-1-2, 2005] method, Eq. (3.2)). It should be noted that the reduction factor $k_{0.2p,\theta}$ is used to calculate ultimate shear resistance (not shear buckling resistance) for class 4 steel sections. The use of this method is justified, because the three components of the ultimate shear resistance of thin plate (Fig. 1.2) are not considered separately in EN 1993-1-2 [EN 1993-1-2, 2005], but reduced using one reduction factor ($k_{0.2p,\theta}$). In other words, also shear buckling resistance is reduced using factor $k_{0.2p,\theta}$. However, the comparison to methods a-f is complicated in this case.

All results more than 10 % on the unsafe side compared to FEM results are marked with shading while all results more than 20 % on the safe side compared to FEM results are surrounded by a thick line. Method e does not produce a result for the distribution where $T_{cold} > 500$ °C even though the reduction factor may in some cases be even close to 0,35 according to FEM results.

Table 6.1. Comparison of results of methods and FEM calculations (carbon steel).

> 10 % unsafe **> 20 % safe**	Reduction factor $k_{E,\theta}$							
	Method							
Temperature distribution	FEM_{min}	a	b	c	d	e	f	EN
1. 100-300 °C linear	0,897	0,900	0,900	0,894	0,896	0,900	0,867	0,890
2. 100-500 °C linear	0,788	0,800	0,800	0,788	0,783	0,800	0,733	0,780
3. 100-700 °C linear	0,567	**0,700**	0,610	0,584	**0,450**	0,533	0,510	**0,650**
4. 100-900 °C linear	0,287	**0,600**	**0,556**	**0,528**	**0,343**	**0,400**	0,306	**0,530**
5. 200-500 °C linear	0,743	0,750	0,751	0,741	0,740	0,750	0,700	0,715
6. 300-600 °C linear	0,605	0,650	0,587	0,572	0,544	**0,467**	0,540	0,590
7. 400-700 °C linear	0,376	**0,455**	**0,428**	0,411	0,346	**0,217**	0,314	0,415
8. 500-800 °C linear	0,193	**0,220**	**0,303**	**0,288**	**0,228**	-	0,175	0,215
9. 600-900 °C linear	0,114	0,110	**0,163**	**0,155**	**0,132**	-	0,102	0,100
10. 100-300 °C non-linear	0,953	0,975	0,925	0,919	0,921	0,975	0,927	0,945
11. 100-500 °C non-linear	0,901	0,950	0,850	0,838	0,829	0,950	0,855	0,890
12. 100-700 °C non-linear	0,809	**0,923**	0,684	**0,658**	**0,493**	0,829	0,761	0,835
13. 100-900 °C non-linear	0,638	**0,899**	0,656	0,691	**0,394**	0,753	0,697	**0,780**
14. 200-500 °C non-linear	0,827	0,862	0,787	0,778	0,775	0,862	0,791	0,808
15. 300-600 °C non-linear	0,715	0,762	0,624	0,609	**0,574**	0,677	0,678	0,683
16. 400-700 °C non-linear	0,561	**0,662**	0,497	0,480	**0,392**	0,476	0,544	0,560
17. 500-800 °C non-linear	0,351	**0,490**	**0,393**	0,378	0,298	-	0,334	0,358
18. 600-900 °C non-linear	0,182	**0,242**	**0,207**	0,199	0,172	-	0,163	0,173

Table 6.1 shows that when the hottest temperature of the plate is not more than 500 °C, all methods give good results, but when the hottest temperature of the plate exceeds 500 °C, only method f gives reliable results compared to FEM calculations. Results shown in Table 6.1 are also presented in Figures 6.3-6.6.

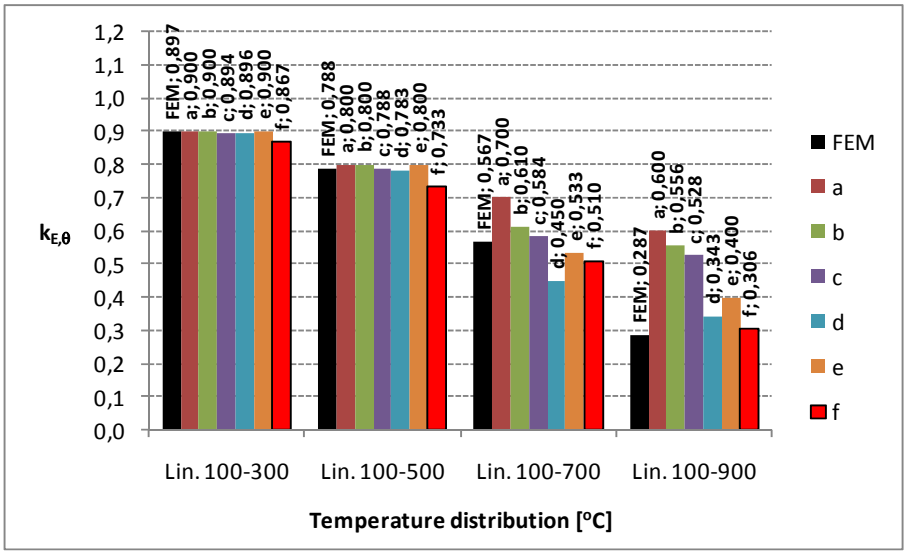

Figure 6.3. Comparison of methods and FEM calculations (carbon steel, temperature distributions 1-4).

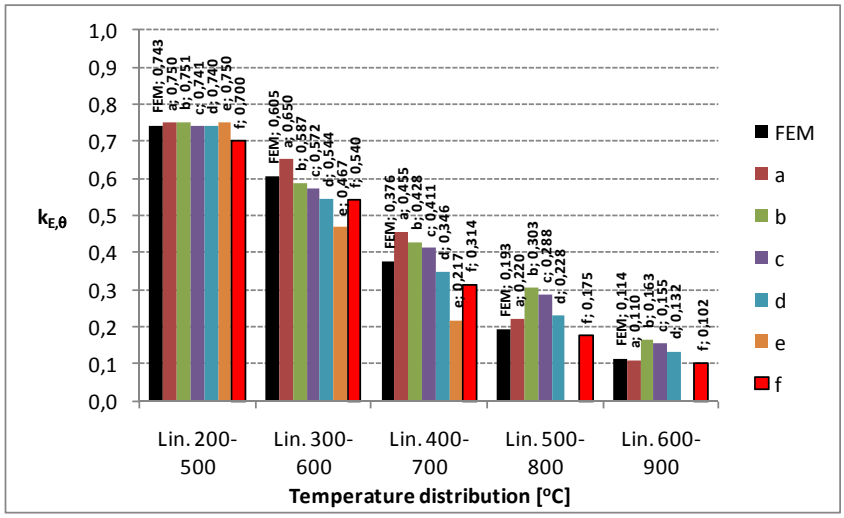

Figure 6.4. Comparison of methods and FEM calculations (carbon steel, temperature distributions 5-9).

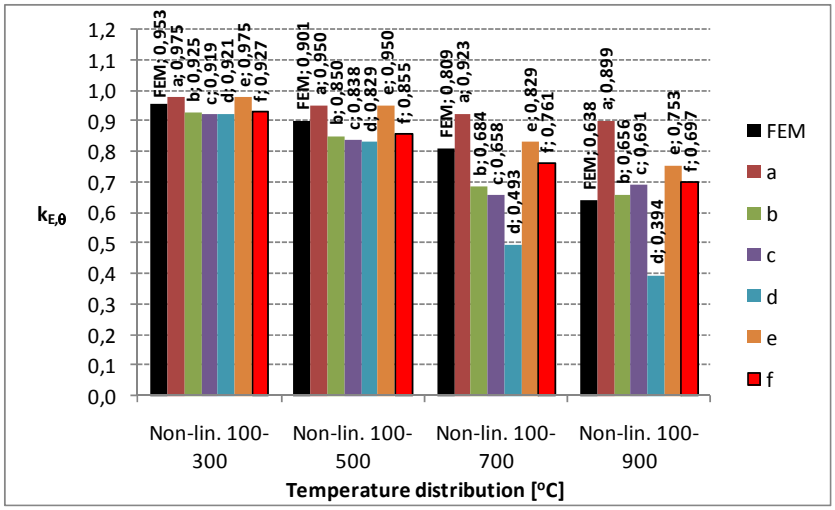

Figure 6.5. Comparison of methods and FEM calculations (carbon steel, temperature distributions 10-13).

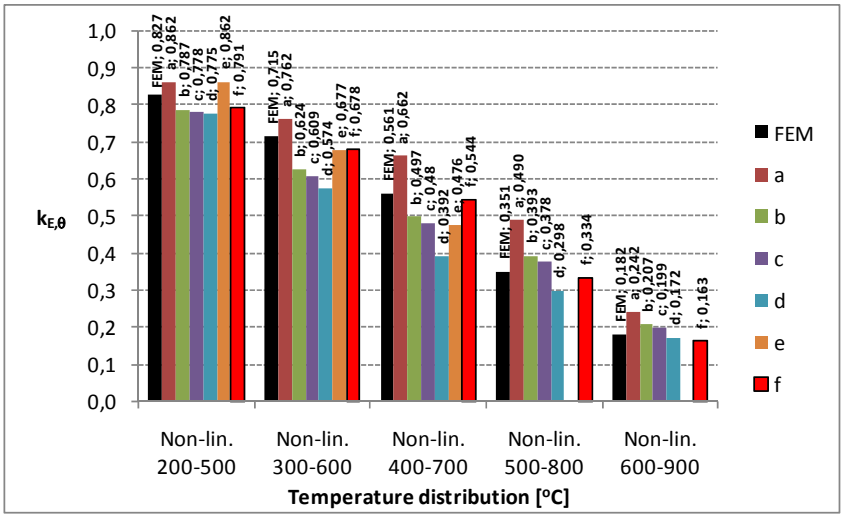

Figure 6.6. Comparison of methods and FEM calculations (carbon steel, temperature distributions 14-18).

Based on Figures 6.3-6.6 it can be concluded that there is more scattering in the results when the temperature difference between the edges of the plate or the hottest temperature increases. Method a gives poor results in almost all of the cases. Especially when the hottest temperature of the plate (T_{hot}) is more than 500 °C the results are clearly on the unsafe side. Methods b and c give mostly conservative results compared to FEM when $T_{hot} \leq 600$ °C. All results of method d are on the safe side (in some case over 60 %) when $T_{hot} \leq 700$ °C. Method e gives slightly unconservative or conservative results when $T_{hot} \leq 700$ °C. All results from method f are relatively close to those from FEM calculations.

Figure 6.7 gives the minimum, average and maximum values and standard deviation of the ratio $k_{E,\theta,FEM} / k_{E,\theta,method}$ for each presented method. If the ratio is more than 1, the

result from the method is conservative compared to the FEM result. Table 6.2 shows the ranges of ratio for each method.

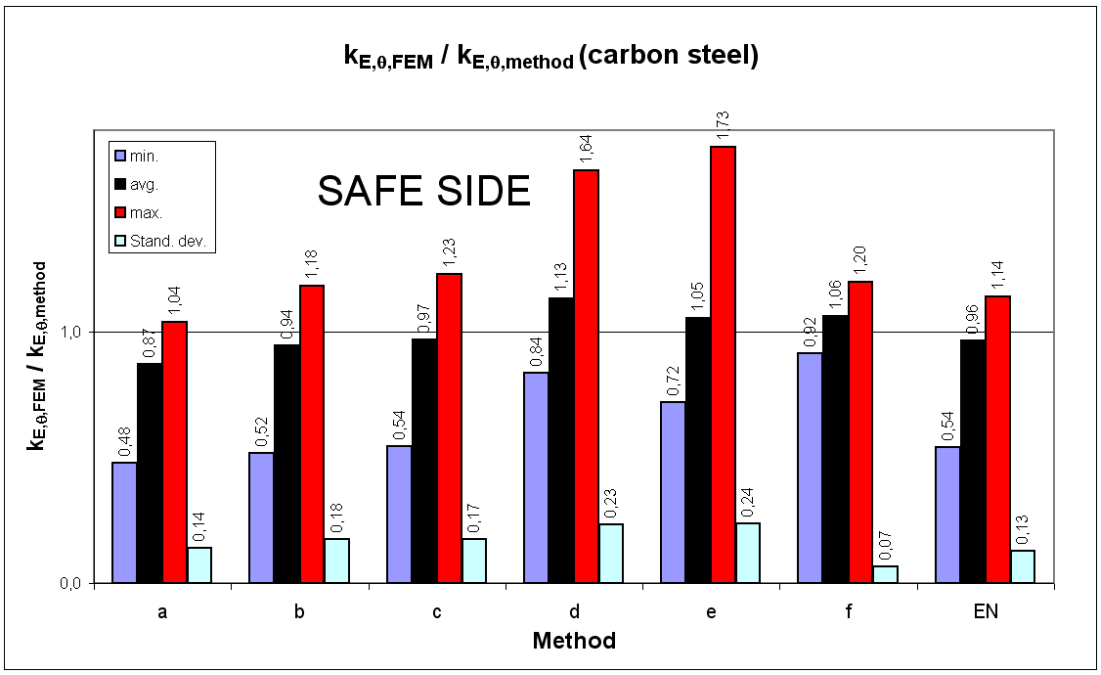

Figure 6.7. Comparison of the methods (carbon steel).

Table 6.2. Ranges of the ratio $k_{E,\theta,FEM}$ / $k_{E,\theta,method}$.

Method	0,95 - 1,10	0,90 – 0,95 or 1,10 -1,20	> 1,20	< 0,90	< 0,80
a	7	2		5	4
b	8	4		3	3
c	8	6	1		3
d	8	2	5	3	
e	9	1	2	1	1
f	12	6			
EN	12	3		2	1

Figures 6.8 and 6.9 show a comparison of the results from FEM calculations and method f as well as the upper and lower limits of reduction factor $k_{E,\theta}$ for all 18 cases. At the upper limit of the reduction factor reduction is done using the coldest temperature while at the lower limit it is done using the hottest temperature of the plate. Temperature distributions are numbered similarly as in Table 6.1.

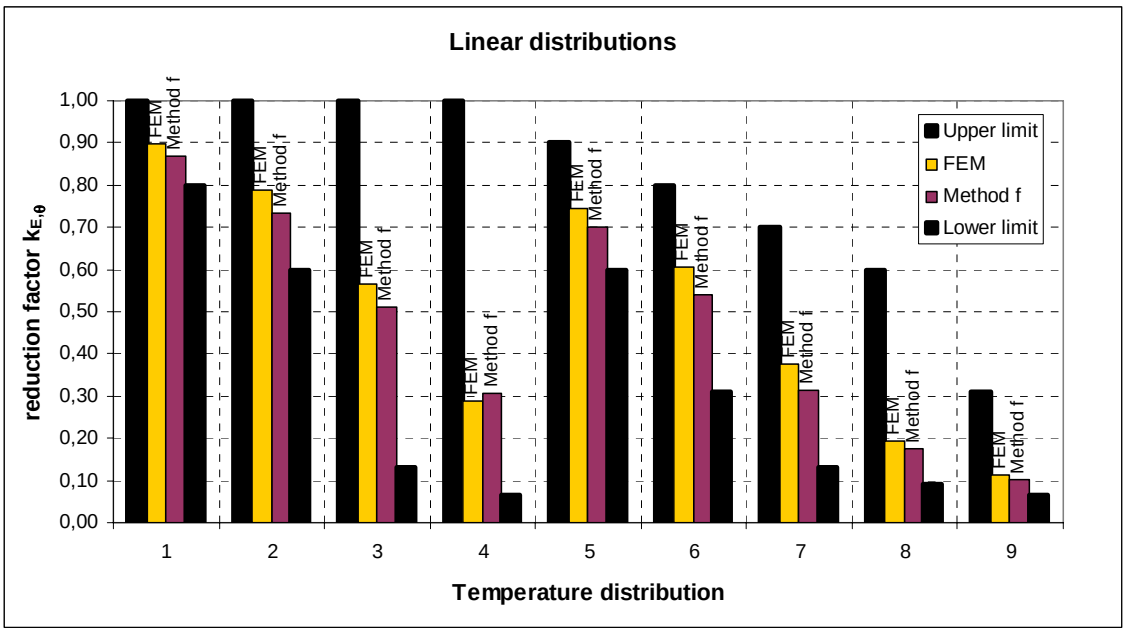

Figure 6.8. Comparison of results from method f and FEM calculations (linear distributions).

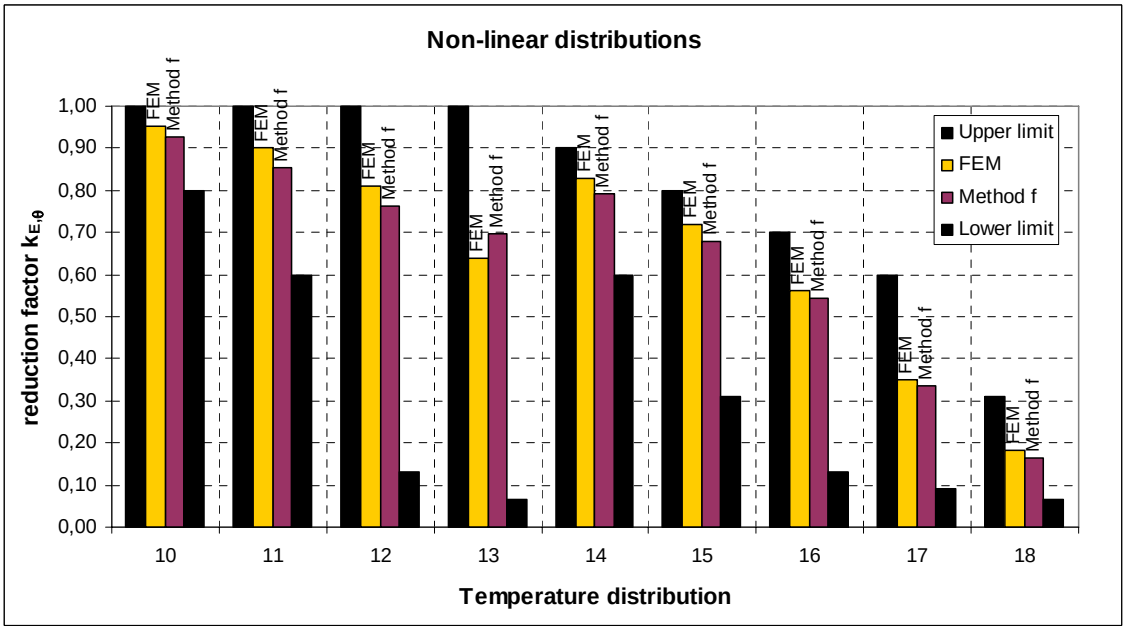

Figure 6.9. Comparison of results from method f and FEM calculations (non-linear distributions).

Based on Tables 6.1 and 6.2 and Figures 6.3-6.6 it can be said that method f gives the best results for carbon steel compared to the results of FEM calculations. The accuracy of method f seems to be independent of temperature distribution and hottest temperature, unlike the other presented methods. The method presented in EN 1993-1-2 [EN 1993-1-2, 2005] (see also Eq. 3.2) was also included in the comparison, even though it is generally used for calculating ultimate shear resistance at elevated temperatures. It would seem to work well also in determining shear buckling stresses in

most of the cases considered, but in three cases the results were clearly on the unsafe side.

6.2. Aluminium and stainless steel

Methods a-d and f were considered for aluminium and stainless steel in the comparison. Method e was not included in the analysis, because the temperature, which defines the cold and hot parts of the plate, should have been changed, and the method did not give promising results for carbon steel (see Table 6.1 and Fig. 6.3-6.6).

Table 6.3 shows all the calculated reduction factors for aluminium. In the case of aluminium and stainless steel, all results more than 5 % on the unsafe side compared to FEM results are marked with shading while all results more than 10 % on the safe side compared to FEM results are surrounded by a thick line. It should be noted that the percentages are not the same as in the comparison with carbon steel. The main purpose of the marked results is to indicate those temperature distributions for which it is difficult for the methods to predict correct reduction factors.

Table 6.3. Comparison of results of the methods and FEM calculations (aluminium).

> 5 % unsafe **> 10 % safe**	Reduction factor $k_{E,\theta}$					
	Method					
Temperature distribution	FEM_{min}	a	b	c	d	f
1. 100-200 °C linear	0,932	0,930	0,920	0,917	0,919	0,903
2. 100-300 °C linear	0,853	0,860	0,837	0,828	0,828	0,796
3. 100-400 °C linear	0,731	**0,780**	0,717	0,699	0,671	**0,642**
4. 100-500 °C linear	0,544	**0,680**	**0,594**	0,569	**0,444**	**0,461**
5. 150-300 °C linear	0,820	0,820	0,810	0,802	0,803	0,774
6. 200-350 °C linear	0,721	0,720	0,710	0,700	0,697	0,667
7. 250-400 °C linear	0,595	0,610	0,597	0,585	0,575	**0,535**
8. 300-450 °C linear	0,453	**0,470**	0,472	0,460	0,440	**0,401**
9. 350-500 °C linear	0,306	**0,333**	**0,335**	0,323	0,288	**0,267**
10. 100-200 °C non-linear	0,959	0,960	0,930	0,927	0,929	0,938
11. 100-300 °C non-linear	0,927	0,950	0,867	0,858	0,856	0,889
12. 100-400 °C non-linear	0,877	**0,940**	**0,770**	**0,753**	**0,714**	0,825
13. 100-500 °C non-linear	0,797	**0,860**	**0,654**	**0,629**	**0,481**	0,757
14. 150-300 °C non-linear	0,886	0,903	0,838	0,830	0,830	0,850
15. 200-350 °C non-linear	0,803	0,830	0,743	0,734	0,728	0,765
16. 250-400 °C non-linear	0,702	0,742	0,641	**0,629**	**0,614**	0,661
17. 300-450 °C non-linear	0,574	**0,627**	0,525	**0,512**	**0,485**	0,529
18. 350-500 °C non-linear	0,427	**0,487**	0,387	**0,374**	**0,327**	0,390

Figure 6.10 shows the minimum, average and maximum values and standard deviations of the ratio $k_{E,\theta,FEM}$ / $k_{E,\theta,method}$ for aluminium.

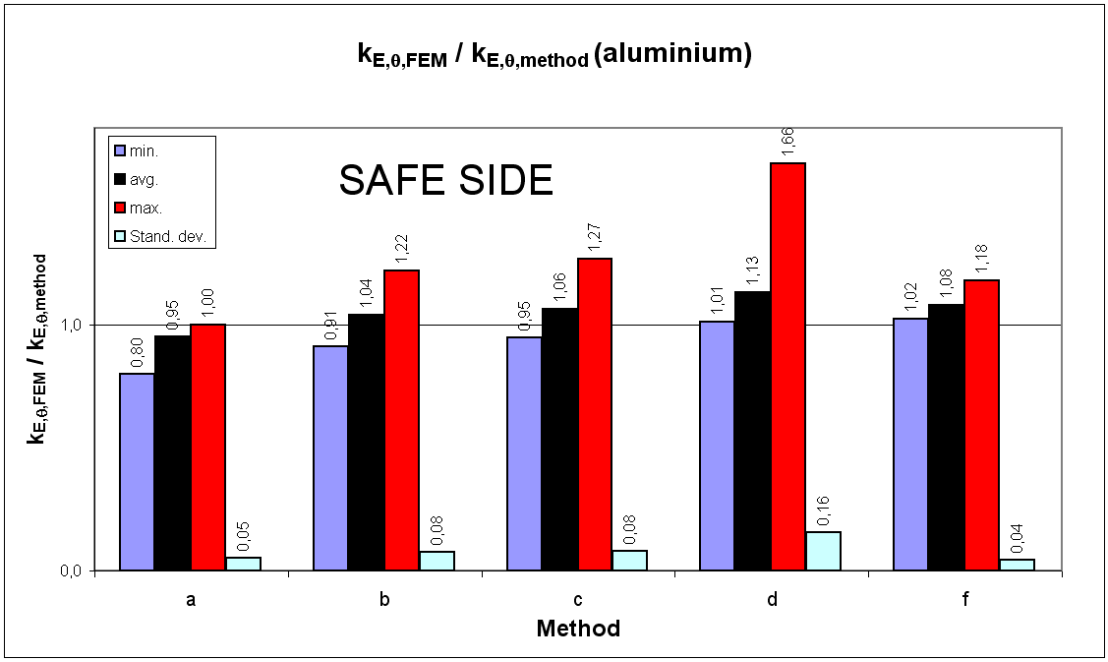

Figure 6.10. Comparison of the methods (aluminium).

The results for stainless steel are presented in Table 6.4 and in Figure 6.11.

Table 6.4. Comparison of results of the methods and FEM calculations (stainless steel).

> 5 % unsafe **> 10 % safe**	Method					
	Reduction factor $k_{E,\theta}$					
Temperature distribution	FEM_{min}	a	b	c	d	f
1. 100-400 °C linear	0,899	0,900	0,900	0,896	0,899	0,880
2. 100-600 °C linear	0,857	0,860	0,860	0,854	0,856	0,827
3. 100-800 °C linear	0,810	0,820	0,803	0,793	0,792	0,763
4. 100-1000 °C linear	0,708	**0,780**	**0,647**	**0,624**	**0,531**	**0,626**
5. 200-600 °C linear	0,838	0,840	0,840	0,835	0,837	0,813
6. 300-700 °C linear	0,797	0,800	0,797	0,792	0,794	0,771
7. 400-800 °C linear	0,750	0,760	0,743	0,737	0,738	0,718
8. 500-900 °C linear	0,678	0,710	0,653	0,643	0,635	0,627
9. 600-1000 °C linear	0,539	**0,630**	0,530	0,513	0,458	**0,462**
10. 100-400 °C non-linear	0,933	0,945	0,915	0,911	0,913	0,916
11. 100-600 °C non-linear	0,913	0,935	0,885	0,879	0,880	0,887
12. 100-800 °C non-linear	0,892	0,925	0,838	0,828	0,824	0,854
13. 100-1000 °C non-linear	0,854	**0,915**	**0,692**	**0,669**	**0,560**	0,807
14. 200-600 °C non-linear	0,883	0,900	0,860	0,855	0,857	0,862
15. 300-700 °C non-linear	0,843	0,860	0,817	0,812	0,813	0,821
16. 400-800 °C non-linear	0,800	0,820	0,763	0,757	0,757	0,778
17. 500-900 °C non-linear	0,750	0,780	**0,677**	**0,666**	**0,655**	0,726
18. 600-1000 °C non-linear	0,674	**0,735**	**0,565**	**0,548**	**0,482**	0,653

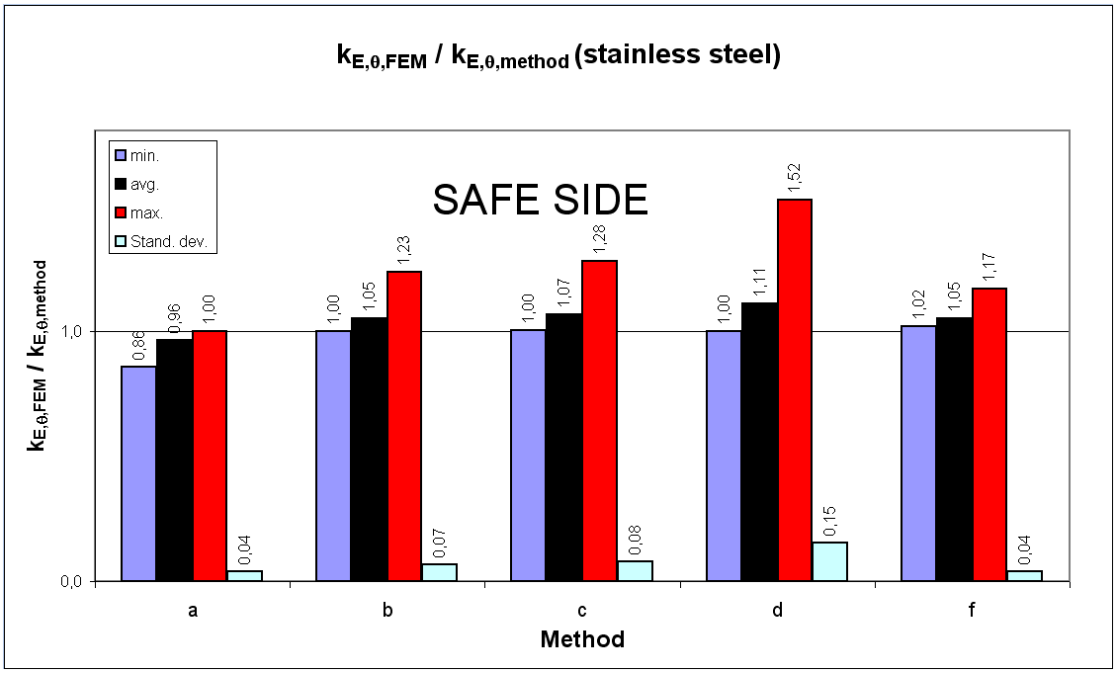

Figure 6.11. Comparison of the methods (stainless steel).

Method f seems to give reliable results also for plates made of aluminium and stainless steel. It should be noted that the temperature distributions were different for all materials considered. Therefore, Figures 6.7, 6.10 and 6.11 cannot be compared directly to each other, and they cannot be used to determine whether one method is better suited for some material than another.

6.3. Summary of the results

Figures 6.12–6.16 show all the calculated $k_{E,\theta,FEM}$ / $k_{E,\theta,method}$ values for methods a-d and f. Results are presented as a function of the hottest temperature of the plate T_{hot}.

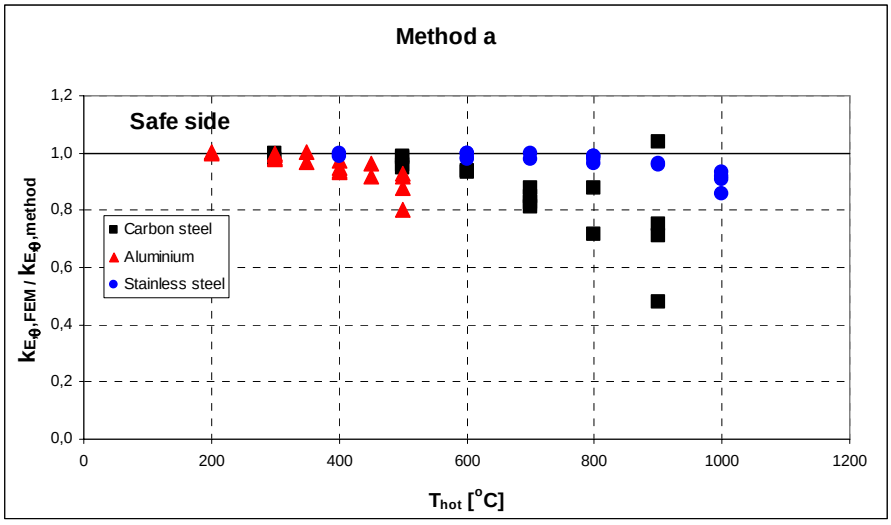

Figure 6.12. Method a (all results).

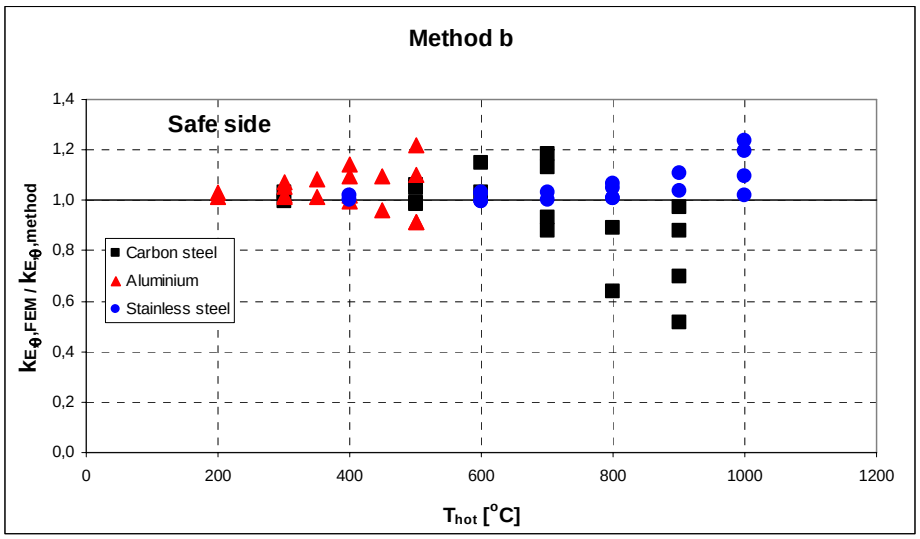

Figure 6.13. Method b (all results).

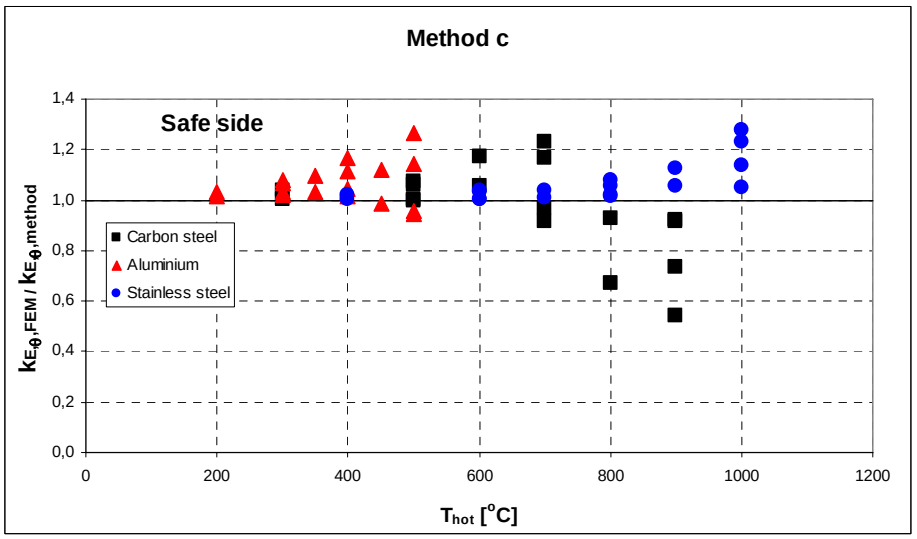

Figure 6.14. Method c (all results).

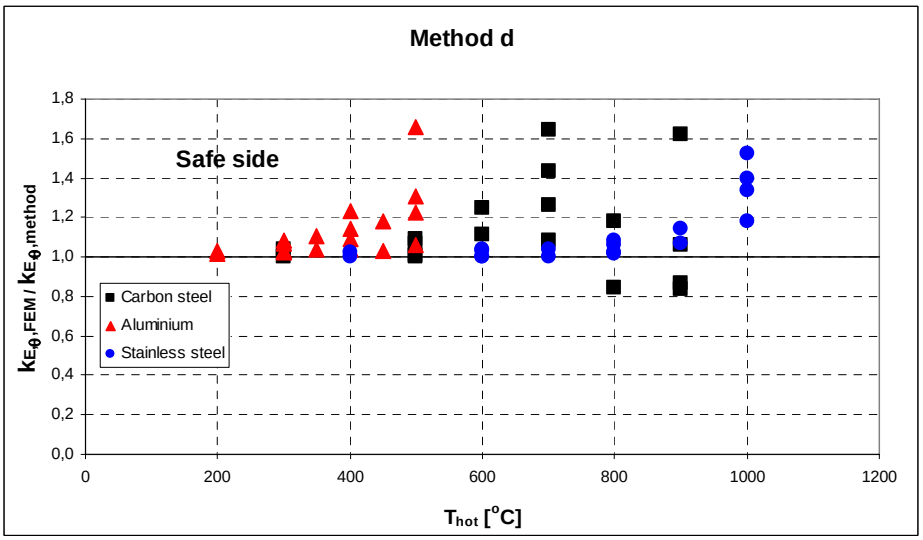

Figure 6.15. Method d (all results).

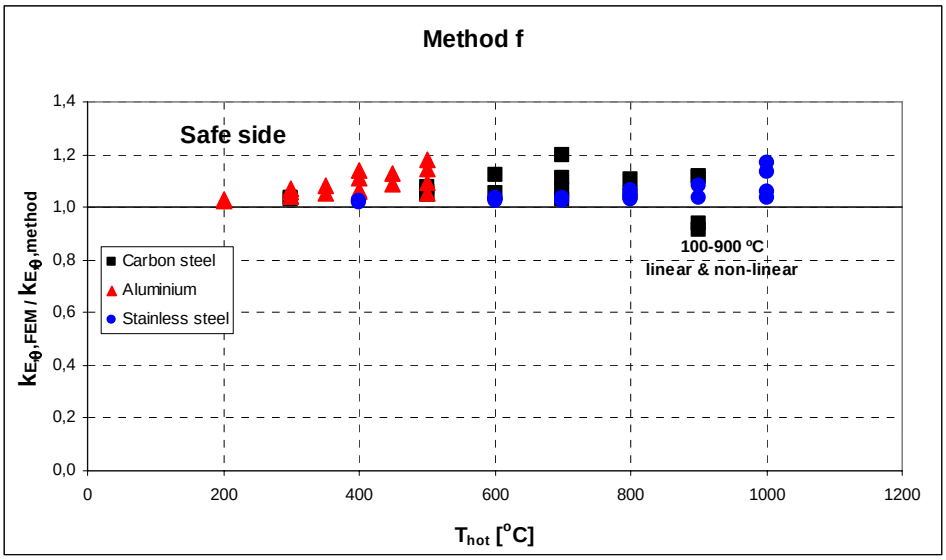

Figure 6.16. Method f (all results).

Figures 6.12–6.16 reveal that method a yields unconservative results in almost every case. It is very unreliable especially for carbon steel when $T_{hot} \geq 800$ °C. Results of methods b and c are mostly on the safe side as to aluminium and stainless steel, but for carbon steel they are not reliable. Almost all results of method d and f are on the safe side, but with method f the $k_{E,\theta,FEM}$ / $k_{E,\theta,method}$ values are all in the 0,92–1,20 range. Deviation between the results of method d is much larger.

Based on Figures 6.3–6.16 and Tables 6.1–6.4, it can be concluded that method f seems to offer a reliable way of predicting the shear buckling load at non-uniform elevated temperatures for carbon steel, aluminium and stainless steel plates. Only two results out of 54 were on the unsafe side compared to FEM calculations. These unsafe cases were the linear and non-linear 100-900 °C temperature distributions for carbon steel. In these cases the $k_{E,\theta,FEM}$ / $k_{E,\theta,method}$ ratio was 0,94 for linear distribution and 0,92 for non-linear distribution. Based on Table 6.1, it can be said that these distributions for carbon steel were difficult for most of the methods. Especially in the case of the linear 100-900 °C distribution for carbon steel, all other proposed methods yielded clearly more unsafe result.

Based on the comparisons and discussions of this chapter, method f was chosen for the example calculation presented in the next chapter. All other methods were eliminated.

7. EXAMPLE CASE

This chapter begins with a short introduction to general heat transfer theory. Then the temperature distributions of an all-metal sandwich panel are defined at different elevated temperatures and compared to tests results. Finally, the shear buckling resistance of the panel web at elevated temperatures is calculated using FEM and method f presented in Chapter 5.3.

This example case is based on tests done in the Fire Laboratory of Tampere University of Technology in 2006 [Heinisuo, Ylihärsilä, 2006]. Tests at elevated temperatures were conducted on three different all-metal sandwich panels. The all-metal sandwich panel tested in this example case is illustrated in Figure 7.1. The length of the specimen was 500 mm. The welds between the faces and the cores were arc spot welds done in the Fire Laboratory. The spacing of the welds was about 30 mm.

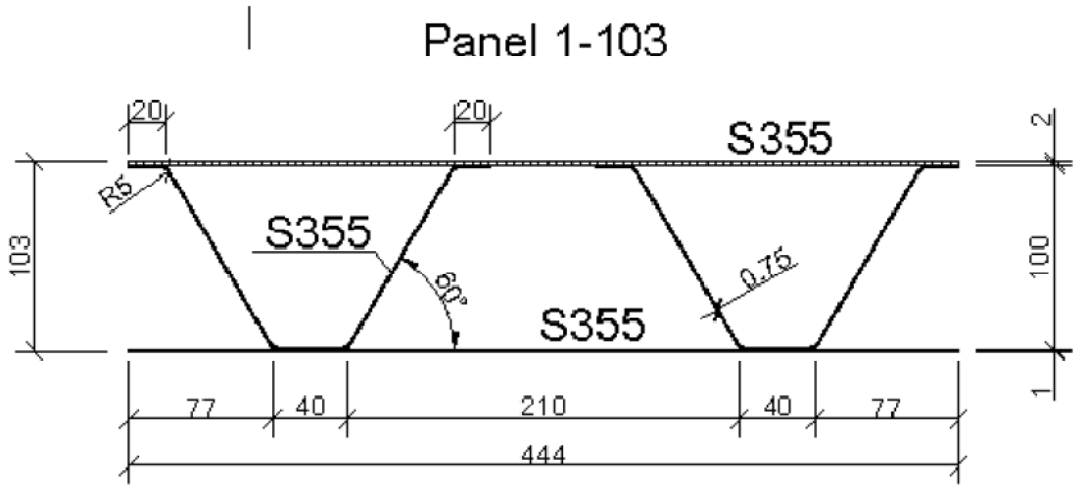

Figure 7.1. All-metal sandwich panel tested in the example case [Heinisuo, Ylihärsilä, 2006].

The all-metal sandwich panel used in this example case is the kind of structure mainly used in ships. Such a panel can resist safely (simply supported, span 4 m) a uniform live load of about 12 kN/m^2 when adhering to the safety concepts of the Eurocodes [Heinisuo, Ylihärsilä, 2006].

7.1. Temperature analysis

7.1.1. General heat transfer theory

The general equations for temperature analysis are found in all basic textbooks on heat transfer such as [Drysdale, 2004]. The following formulas are also presented in EN 1991-1-2 [EN 1991-1-2, 2002]. The net heat flux $\dot{h}_{net}$ [W/m^2] on the fire exposed surface is determined by taking into account convection and radiation as follows:

$$\dot{h}_{net} = \dot{h}_{net,c} + \dot{h}_{net,r}\,, \tag{7.1}$$

where
- $\dot{h}_{net,c}$ is the net convective heat flux component,
- $\dot{h}_{net,r}$ is the net radiative heat flux component.

The net convective heat flux component is calculated as follows:

$$\dot{h}_{net,c} = \alpha_c \cdot (T_g - T_m)\,, \tag{7.2}$$

where
- α_c is the heat transfer coefficient [W/m^{2}K],
- T_g is the gas temperature in vicinity of the fire exposed member [^{o}C],
- T_m is the surface temperature of the member [^{o}C].

Typical values for α_c lie in the 5-25 W/m^{2}K range for free convection [Drysdale, 2004]. EN 1991-1-2 [EN 1991-1-2, 2002] states that α_c = 25 W/m^{2}K, when using the standard (ISO) temperature-time curve.

The net radiative heat flux component per unit surface area is calculated as follows:

$$\dot{h}_{net,r} = \Phi \cdot \varepsilon_m \cdot \varepsilon_f \cdot \sigma \cdot \left[(T_r + 273)^4 - (T_m + 273)^4 \right] \tag{7.3}$$

where
- Φ is the configuration factor (1,0 in this study [EN 1991-1-2, 2002]),
- ε_m is the surface emissivity of the member (0,7 for carbon steel [EN 1993-1-2, 2005]),
- ε_f is the emissivity of the fire (1,0 in this study [EN 1991-1-2, 2002]),

- σ is the Stephan Boltzmann constant (= $5{,}67 \cdot 10^{-8} W/m^2K^4$),
- T_r is the effective radiation temperature of the fire environment [^{o}C],
- T_m is the surface temperature of the member [^{o}C].

In the following calculations it is assumed that the temperature in the furnace T_{test} equals T_g and T_r.

7.1.2. Tests

In the tests [Heinisuo, Ylihärsilä, 2006] the temperature in the electrical furnace was raised to 900 ^{o}C. The total duration of a test was almost four hours meaning that the temperature did not follow the ISO fire curve. The locations where temperatures were measured are shown in Figure 7.2. All temperatures were measured from the surfaces of the steel plates. The lower flange (t = 1 mm) of the all-metal sandwich panel was exposed to the elevated temperatures.

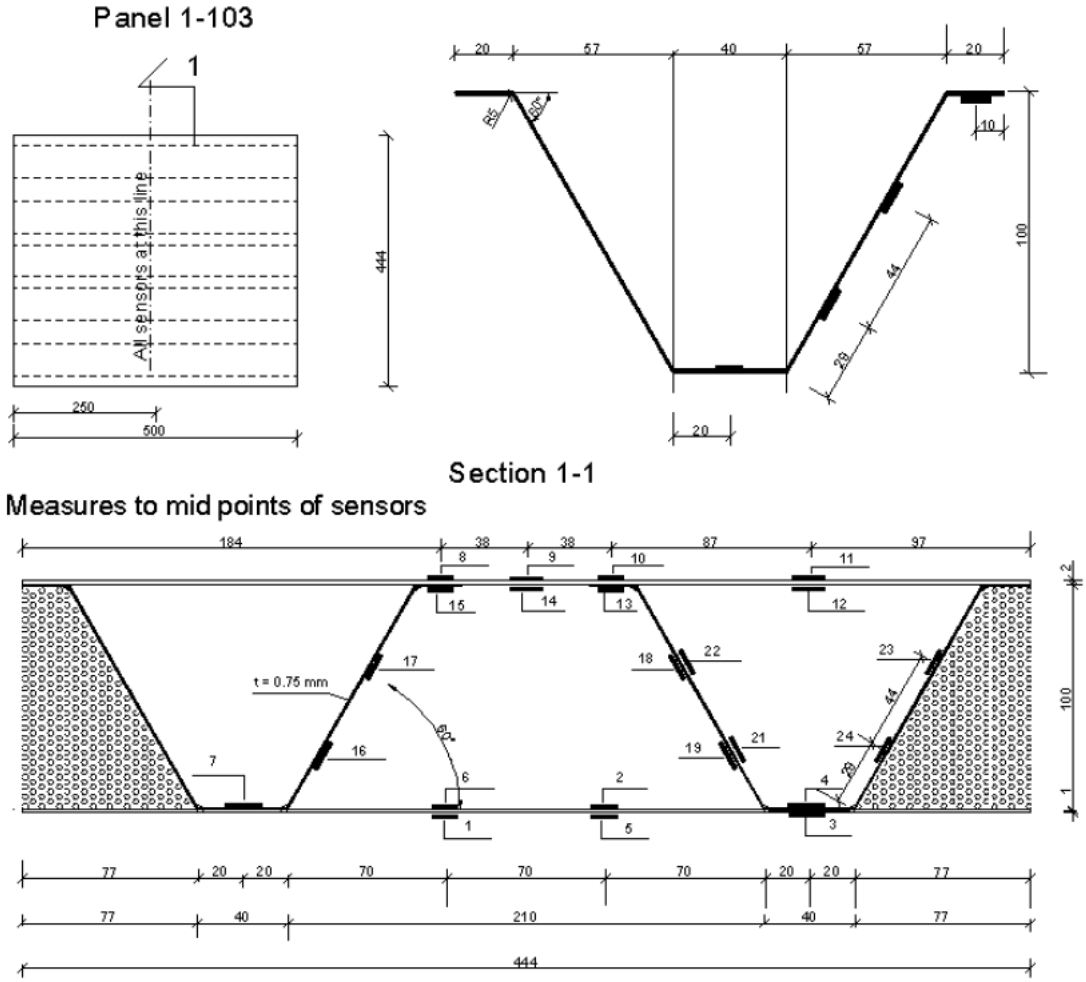

Figure 7.2. Sensors of all-metal sandwich panel [Heinisuo, Ylihärsilä, 2006].

The all-metal sandwich panel and the testing frame were attached to the furnace so as to form a door for it. The panel was insulated from the steel frame by fire resistant mineral wool. The test specimen is shown in Figure 7.3. During the test it was in the vertical position so that its height was 500 mm. The modelling of the specimen was done in 2D assuming that there was no flow in the plane of cavities.

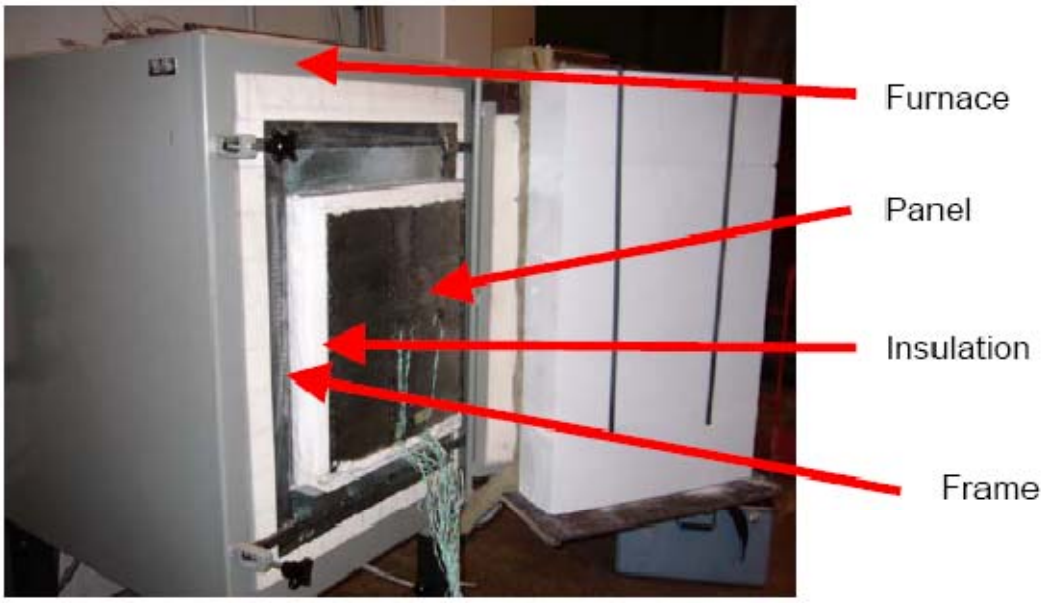

Figure 7.3. All-metal sandwich panel used in the test [Heinisuo, Ylihärsilä, 2006].

7.1.3. FEM calculations on the tested panel

Thermal FEM analyses were performed using *COMSOL Multiphysics* software [COMSOL, 2008]. The cross-section of the tested all-metal sandwich panel was modeled in 2D. The insulation in the outermost cavities and roundings of the web were taken into account. The points where two plates came into contact were considered as if continuous. The program's default triangular element type (Lagrange-T_2J_1) was used. It uses order 1 for the radiosity variable and order 2 for the temperature [COMSOL, 2008]. The mesh and boundary conditions used in the calculations are shown in Figure 7.4. The value used for the emissivity in the cavities of the tested panel was 0,7.

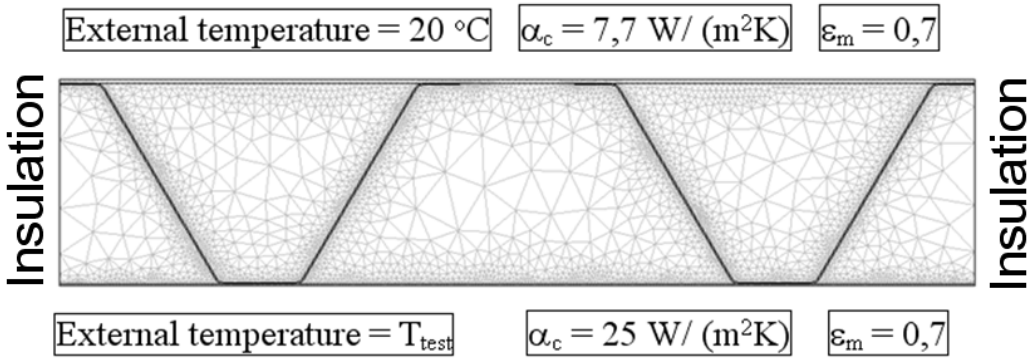

Figure 7.4. Mesh and boundary conditions of the all-metal sandwich panel.

For specific heat and thermal conductivity of carbon steel, the temperature-dependent relationships defined in EN 1993-1-2 [EN 1993-1-2, 2005] were used as shown in Figure 7.5.

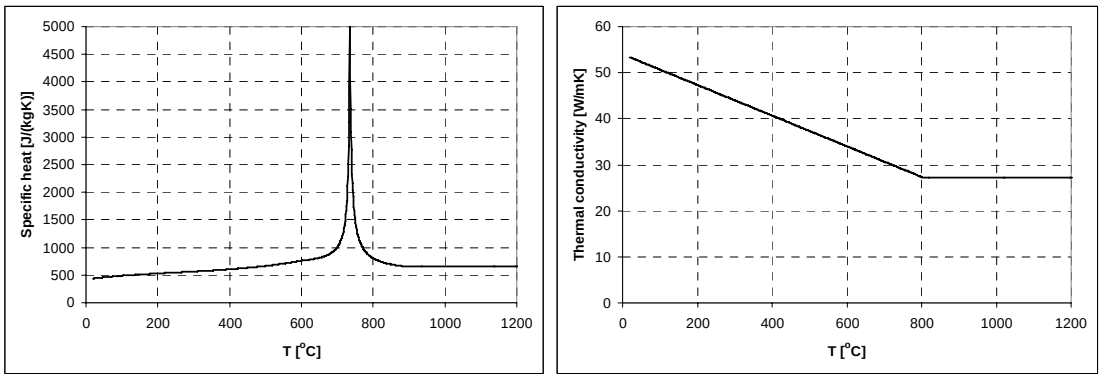

Figure 7.5. Specific heat and thermal conductivity of carbon steel as a function of temperature according to EN 1993-1-2 [EN 1993-1-2, 2005].

The values for the insulation material given by the manufacturer were the following:

- density $\rho = 128$ kg/m^3,
- specific heat $c_i = 840$ J/(kgK),
- thermal conductivity λ_i (200 °C) = 0,066 W/(mK),
- λ_i (400 °C) = 0,117 W/(mK),
- λ_i (600 °C) = 0,168 W/(mK).

The temperature-dependent values of thermal conductivity of the insulation material were inter- and extrapolated linearly between and outside the given points. The values used for λ_i are shown as a function of temperature in Figure 7.6. The sensitivity of the temperatures at points C and E (locating near the insulation) for increase of λ_i was studied by using given values multiplied by ten (0,66; 1,17 and 1,68 W/(mK)). Temperatures from this analysis are presented in Figures 7.12 and 7.14 (line FEM 2).

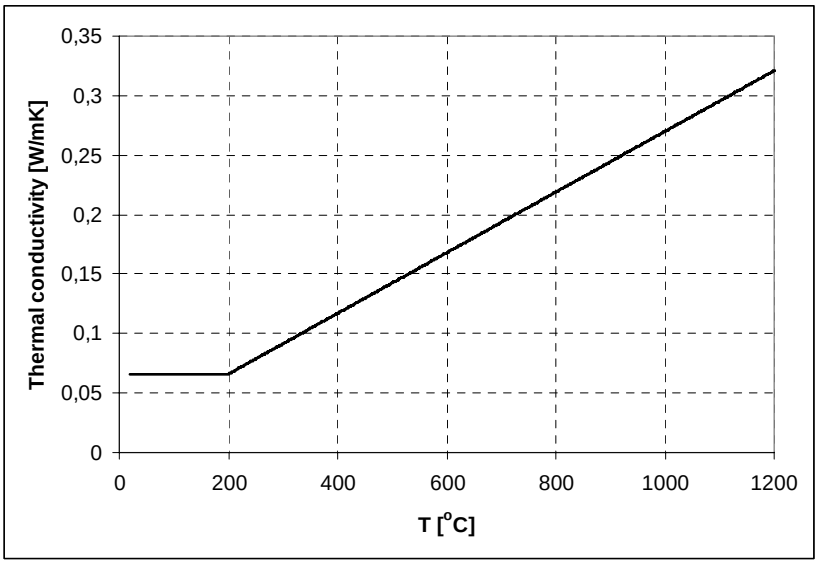

Figure 7.6. Thermal conductivity of the insulation material as a function of temperature.

All used values and temperature-dependent functions are found in Appendix B. The convective heat transfer coefficient for a vertical surface α_c = 7,7 W/(m^{2}K) for the unexposed side of the panel was taken from Finnish building regulations [RakMK C4, 2003].

Figure 7.7 shows the function for T_{test}, which is used to calculate the temperature of the exposed side as shown in Figure 7.4. The function for T_{test} is defined in four parts so that for every measured time the difference between T_{test} and the average furnace temperature is less than 3 ^{o}C. There were two sensors in the furnace measuring temperatures during the test. The biggest temperature difference these two sensors measured at the same time during 234 minutes was 23 ^{o}C [Heinisuo, Ylihärsilä, 2006].

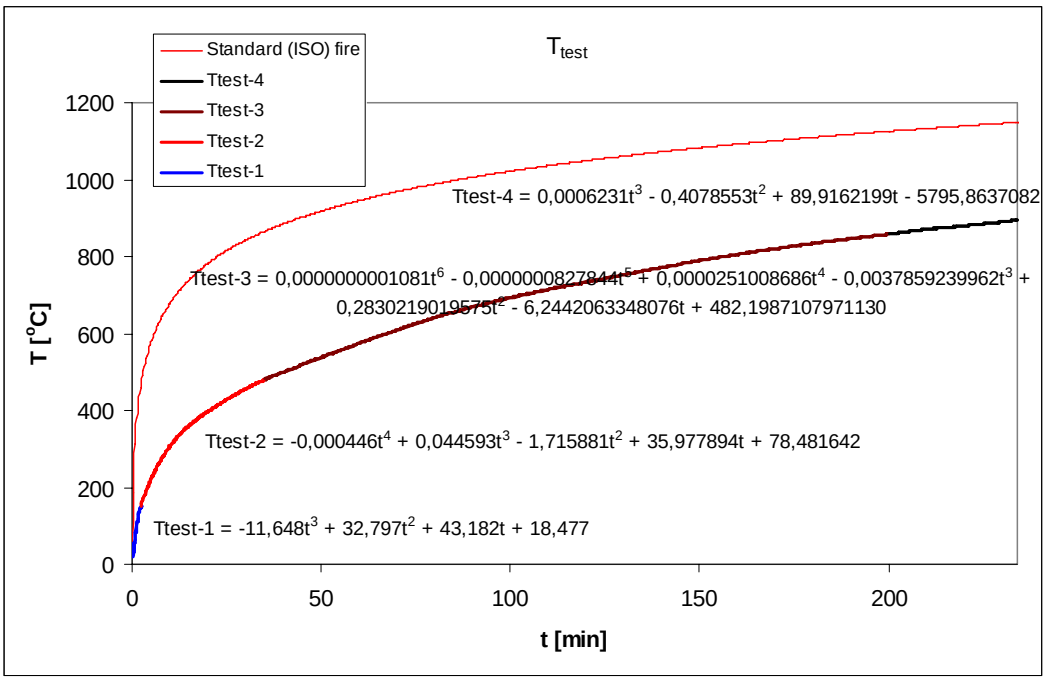

Figure 7.7. Average temperature of the furnace as a function of time t [min].

Figure 7.8 shows the calculated temperature distribution of the panel at the end of the test.

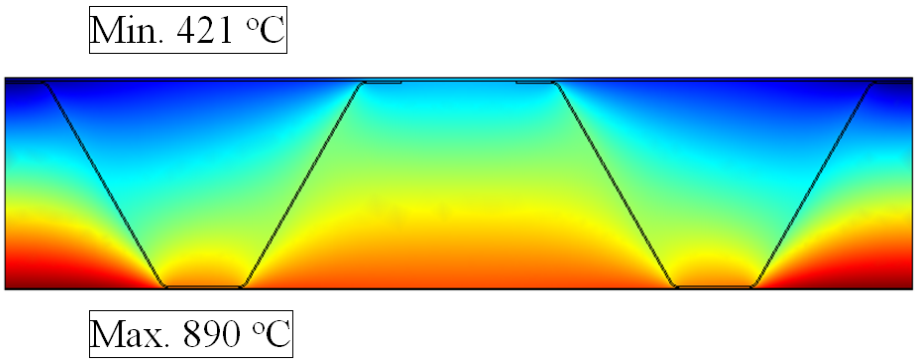

Figure 7.8. Temperature distribution of the panel after 234 minutes.

Figure 7.9 shows the points where the temperatures were calculated and to which the test results (Figure 7.2.) compared. The points considered in the FEM calculations (A-I) were in the middle of the thickness of the plate while temperatures measured in tests were from the surface of the plates. Points A and H were located in the middle of the two plate thicknesses, because the whole cross-section was modelled as if continuous.

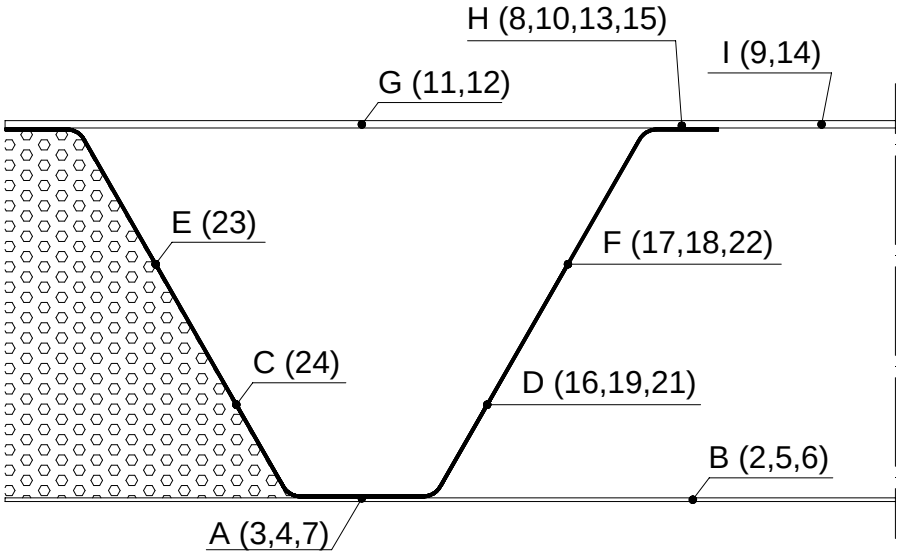

Figure 7.9. Plotted points in FEM calculation.

A complete report on the FEM calculation is shown in Appendix B. Figures 7.10–7.18 show the comparisons between the test results and the FEM calculations. Sensitivity to different ε-values (0,5 and 0,9) is considered in Figures 7.11, 7.13 and 7.18.

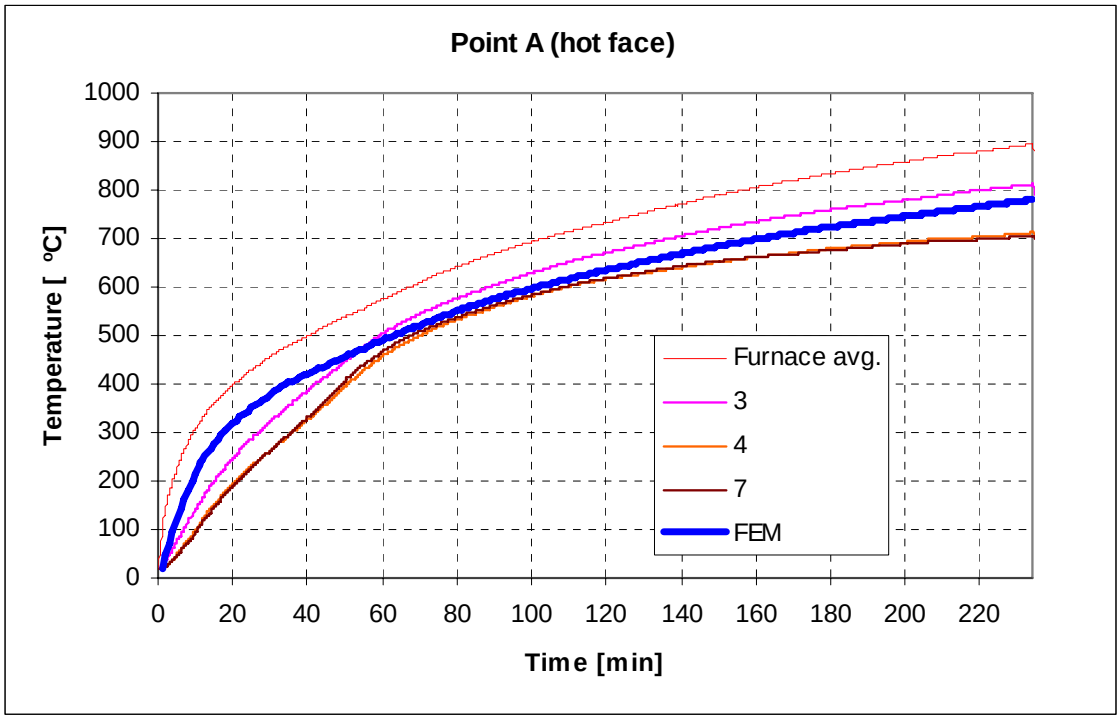

Figure 7.10. Temperatures at point A.

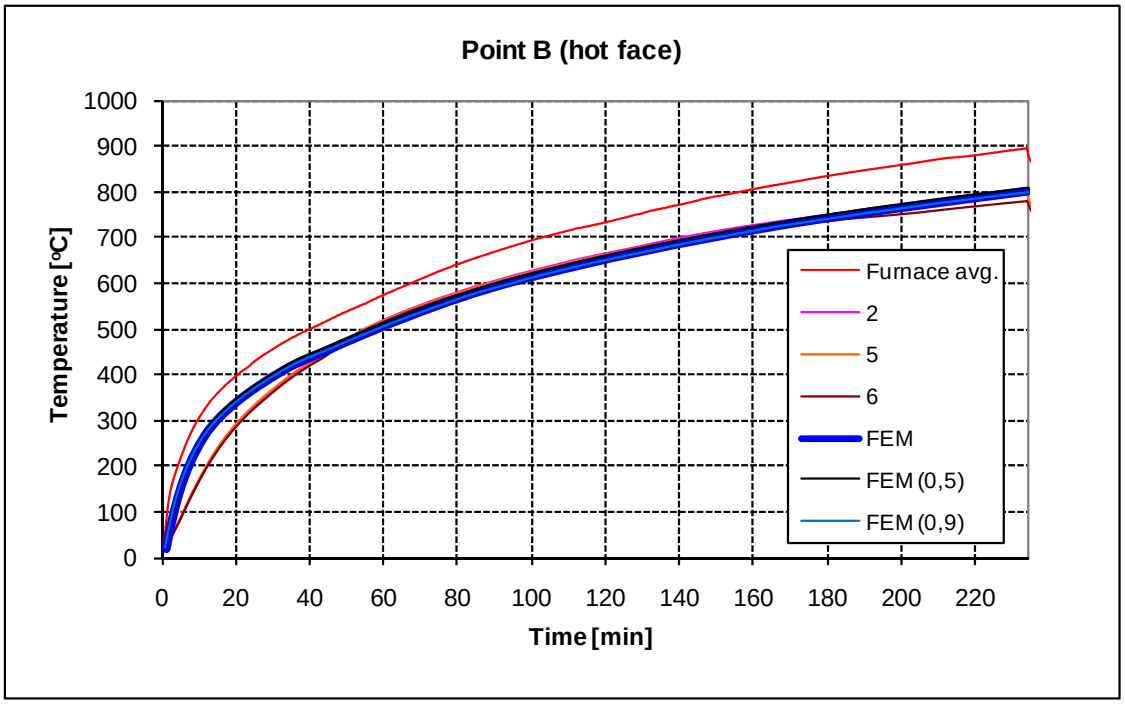

Figure 7.11. Temperatures at point B.

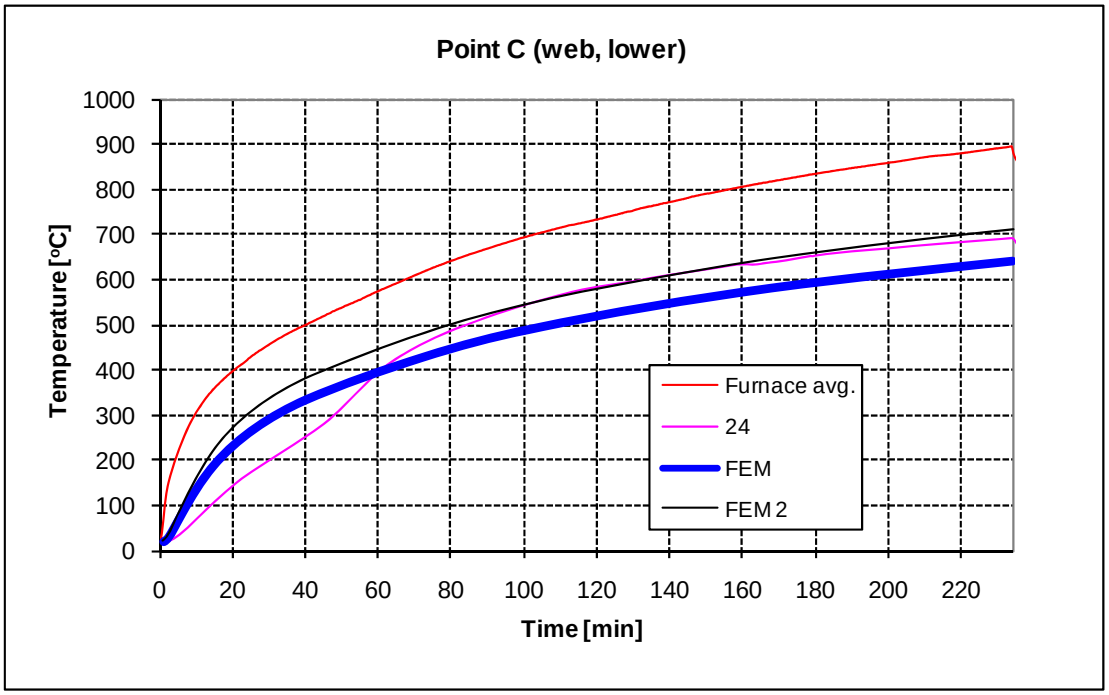

Figure 7.12. Temperatures at point C.

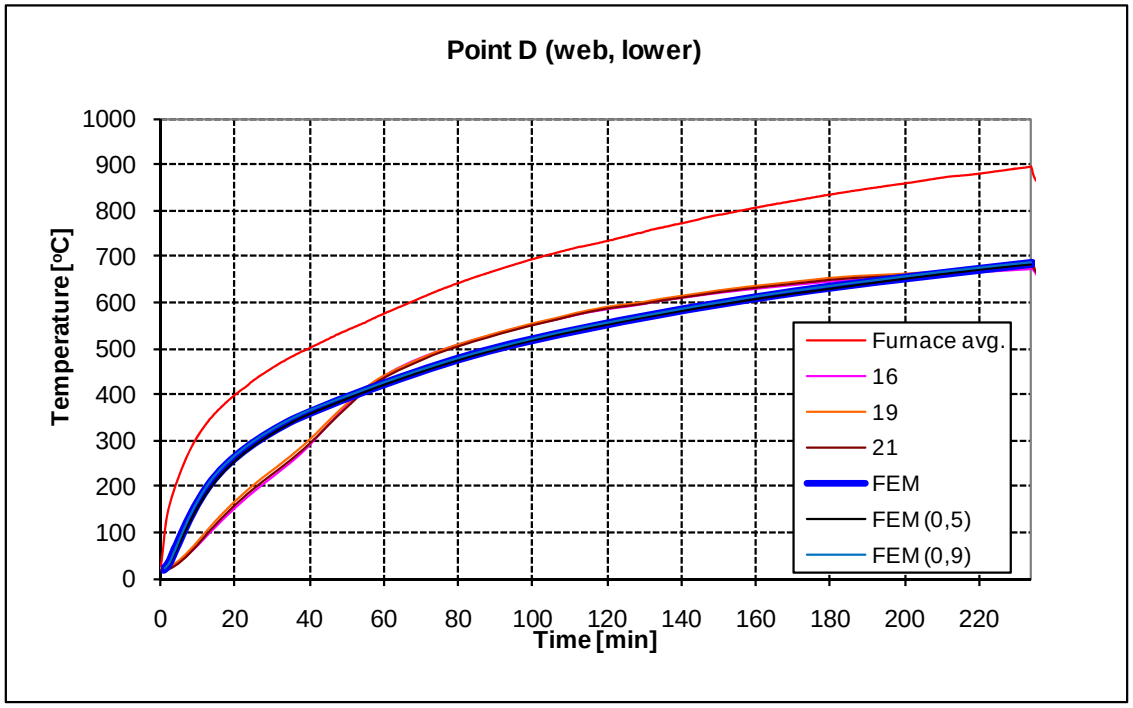

Figure 7.13. Temperatures at point D.

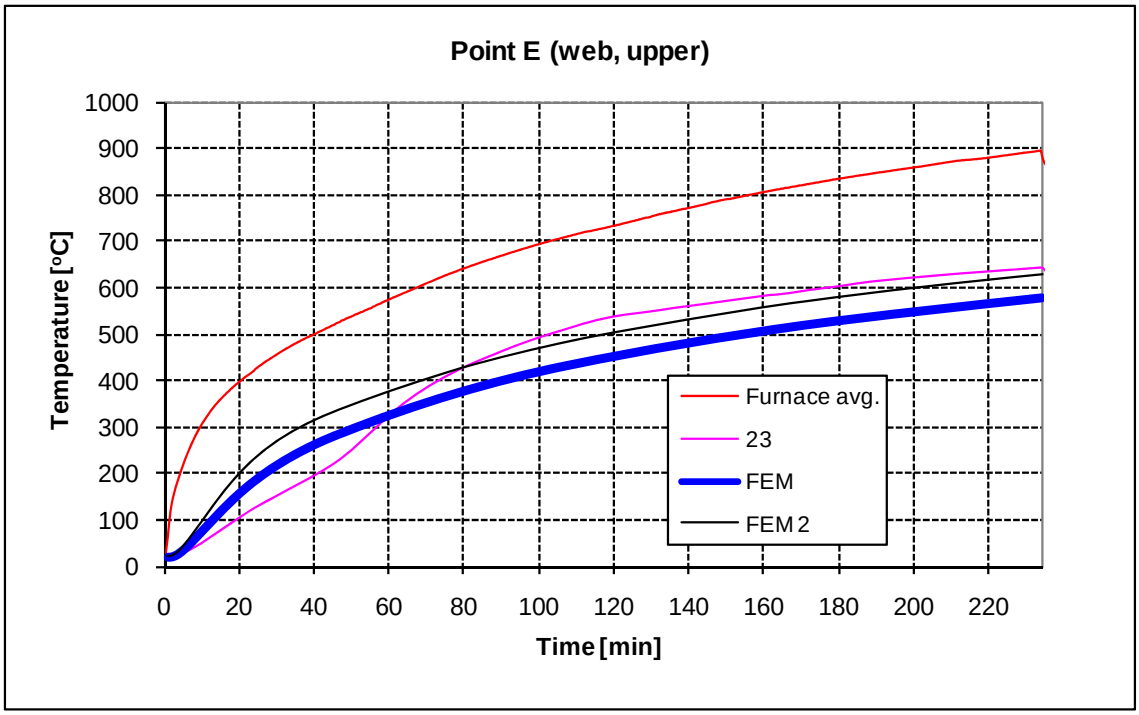

Figure 7.14. Temperatures at point E.

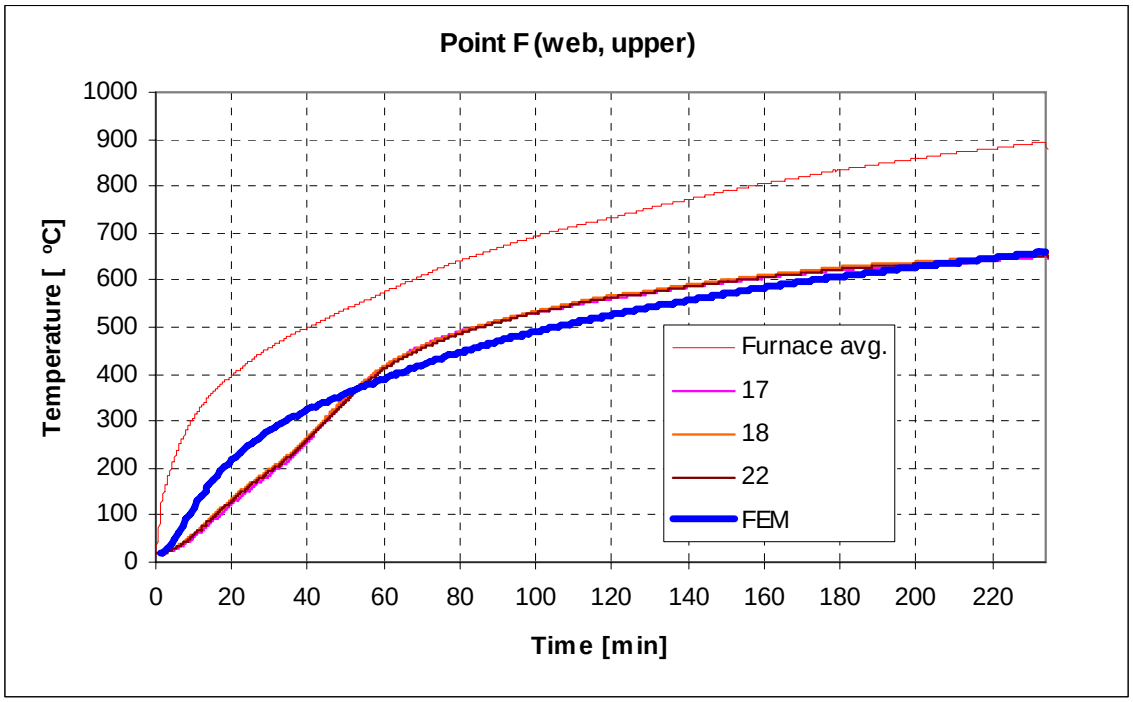

Figure 7.15. Temperatures at point F.

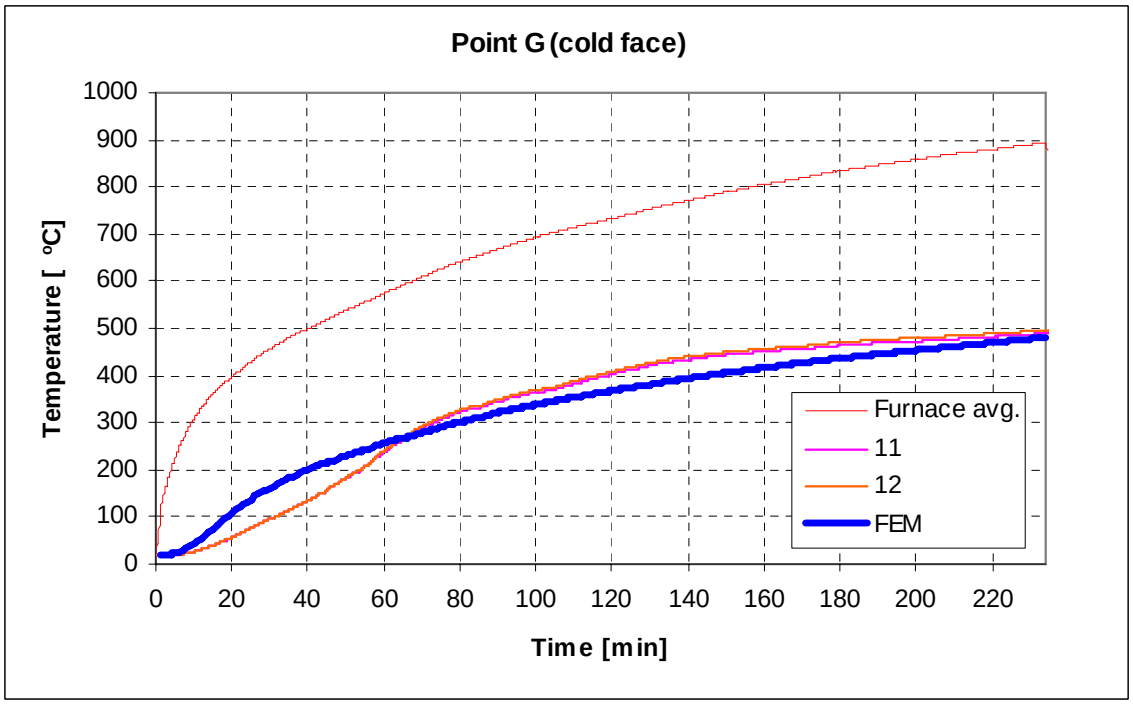

Figure 7.16. Temperatures at point G.

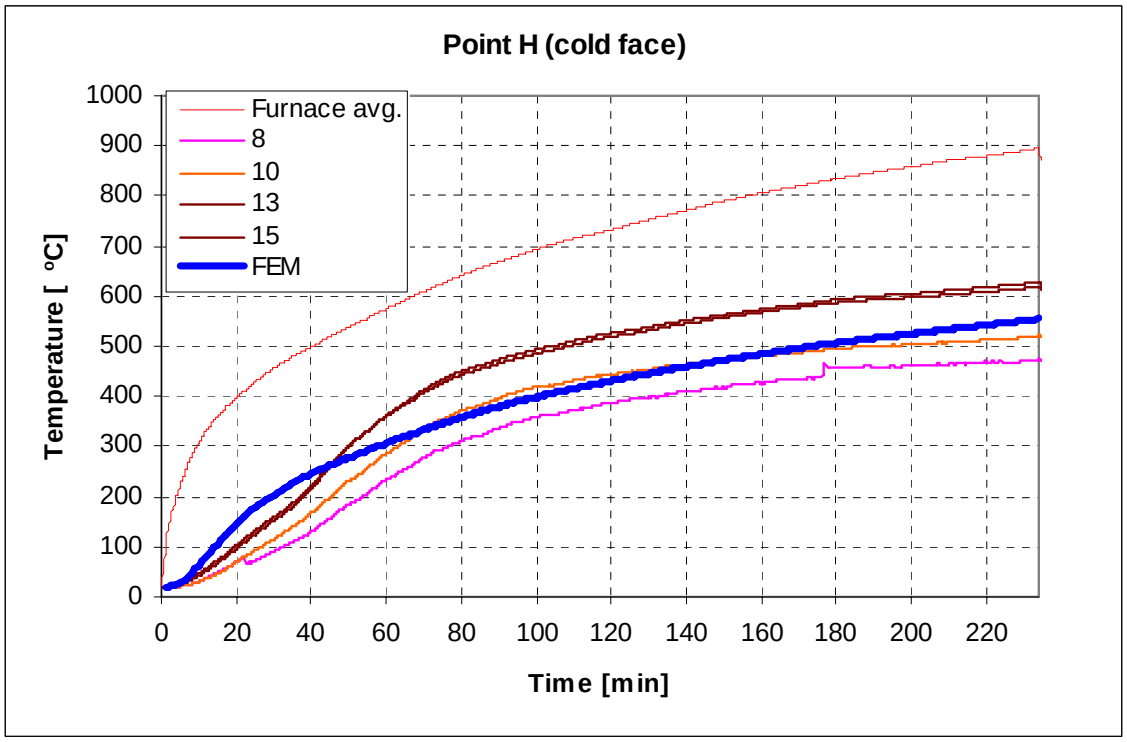

Figure 7.17. Temperatures at point H.

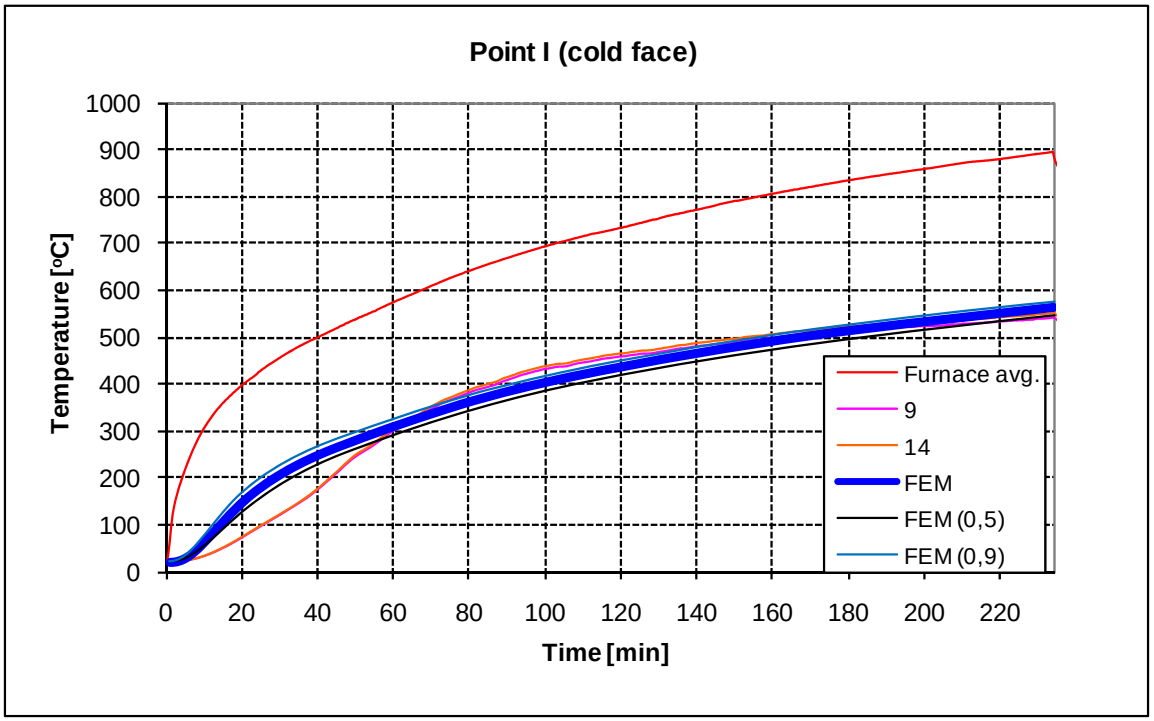

Figure 7.18. Temperatures at point I.

Based on Figures 7.10–7.18, it can be concluded that the temperatures from the FEM analysis were too hot in the beginning of the test (within 60 minutes from the start). Thereafter, the temperature curves based on FEM calculations are slightly below the curves based on test results at most points. Similar behaviour has been observed in other comparisons between elevated temperatures of tests and numerical calculations including the references [Ala-Outinen et al, 2006] and [Franssen et al, 1995]. According to Figures 7.11, 7.13 and 7.18 the temperatures of the panel are not sensitive for small changes of emissivity of steel. Especially in the hot face and web, the effect of changing the emissivity to 0,5 or 0,9 had very small effect on the temperatures. At the end of the test, the biggest differences between the temperatures from FEM and tests existed at points C and E, which located near the insulation. The effect of the thermal conductivity λ_i of the insulation material was studied by multiplying the given values by ten. From Figures 7.12 and 7.14 it can be seen that with these multiplied values of λ_i, the temperatures at the end of the FEM calculation are close to those from the tests. The differences between the temperatures from FEM and tests at points C and E cannot be entirely explained by the properties of the insulation material, but they may be one possible reason for the scattering. However, the temperatures from the test and FEM calculations correlate quite well and the numerical model seems to be reliable.

7.1.4. FEM calculations for standard fire

The FEM model was validated by comparison to test results. Therefore, other fire curves may also be used in calculations on the same panel. This study uses next the EN 1991-1-2 [EN 1991-1-2, 2002] standard (ISO) temperature-fire curve which can be expressed as:

$$T_{stand} = T_g = 20 + 345 \log_{10} (8\,t + 1) \qquad (7.4)$$

where T_g is the gas temperature in the fire compartment [^oC],
t is time [min].

In comparison to test results, the entire cross-section including the insulation was modelled exactly the same as in the test. In standard fire calculations there is no insulation inside the profile. Therefore, a smaller part of the panel was modelled as shown in Figure 7.19.

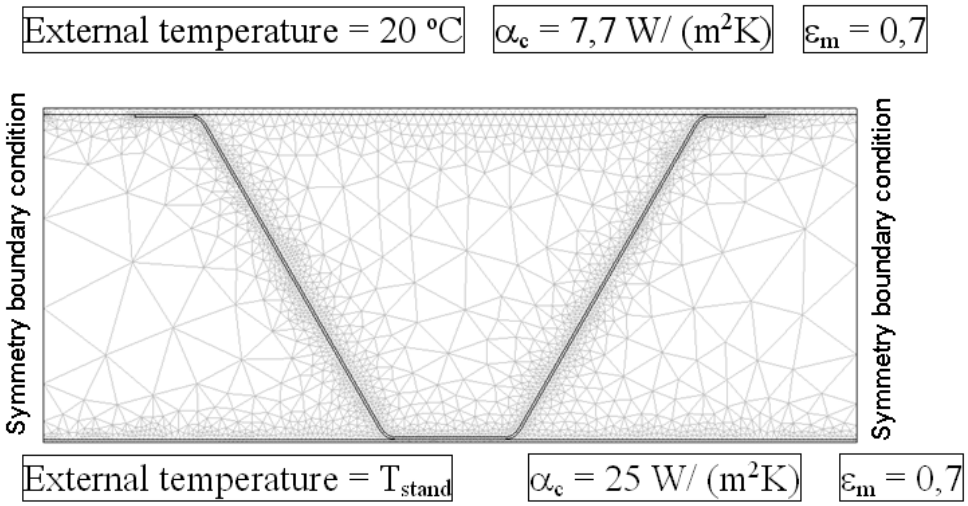

Figure 7.19. Mesh and boundary conditions of the all-metal sandwich panel in ISO fire.

The calculation covered a period of 60 minutes. Figure 7.20 shows the temperature distribution of the panel at the end of the calculation.

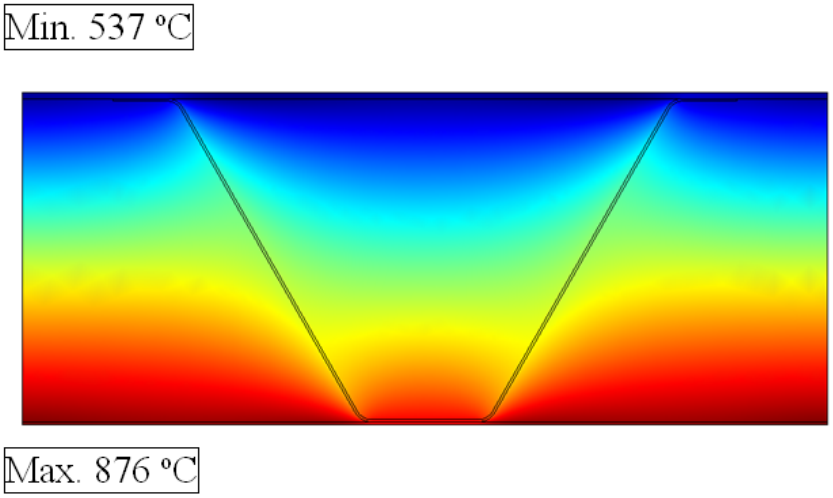

Figure 7.20. Temperature distribution of the all-metal sandwich panel after 60 minutes of ISO fire exposure.

Figure 7.21 shows the temperatures at points A, B, D, F, G and I (see Fig. 7.9) as a function of time.

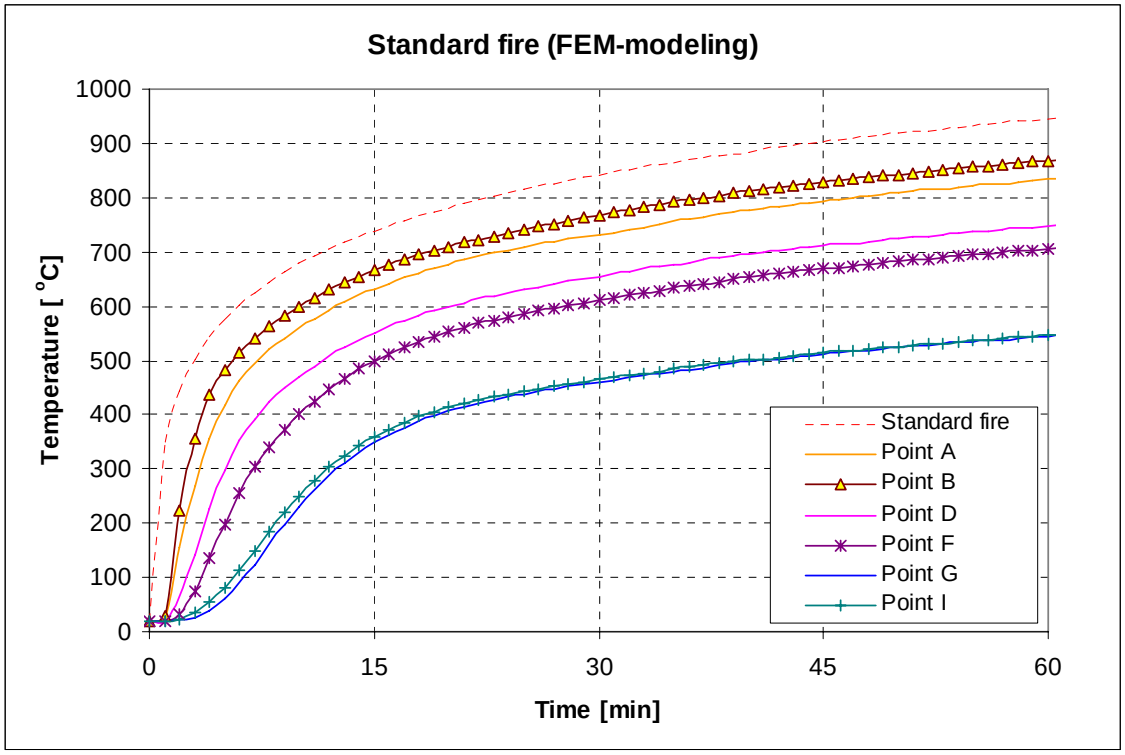

Figure 7.21. Temperatures across the all-metal sandwich panel during 60 minutes of ISO fire exposure.

Figures 7.23 and 7.24 show the temperature distributions of the hot face and the cold face of the panel. The origin of the used co-ordinate system is above the lower flange of the left edge of the modelled part as shown in Figure 7.22.

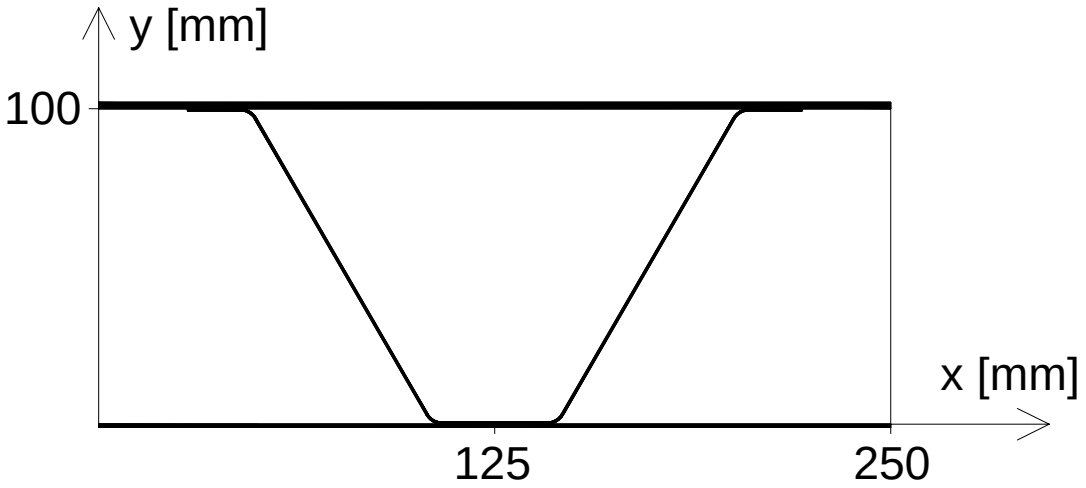

Figure 7.22. Co-ordinate system of the modelled part of the all-metal sandwich panel.

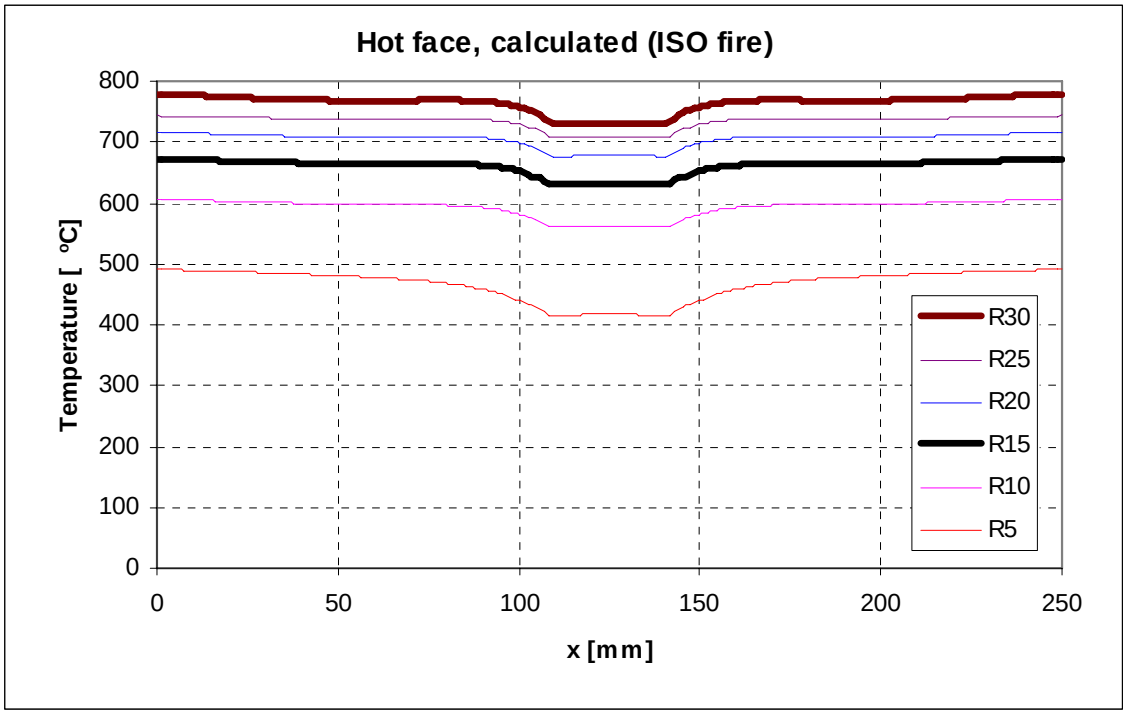

Figure 7.23. Temperatures across the hot face of the all-metal sandwich panel during 30 minutes of standard (ISO) fire exposure.

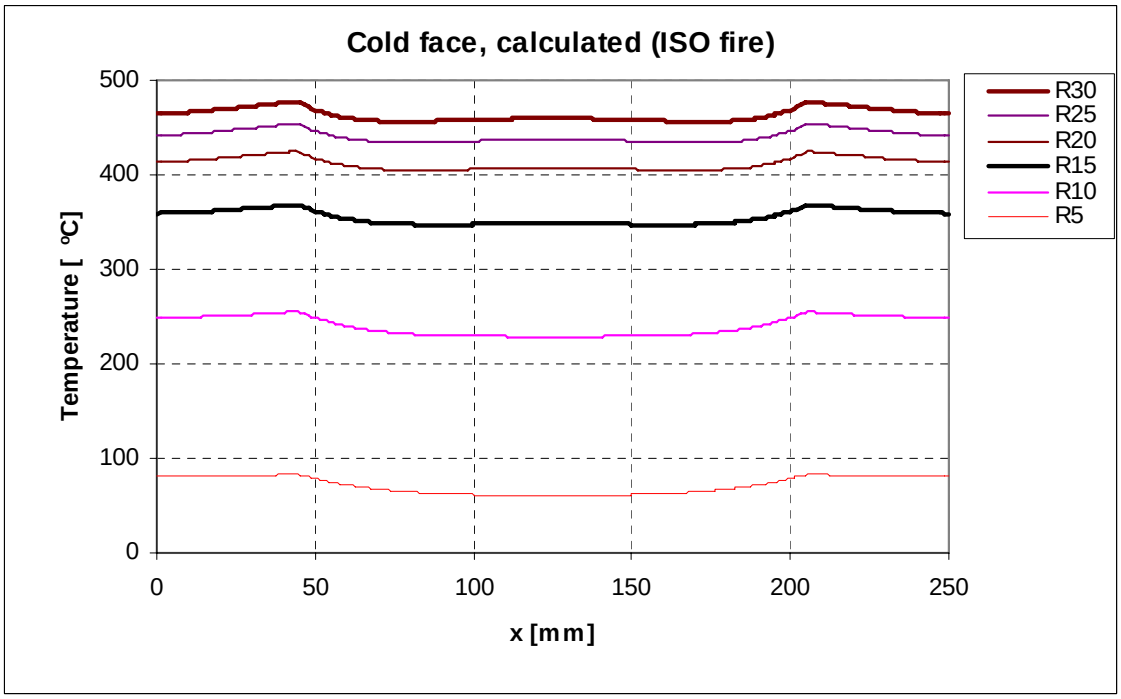

Figure 7.24. Temperatures across the cold face of the all-metal sandwich panel during 30 minutes of ISO fire exposure.

Figures 7.25 and 7.26 show the ISO fire curve and the maximum temperatures of the hot face and the cold face. Partly defined functions for the temperatures of the faces were formulated. The difference between the average and the maximum temperature was very small, so equations were formulated based on the maximum value. The temperature equations are needed later to calculate the strength of the panel at elevated temperatures as a function of time.

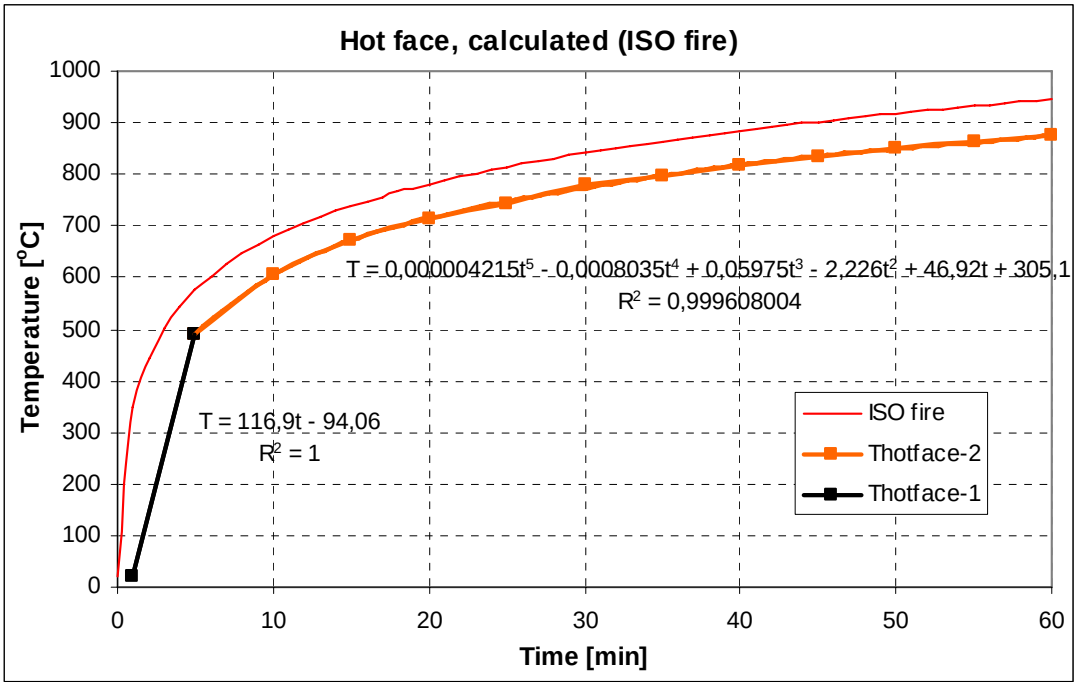

Figure 7.25. Maximum temperature of the hot face.

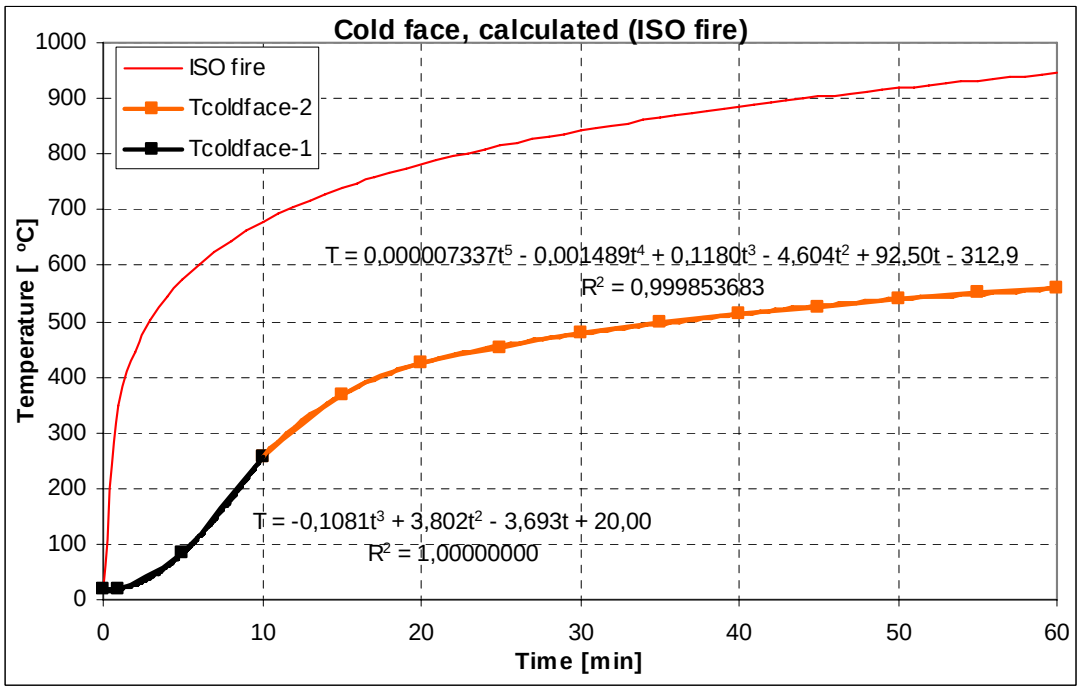

Figure 7.26. Maximum temperature of the cold face.

The temperatures of the web were defined as a function of the y-co-ordinate as shown in Figure 7.22. The distributions at different elevated temperatures are shown in Figure 7.27.

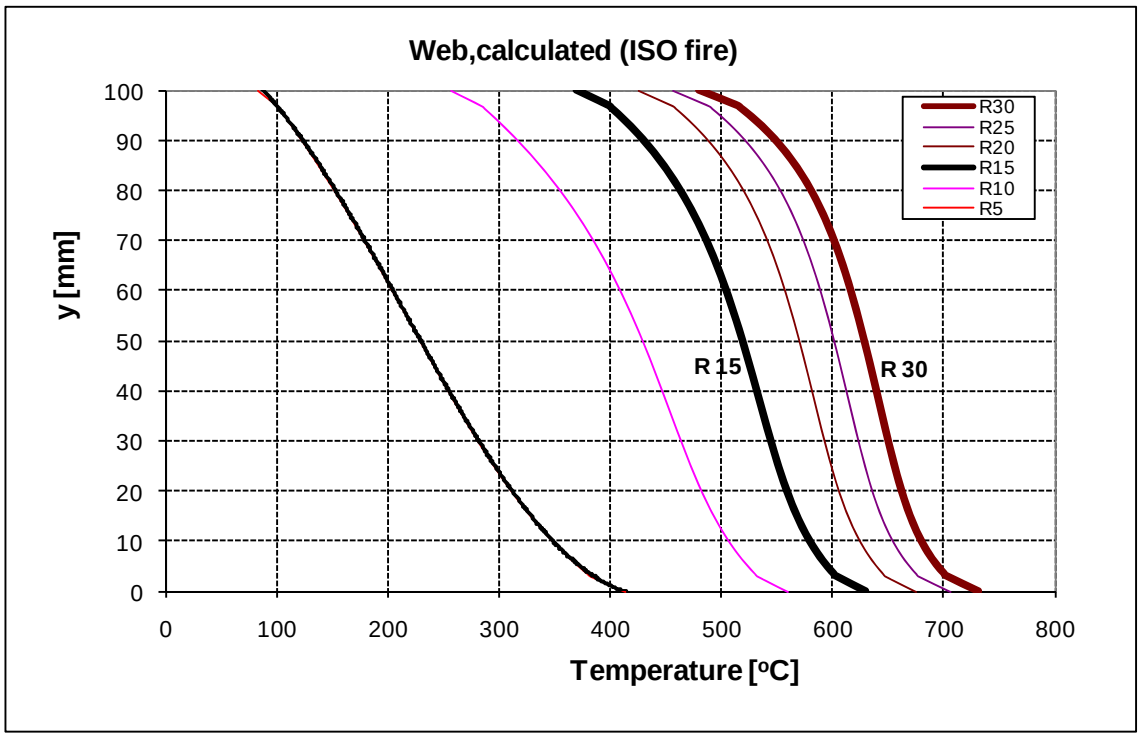

Figure 7.27. Temperature distribution of the web as a function of the y-co-ordinate.

Figure 7.28 shows the relative temperatures of the web as a function of relative height position, which are defined as:

$$\text{Relative height position} = \frac{y}{h_w}, \tag{7.5}$$

where
- y is the vertical position (Fig. 7.20) [mm],
- h_w =100 mm, the height of the web (projection in y-direction).

$$\text{And Relative temperature} = \frac{T - T_{uf}}{T_{lf} - T_{uf}}, \tag{7.6}$$

where
- T is the calculated temperature,
- T_{uf} is the maximum temperature of the upper (cold) face of the panel,
- T_{lf} is the maximum temperature of the lower (hot) face of the panel.

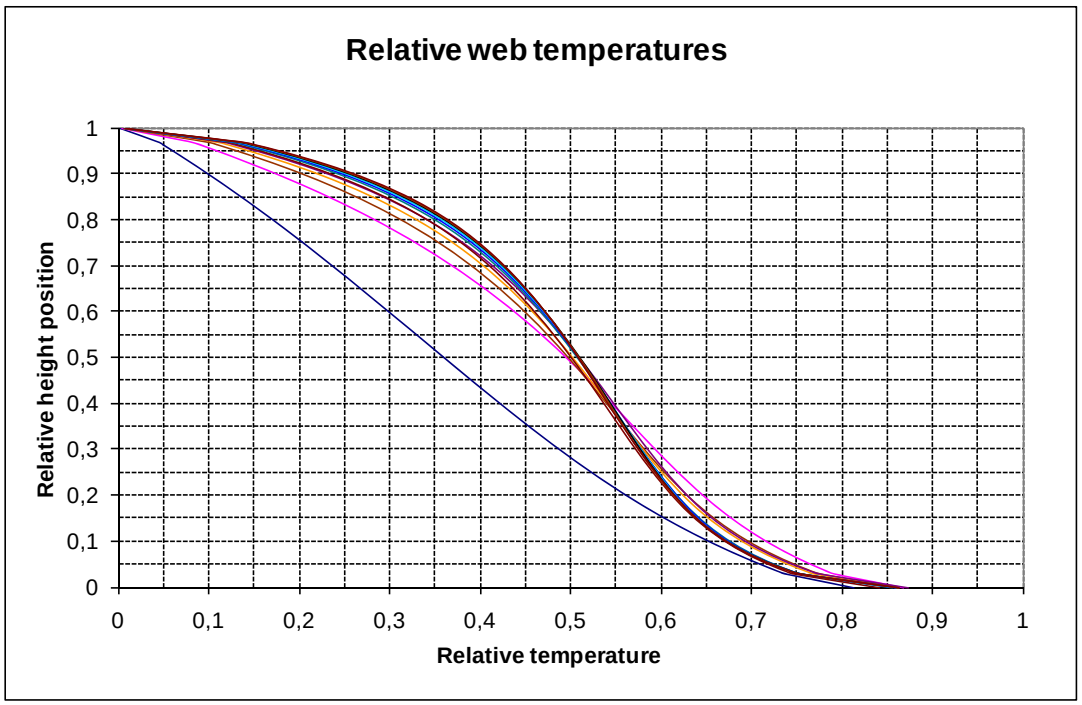

Figure 7.28. Relative temperatures of the web from R5 to R60.

The lowest line in Figure 7.28 shows the temperature distribution at t=5 min. It can be seen that all other subsequent relative distributions (R10–R60) are very close to each other in size. However, the temperature distributions of the web for FEM calculations were formulated separately for each time as follows:

R5: $$T_{web} = -88117141\left(\frac{y}{1000}\right)^5 + 24511238\left(\frac{y}{1000}\right)^4 - 2734346\left(\frac{y}{1000}\right)^3 + 152805\left(\frac{y}{1000}\right)^2 - 6810\left(\frac{y}{1000}\right) + 405 \quad (7.7)$$

R10: $$T_{web} = -112474400\left(\frac{y}{1000}\right)^5 + 30001126\left(\frac{y}{1000}\right)^4 - 170834\left(\frac{y}{1000}\right)^3 + 170834\left(\frac{y}{1000}\right)^2 - 5783\left(\frac{y}{1000}\right) + 551 \quad (7.8)$$

R15: $$T_{web} = -141725441\left(\frac{y}{1000}\right)^5 + 35986955\left(\frac{y}{1000}\right)^4 - 3713401\left(\frac{y}{1000}\right)^3 + 184632\left(\frac{y}{1000}\right)^2 - 5591\left(\frac{y}{1000}\right) + 621 \quad (7.9)$$

R20: $$T_{web} = -165150618\left(\frac{y}{1000}\right)^5 + 41170614\left(\frac{y}{1000}\right)^4 - 4118278\left(\frac{y}{1000}\right)^3 + 198431\left(\frac{y}{1000}\right)^2 - 5640\left(\frac{y}{1000}\right) + 666 \quad (7.10)$$

R25: $$T_{web} = -183852832\left(\frac{y}{1000}\right)^5 + 45554392\left(\frac{y}{1000}\right)^4 - 4493775\left(\frac{y}{1000}\right)^3 + 212903\left(\frac{y}{1000}\right)^2 - 5848\left(\frac{y}{1000}\right) + 696 \quad (7.11)$$

R30: $$T_{web} = -197751150\left(\frac{y}{1000}\right)^5 + 48529439\left(\frac{y}{1000}\right)^4 - 4709376\left(\frac{y}{1000}\right)^3 + 218237\left(\frac{y}{1000}\right)^2 - 5810\left(\frac{y}{1000}\right) + 721 \quad (7.12)$$

The temperatures required for shear buckling calculation method f are T_{hot}, T_{mid} and T_{avg}. These values were derived from the distributions shown in Figure 7.28. Table 7.1 shows the relative maximum, middle and average temperatures.

Table 7.1. Relative temperatures T_{hot}, T_{mid} and T_{avg}.

	$\frac{T - T_{uf}}{T_{lf} - T_{uf}}$			
Web temperatures	R15	R30	R45	R60
T_{hot}	0,833	0,807	0,820	0,819
T_{mid}	0,498	0,501	0,511	0,510
T_{avg}	0,473	0,477	0,487	0,488

Figure 7.28 and Table 7.1 reveal that the maximum temperature of the web is clearly less than the maximum temperature of the hot face (< 85 %). It can also be concluded that the values T_{avg} and T_{mid} are close to value $\frac{T_{lf} + T_{uf}}{2}$.

7.1.5. Sensitivity analysis

This sensitivity analysis considers the effects of emissivity ε_m and the heat transfer coefficient α_c. It begins with a hand-calculation example concerning a rectangular hollow section. The section considered in the example is 200 x 200 x 10 mm^3 (Fig. 7.29) which is exposed to fire on all sides.

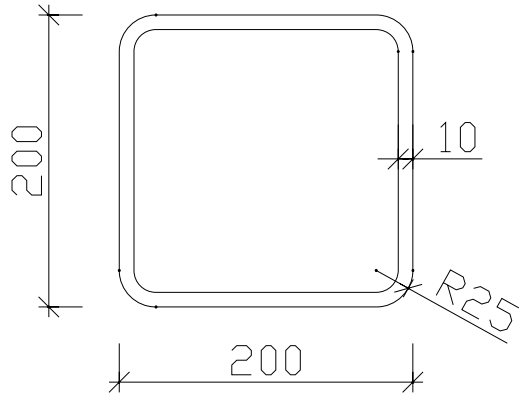

Figure 7.29. Dimensions of the rectangular hollow section.

The calculation is done according to the ISO fire curve in five second steps the same as in the reference [Rautaruukki, 2000] using the following values:

c_a = 600 J/kgK
ρ_a = 7850 kg/m^3
ε_m = 0,7
α_c = 25 W/m^2K

Sensitivity to different ε-values is considered in Figures 7.30 and 7.31 and sensitivity to different α_c-values in Figures 7.32 and 7.33. Calculated temperatures are plotted for relatively long (3 hours) and relatively short (15 min) periods.

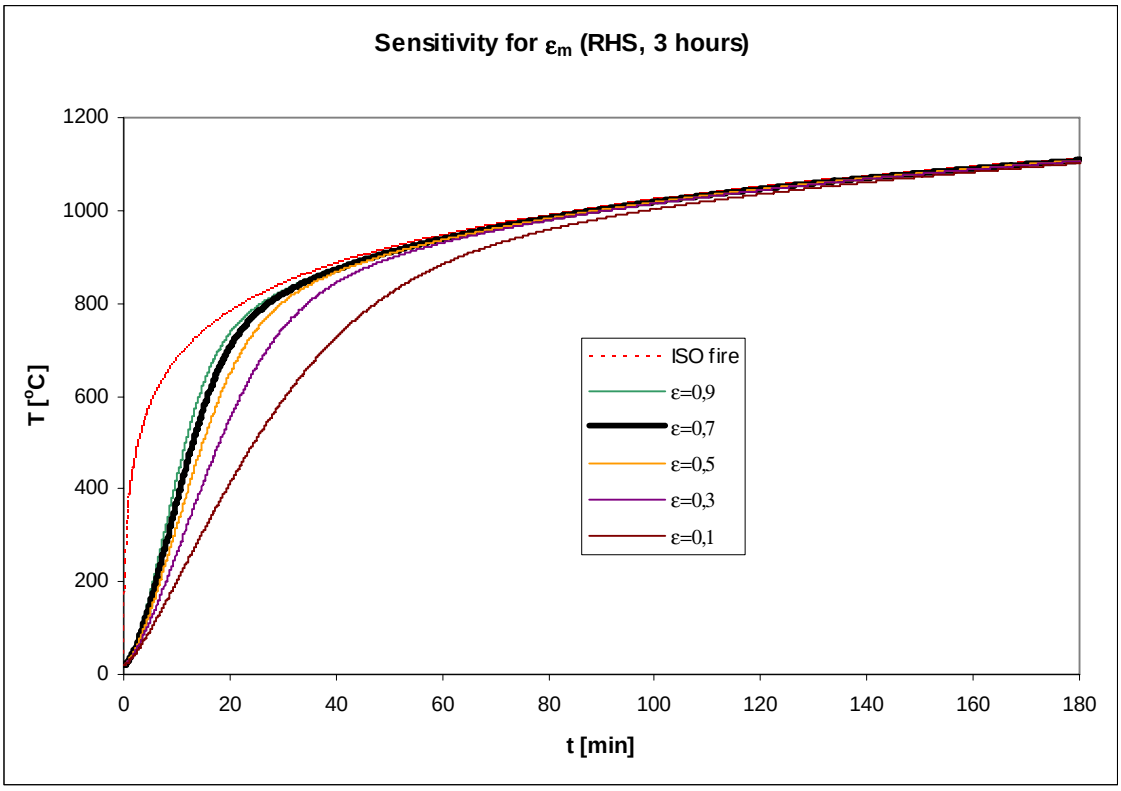

Figure 7.30. Effect of ε_m in hand-calculation (RHS, 3 hours).

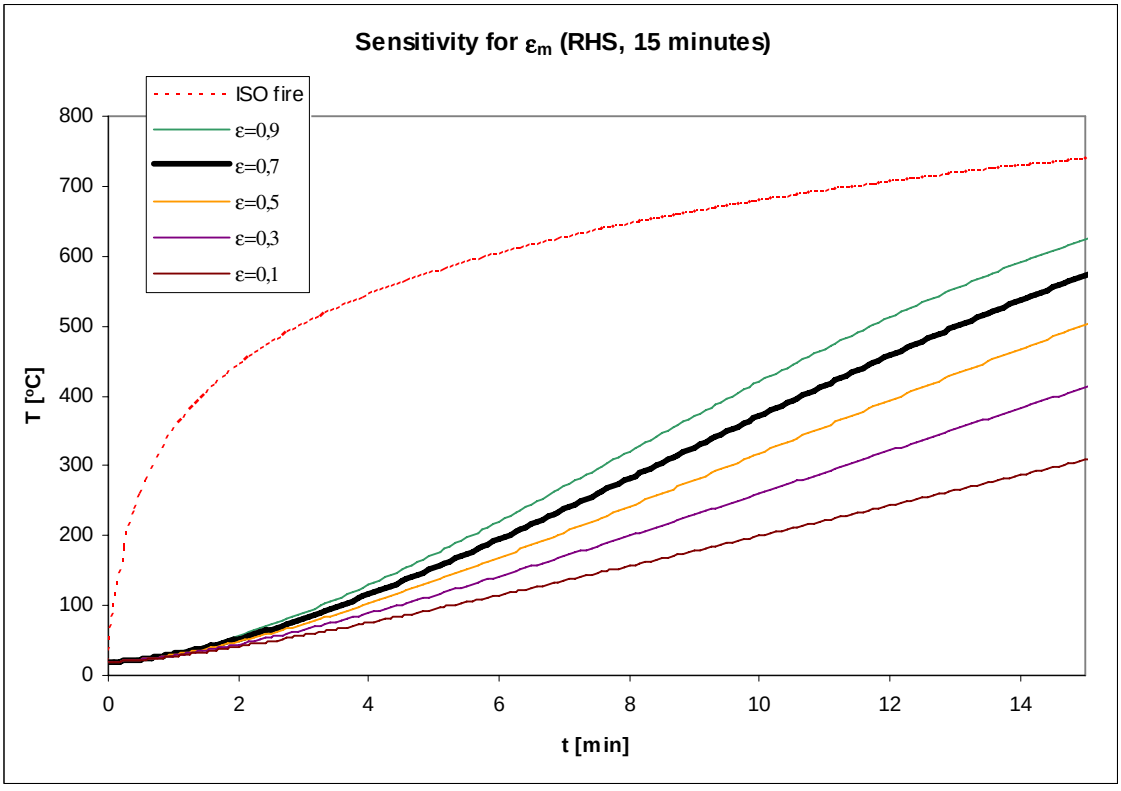

Figure 7.31. Effect of ε_m in hand-calculation (RHS, 15 minutes).

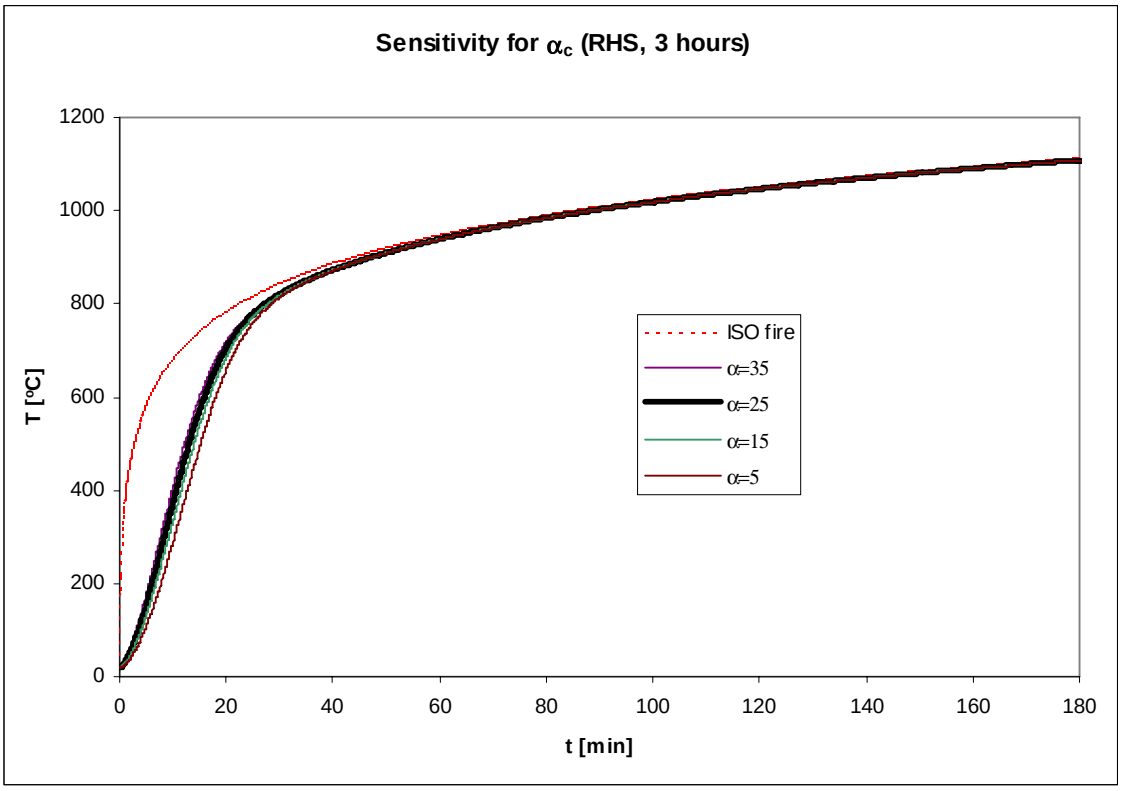

Figure 7.32. Effect of α_c in hand-calculation (RHS, 3 hours).

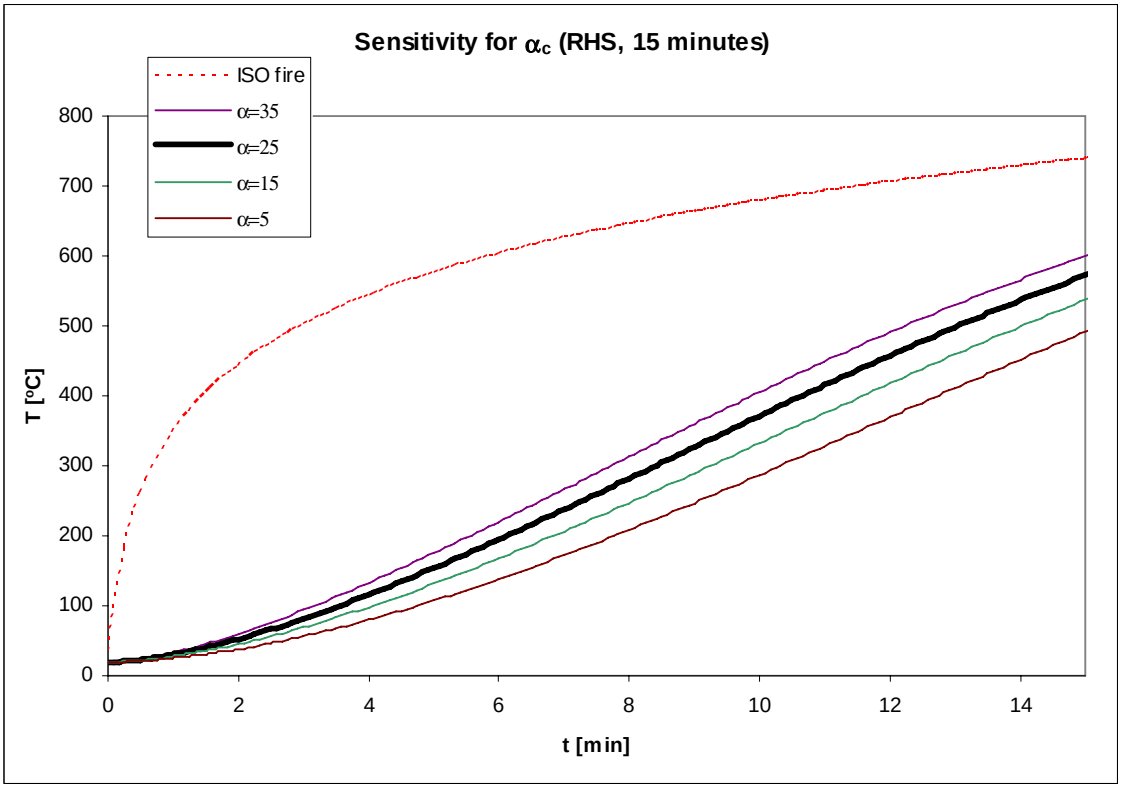

Figure 7.33. Effect of α_c in hand-calculation (RHS, 15 minutes).

As indicated by the results of hand-calculations on the rectangular hollow section (Figures 7.30–7.33), the effect of small changes in ε_m and α_c can be significant when time t is relatively short. That is often the case when calculating the temperatures of metal structures.

The sensitivity analysis of the all-metal sandwich panel considered in the example was done by FEM by changing the emissivity of all surfaces ε_m from 0,7 to 0,5 and 0,3 and the heat transfer coefficient α_c of the hot face from 25 W/(m^{2}K) to 15 and 5. Figures 7.34 and 7.35 show the temperatures at points B, D, I (hot face, web, cold face, see also Fig. 7.9) with the changed values.

This study used the value $\varepsilon_m = 0{,}7$ for carbon steel based on standard EN 1993-1-2 [EN 1993-1-2, 2005] and the value α_c = 25 W/(m^{2}K) based on standard EN 1991-1-2 [EN 1991-1-2, 2002]. The emissivities of mild steel typically lie in the 0,2–0,3 range and the corresponding values for sheet steel with a rough oxide layer are in the 0,8–0,9 range. Typical values for α_c are between 5–25 W/(m^{2}K) in the case of free convection [Drysdale, 2004].

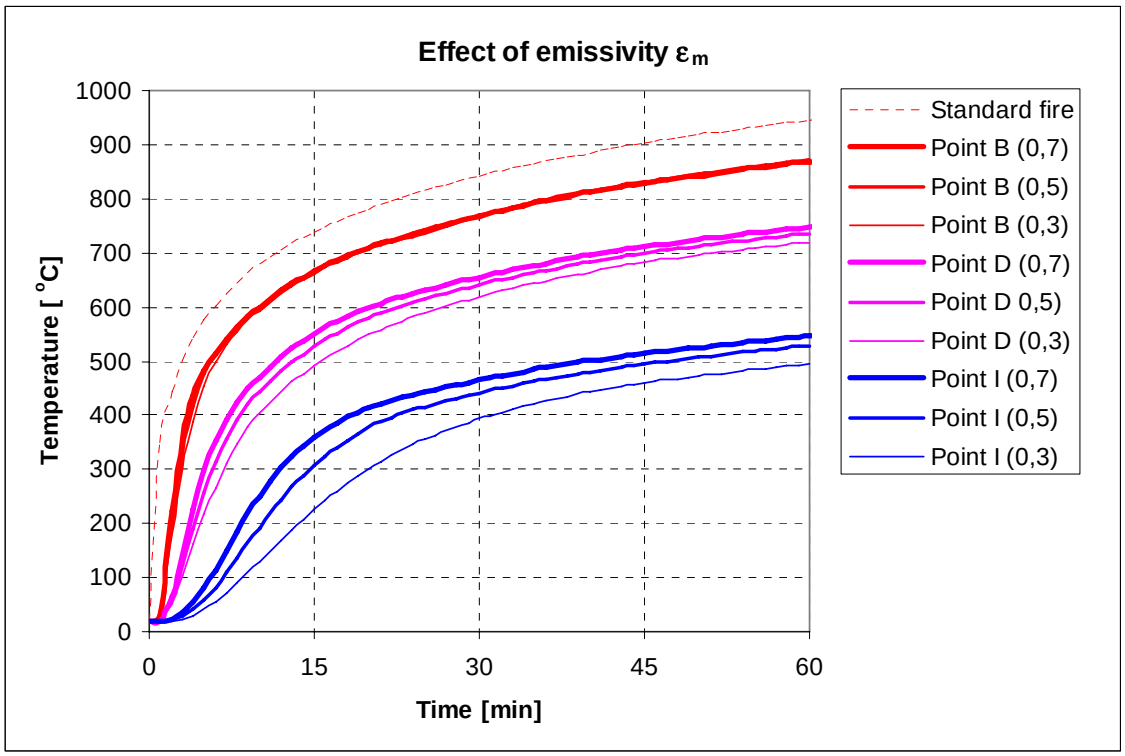

Figure 7.34. Effect of ε_m in FEM calculations (all-metal sandwich panel).

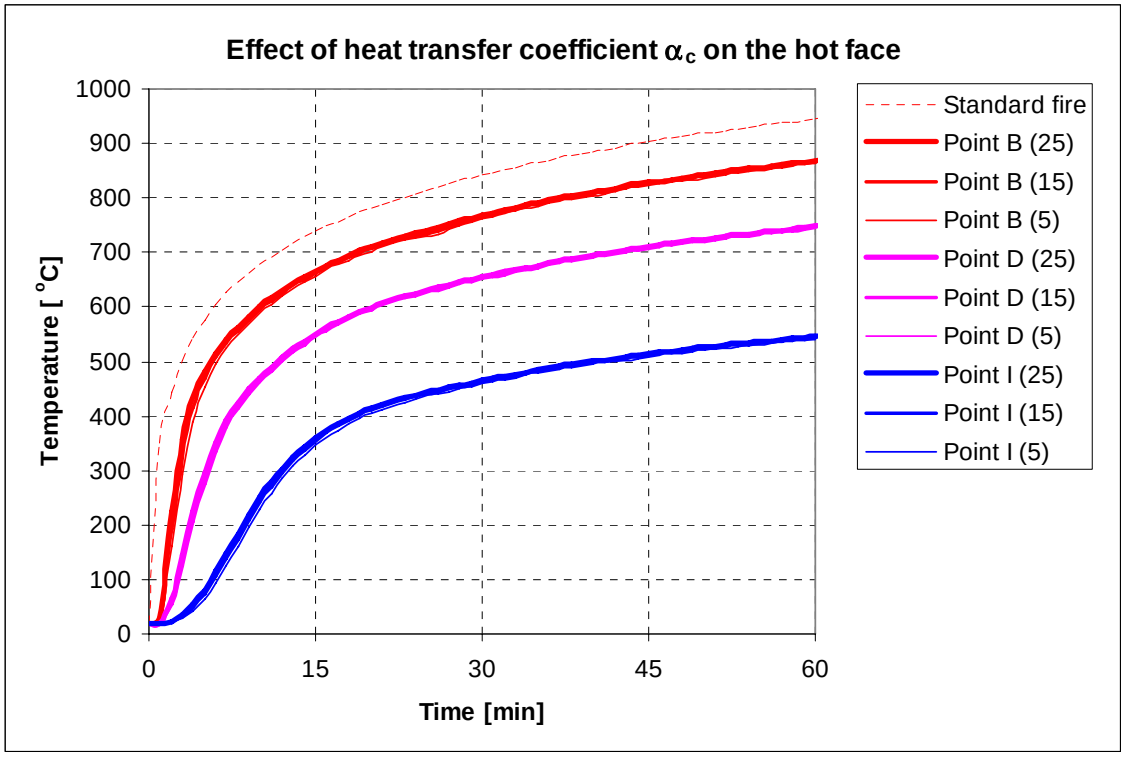

Figure 7.35. Effect of α_c in FEM calculations (all-metal sandwich panel).

Based on Figures 7.34 and 7.35, it can be concluded that small changes in emissivity ε_m may have a considerable effect on the results, but they are not as sensitive to small changes in the heat transfer coefficient α_c. Figure 7.34 shows that the temperature of the hot face is not highly dependent on ε_m, but the temperatures of the web, and especially the cold face, are clearly lower at smaller values of ε_m. Based on Figure 7.35, it can be said that at smaller values of the heat transfer coefficient of the hot face than α_c = 25 W/(m^{2}K) for the heat transfer coefficient of the hot face, the temperatures of the hot face, web and cold face are slightly lower. The sensitivity results from FEM analysis agree well with the results of the hand-calculation example.

7.2. Shear buckling resistance at elevated temperatures

This chapter defines the shear buckling resistance of an all-metal sandwich panel at elevated temperatures using FEM and the hand-calculation method f presented in Chapter 5.3.

The cross-section of the part of the panel considered in the calculations is shown in Figure 7.36. It is assumed that the whole panel can be composed of similar parts by

copying them. Roundings are taken into account in FEM calculations as earlier in the thermal FEM analyses of Chapters 7.1.3 and 7.1.4. Elevated temperatures are derived from the FEM calculations of Chapter 7.1.4. Calculated shear buckling resistances are presented as a function of time subject to up to 30 minutes of standard (ISO) fire.

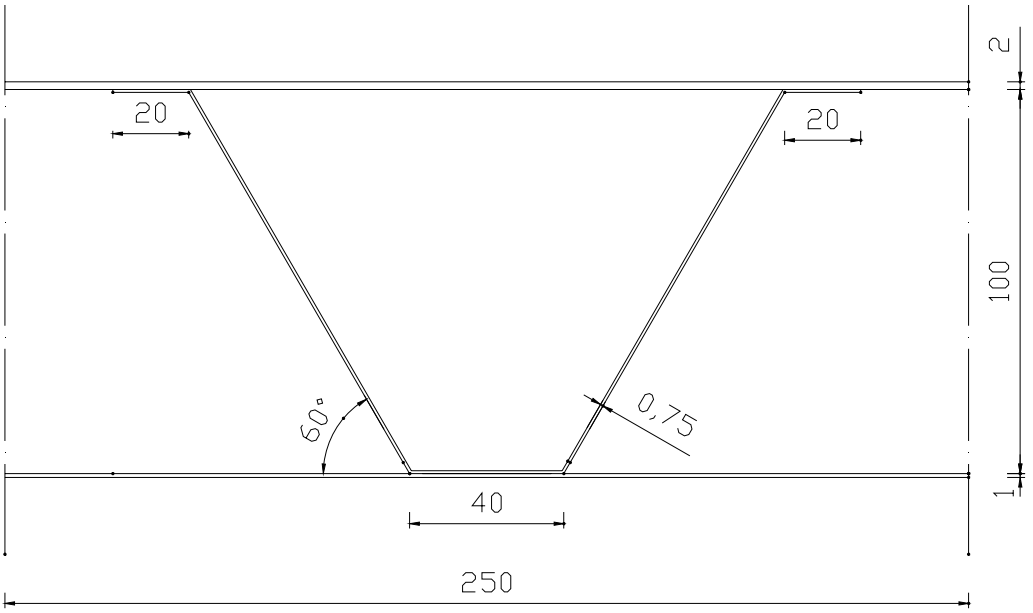

Figure 7.36. Dimensions of the considered cross-section.

7.2.1. FEM calculations for shear buckling at elevated temperatures

FEM calculations were done using *ABAQUS* [ABAQUS, 2007] software. Temperature distributions at times R5, R10, R15, R20, R25 and R30 were derived from thermal FEM analyses for standard fire and the reduction of elastic modulus was done according to EN 1993-1-2 [EN 1993-1-2, 2005].

All calculations were performed for the cross-section shown in Figure 7.36 applying symmetry boundary conditions on both sides of the panel. Two lengths of the panel were considered so, that the ratio a/h_w for the panel web was 0,5 and 1. The modelled structures consisted of two parts of the all-metal sandwich panel (see Fig. 7.36), end plates and a plate in the middle of the span, where the load was applied. All plates were relatively thick (5–10 mm) to ensure that they would not buckle. The whole structure was modelled using the properties of carbon steel. All connections between the plates were modelled as rigid.

A load of 2 kN was applied as a uniform pressure on the upper side of the middle plate in order to produce a 1 kN shear force across the whole length of the panel. Then eigenvalues λ were calculated the way described in Chapter 4 for calculating critical

shear forces. The dimensions and the loading of the modelled structures are shown in Figure 7.37.

Eight-node brick elements with reduced integration (C3D8R) were used for all parts in the model. The meshes of the structures are shown in Figure 7.38. The other endplate was left out of the figure.

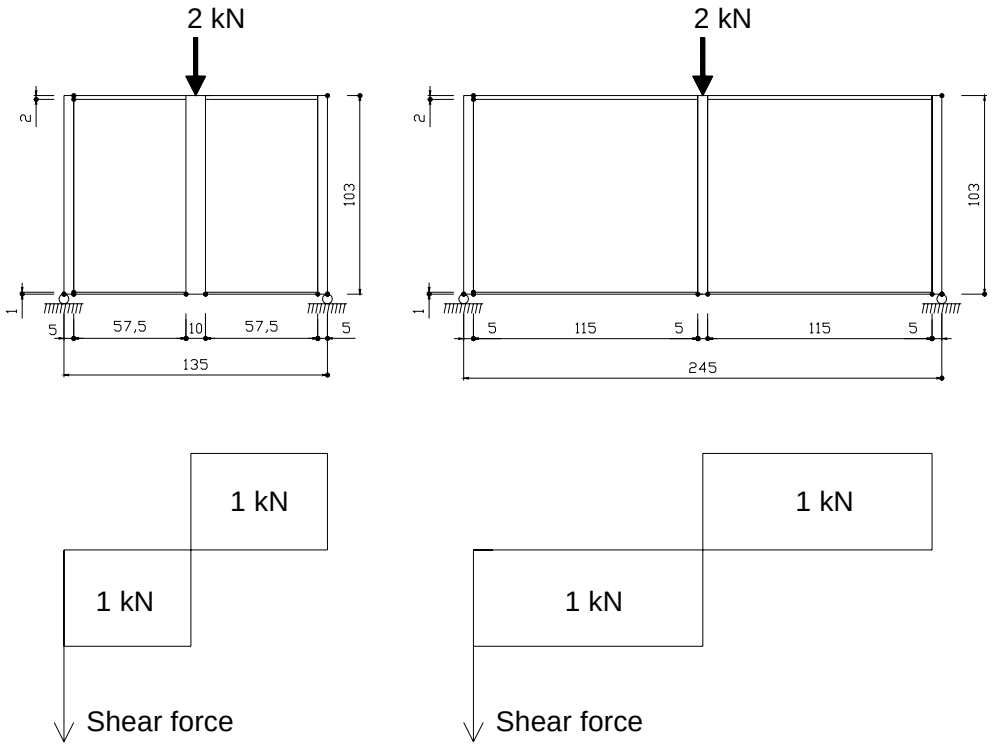

Figure 7.37. Dimensions and loads of the structures.

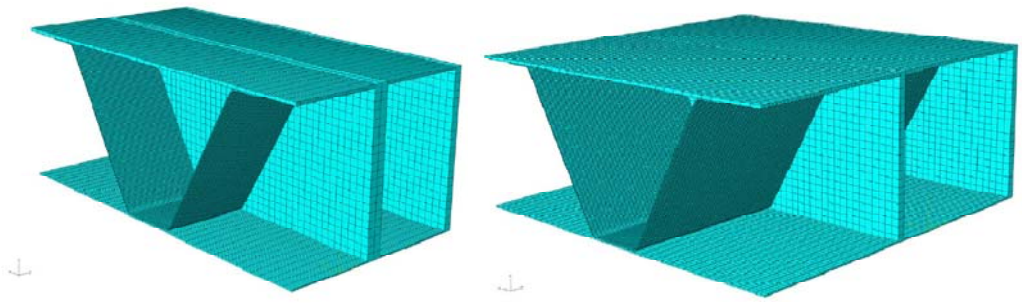

Figure 7.38. *ABAQUS* models of the structures (other endplate left out).

Unlike in the FEM calculations on the plate in Chapter 4, here a bending moment is applied to the structure. The bending moment does not have a considerable effect on the results when it is less than 10 % of the maximum value [Höglund, 1997], [Liang et al, 2004], [Liu et al, 2003]. According to the reference [Heinisuo, Ylihärsilä, 2006], the bending moment resistance of the part of the panel is about 6 kNm at ambient temperature. In this case, the bending moment resistance cannot be determined because it depends on yield strength, which is not relevant for this analysis.

Two different lengths of the part were used in the calculations: a = 57,5 mm and a = 115 mm. The values for ratio a/h_w were 0,5 and 1. They resulted in the following bending moments M_b in the base state (F = 2 kN):

$$a = 57{,}5 \text{ mm: } M_b = \frac{2kN \cdot 0{,}135m}{4} = 0{,}0675 \text{ kNm} \tag{7.13}$$

$$a = 115 \text{ mm: } M_b = \frac{2kN \cdot 0{,}245m}{4} = 0{,}1225 \text{ kNm} \tag{7.14}$$

The height of the web was calculated from the following:

$$h_w = \frac{100mm}{\sin 60^o} = 115 \text{ mm} \tag{7.15}$$

Longitudinal movement of the panel was prevented in same area where the force was applied to allow thermal elongation at the end-posts.

Thermal expansion is taken into account in *ABAQUS* by the coefficient α:

$$\alpha = \frac{\Delta L}{L \Delta T} \tag{7.16}$$

The temperature-dependent values for α were calculated from the relative thermal elongation $\Delta L / L$ of steel defined in EN 1993-1-2 [EN 1993-1-2, 2005] as shown in Figure 7.39.

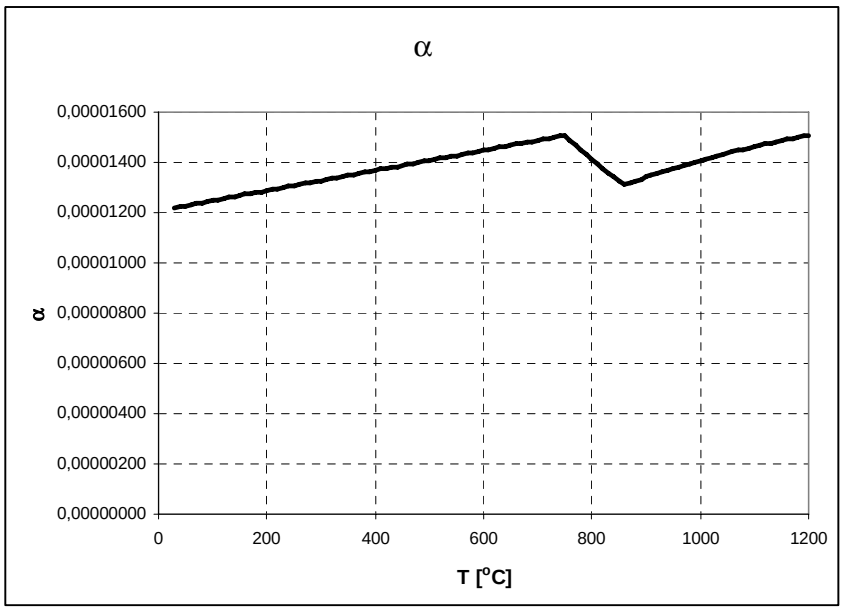

Figure 7.39. Thermal expansion coefficient used in the calculations.

Temperature data were applied in the model so as to produce a non-uniform temperature field across the web and the plates (Fig. 7.27) while uniform temperature based on Figures 7.25 and 7.26 was applied to the flanges.

Table 7.2 shows the smallest eigenvalues at which shear buckling occurred. The negative eigenvalues were also considered. Here, a negative eigenvalue means that the force shown in Figure 7.37 acts upwards. Both positive and negative eigenvalues were taken into account because the cross-section is not symmetric and the effect of the flanges depends on the direction of the applied force.

Table 7.2. Critical shear forces from FEM calculation.

	V_{cr} [kN]			
	$a/h_w = 0,5$		$a/h_w = 1$	
	Positive eigenvalue	Negative eigenvalue	Positive eigenvalue	Negative eigenvalue
Ambient	27,39	30,36	12,57	11,44
R5	25,63	25,23	12,16	9,36
R10	20,90	19,59	10,51	7,21
R15	18,21	15,00	9,63	5,57
R20	15,28	11,43	8,39	4,39
R25	13,08	9,57	7,41	3,84
R30	11,35	8,12	6,67	3,42

The negative eigenvalues are in most of the cases smaller than positive ones because the upper flange is stiffer than lower and in the case of negative eigenvalue, the lower flange is compressed. Figures 7.40 and 7.41 illustrate the buckling modes of the shear

buckled panels at ambient temperature and at 15 and 30 minutes' exposure to standard (ISO) fire. It should be noted that the critical load shown in the following figures is twice the critical shear force shown in Table 7.2 (see Fig. 7.37).

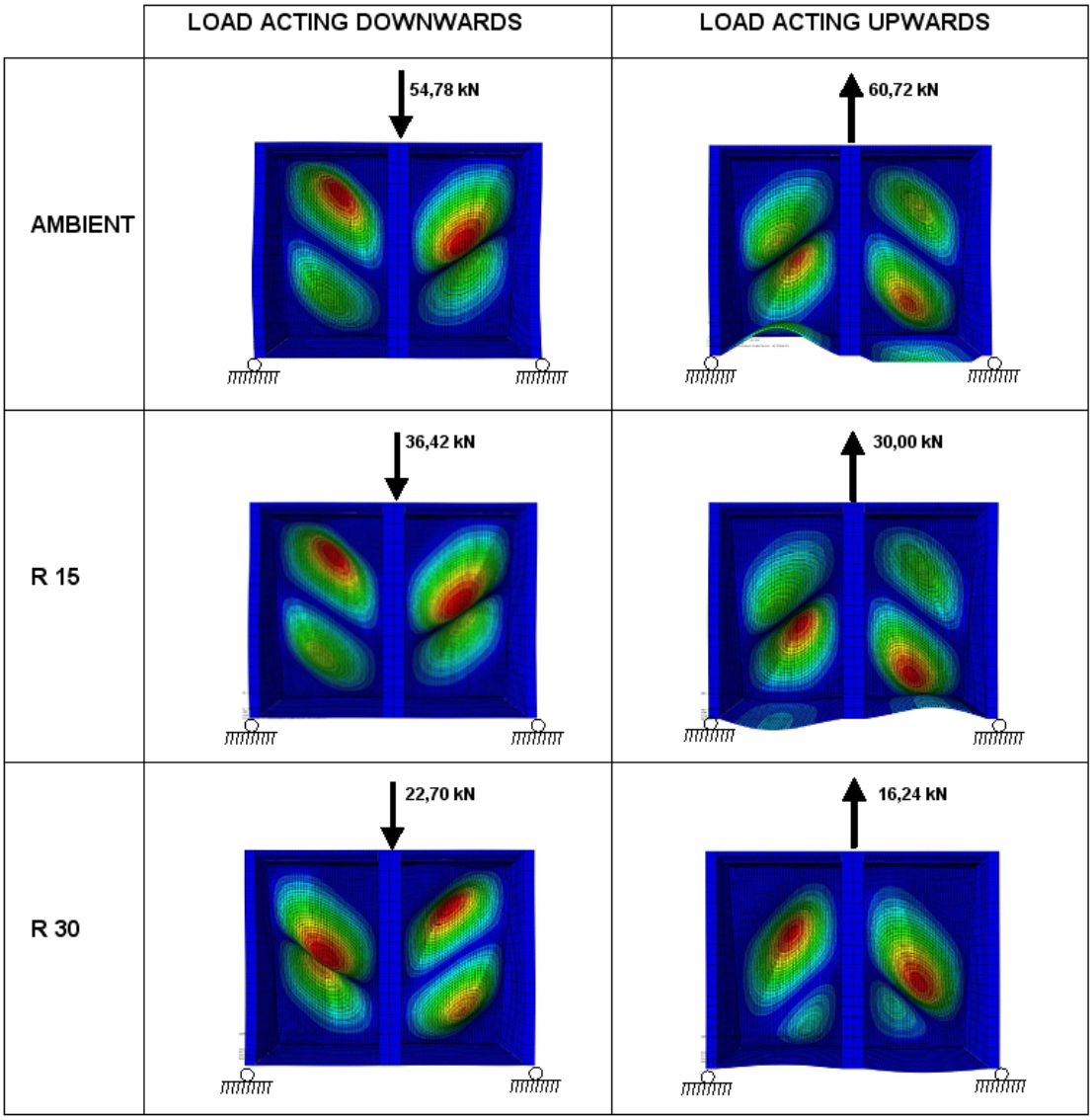

Figure 7.40. Shear buckling modes of the panel web ($a/h_w = 0,5$) at ambient temperature and after 15 and 30 minutes of ISO fire exposure.

Figure 7.40 reveals that when the critical load acts upwards, the slender (t = 1 mm) lower flange is compressed and buckles. The biggest difference between the negative and positive eigenvalues in the case a/hw = 0,5 was 39,8 % compared to the lowest absolute value (R30). The buckling modes of the web are clearly dependent on the direction of the load at R30.

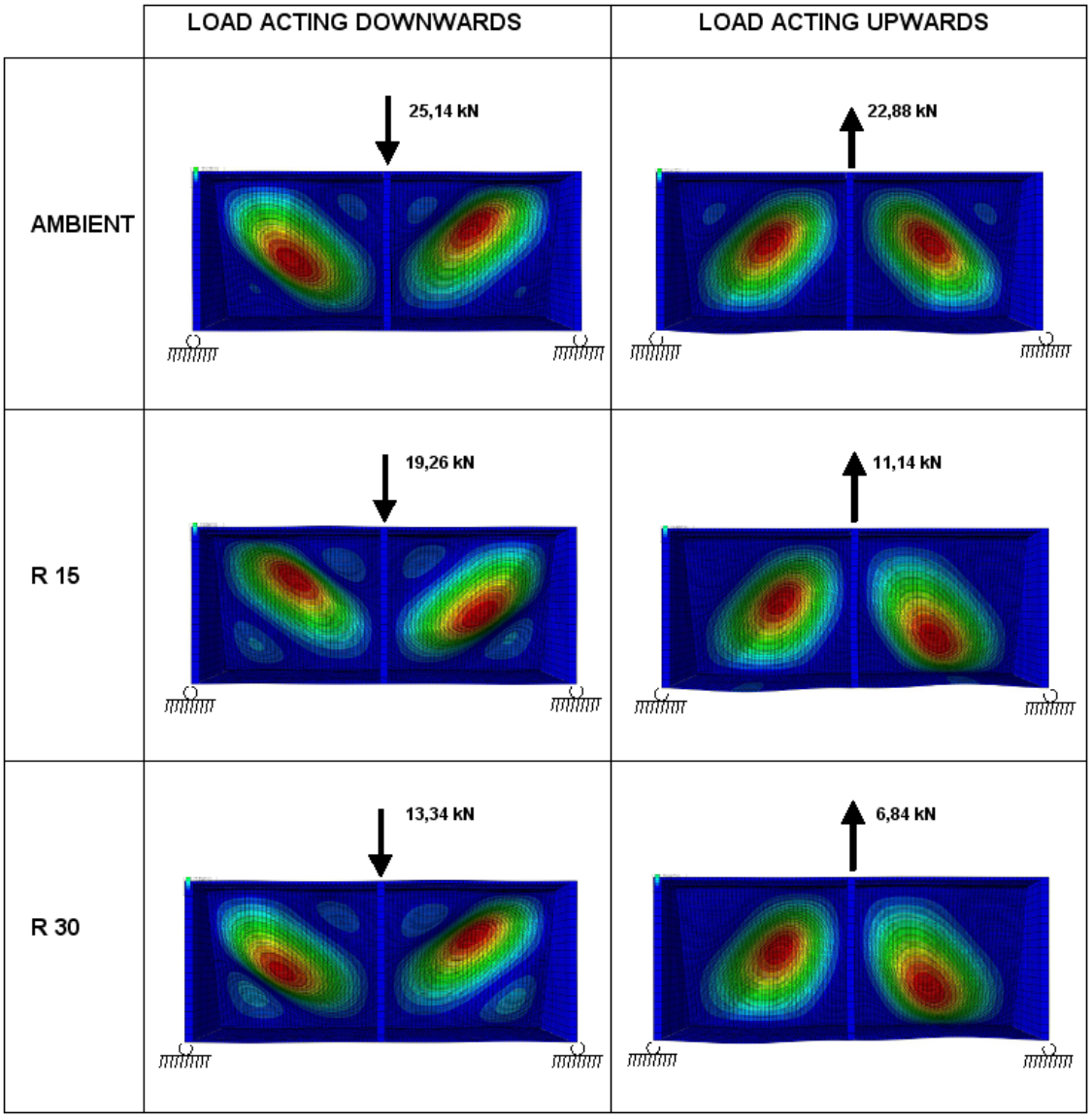

Figure 7.41. Shear buckling modes of the panel web ($a/h_w = 1$) at ambient temperature and after 15 and 30 minutes of ISO fire exposure.

In the longer structure ($a/h_w = 1$), the deformations in the lower flange were also obvious in the case of negative eigenvalues as can be seen from Figure 7.41. The absolute values of the critical load depended more on the direction of the load than with the shorter structure.

The buckling modes of both structures resembled those of Figure 4.5 in Chapter 4. The buckling occured lower because of the smaller elastic modulus.

It can be concluded, that the supporting structures have a significant effect on the shear buckling of the web. Recent studies have shown that the restraint provided by the flanges may enhance the buckling coefficient k_τ [Vimonsatit, Tan, Qian, 2007].

7.2.2. Hand-calculations with method f

The critical shear force for a single web plate ($V_{cr,web}$) is defined first, followed by the shear buckling resistance of the whole structure ($V_{cr,panel}$) at ambient temperature. The calculation applies to the case $a/h_w = 1$ and uses Equations (2.2)–(2.5):

$$\tau_{cr} = 9{,}34\frac{\pi^2 \cdot 210000}{12 \cdot (1-0{,}3^2)} \cdot \left(\frac{0{,}75}{115}\right)^2 = 75{,}40 \text{ N/mm}^2 \quad (7.17)$$

$$V_{cr,web} = 115 \cdot 0{,}75 \cdot 75{,}40 = 6{,}50 \text{ kN} \quad (7.18)$$

$$V_{cr,panel} = 2 \cdot V_{cr,web} \cdot \sin 60^o = \underline{11{,}26 \text{ kN}} \quad (7.19)$$

The critical shear forces for the case $a/h_w = 0{,}5$ are calculated similarly:

$$a/h_w = 0{,}5: \qquad V_{cr,panel} = \underline{30{,}67 \text{ kN}} \quad (7.20)$$

The results according to method f were calculated for each of the 30 minutes of standard (ISO) fire exposure. The needed web temperatures T_{cold}, T_{hot}, T_{mid} and T_{avg} shown in Figure 7.42 were derived from the thermal FEM analysis (see Fig. 7.27). The reduction factors according to method f were calculated using the analytical method illustrated in Figure 5.7. The calculation method used in this case is presented in Table 7.3. The factor $\Delta k_{E,\theta}$ is the difference between the reduction factors at hottest and coldest temperature of the web.

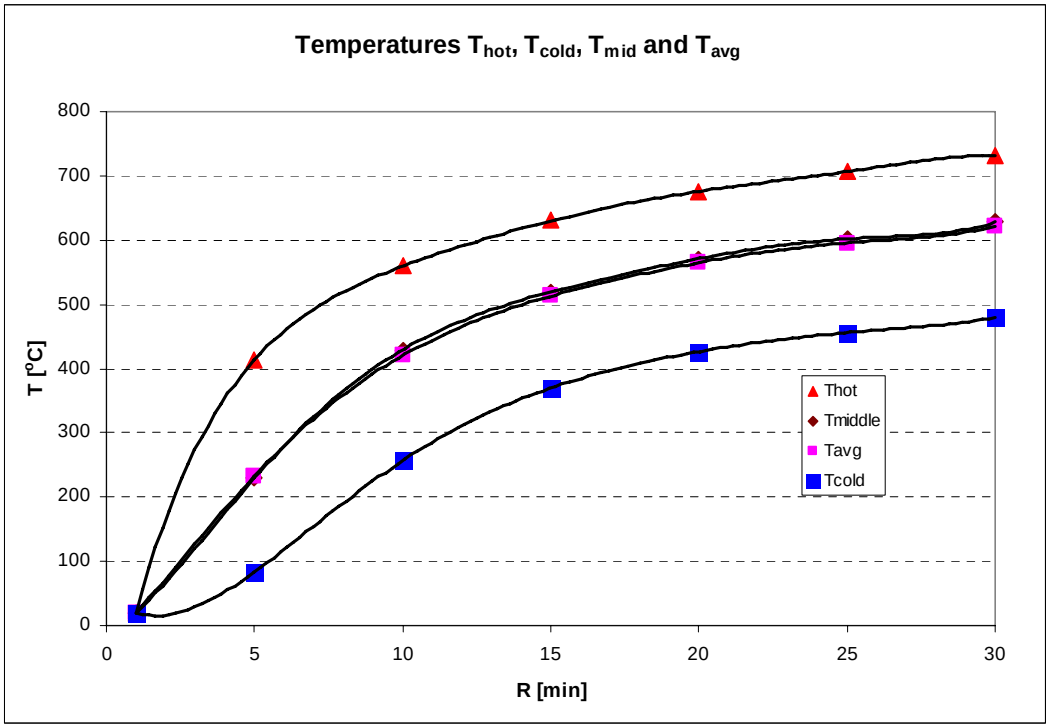

Figure 7.42. Temperatures needed in method f.

Table 7.3. Method f in spreadsheet computation.

	from FEM (see also Fig. 7.42)				EN 1993-1-2		Method f presented in Chapter 5.3 (see Fig. 5.7)								
R [min]	T_{hot}	T_{cold}	T_{mid}	T_{avg}	k_{hot}	k_{cold}	$\Delta k_{E,\theta}$	ϕ	$T_{f,1}$	$T_{f,2}$	$T_{f,3}$	$T_{f,4}$	$T_{f,5}$	T_f	$k_{E,\theta,f}$
0	20	20	20	20	1,000	1,000	0,000							20	**1,000**
1	20	20	20	20	1,000	1,000	0,000	0,0000	100	362	217	-1475	-3244	100	**1,000**
2	165	16	68	73	0,935	1,000	0,065	0,0010	115	301	185	-315	-469	115	**0,985**
3	274	29	121	128	0,826	1,000	0,174	0,0016	179	313	222	-107	-192	179	**0,921**
4	354	53	176	182	0,746	1,000	0,254	0,0019	238	342	265	-1	-67	238	**0,862**
5	414	84	230	233	0,686	1,000	0,314	0,0021	290	370	305	81	26	290	**0,810**
6	459	119	280	280	0,641	0,981	0,340	0,0021	337	399	342	143	94	337	**0,763**
7	492	155	325	322	0,608	0,945	0,337	0,0021	380	426	376	192	145	380	**0,720**
8	519	191	365	360	0,545	0,909	0,364	0,0022	424	452	412	259	220	424	**0,676**
9	541	225	400	392	0,482	0,875	0,393	0,0025	463	476	444	319	287	463	**0,637**
10	559	257	429	421	0,428	0,843	0,415	0,0027	495	497	471	367	341	495	**0,605**
11	576	285	453	445	0,380	0,815	0,434	0,0029	522	515	495	407	385	515	**0,557**
12	591	311	474	466	0,337	0,789	0,453	0,0031	545	531	515	441	422	531	**0,511**
13	605	333	491	483	0,301	0,767	0,465	0,0033	563	544	532	467	451	544	**0,473**
14	618	353	506	499	0,278	0,747	0,469	0,0034	578	555	545	488	473	555	**0,441**
15	630	370	519	513	0,256	0,730	0,474	0,0035	592	564	557	506	492	564	**0,413**
16	641	384	531	525	0,236	0,716	0,480	0,0036	604	573	568	521	509	573	**0,387**
17	651	397	542	536	0,217	0,703	0,485	0,0036	615	582	578	536	524	582	**0,363**
18	661	408	552	546	0,201	0,692	0,491	0,0037	626	590	588	549	538	590	**0,340**
19	669	418	562	556	0,186	0,682	0,496	0,0038	636	597	597	562	551	597	**0,318**
20	676	427	571	565	0,174	0,673	0,500	0,0038	645	604	605	573	563	605	**0,301**
21	682	434	579	573	0,162	0,666	0,504	0,0038	654	610	612	583	574	612	**0,288**
22	688	441	587	580	0,151	0,659	0,508	0,0038	662	616	619	593	584	619	**0,275**
23	694	447	593	586	0,140	0,653	0,513	0,0039	668	621	625	601	592	625	**0,265**
24	700	452	598	591	0,130	0,648	0,519	0,0039	674	625	630	608	599	630	**0,255**
25	707	456	602	596	0,127	0,644	0,517	0,0039	678	628	633	612	603	633	**0,250**
26	713	460	604	599	0,125	0,640	0,515	0,0038	681	630	636	615	607	636	**0,246**
27	720	464	607	602	0,122	0,636	0,514	0,0038	684	632	638	617	610	638	**0,242**
28	726	467	610	606	0,120	0,633	0,513	0,0038	687	634	641	621	613	641	**0,237**
29	730	472	616	612	0,118	0,628	0,510	0,0038	693	638	646	627	620	646	**0,228**
30	731	479	628	622	0,118	0,621	0,503	0,0037	704	645	654	638	631	654	**0,213**

Figure 7.43 provides a graphic representation of method f as regards times R5, R10, R15, R20, R25 and R30 The results are exactly the same as in Table 7.3.

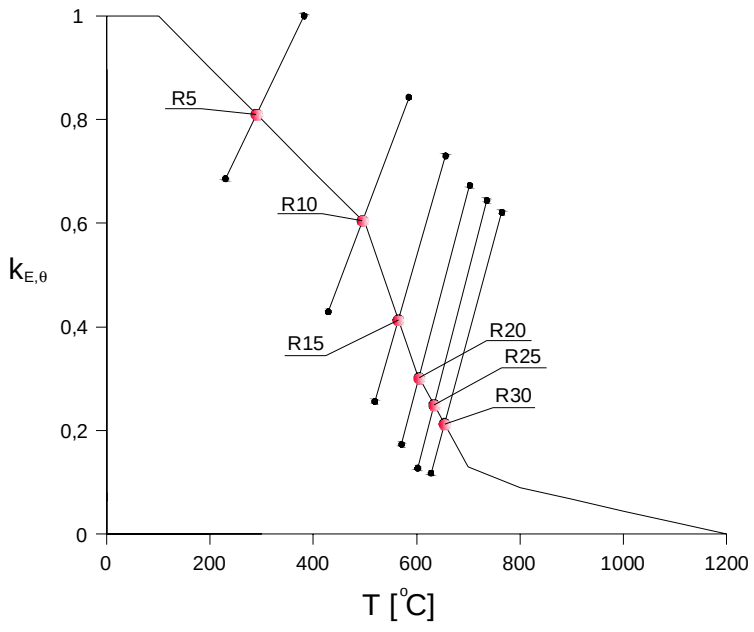

Figure 7.43. Reduction factors according to method f at R5, R10, R15, R20, R25 and R30.

Method f provides reduction factors for elastic modulus which can be used directly to reduce the shear buckling loads calculated in Equations (7.19) and (7.20). Figure 7.44 shows the reduction factors as a function of time. The reduction factors corresponding to temperatures T_{cold} and T_{hot} have also been drawn in the same graph.

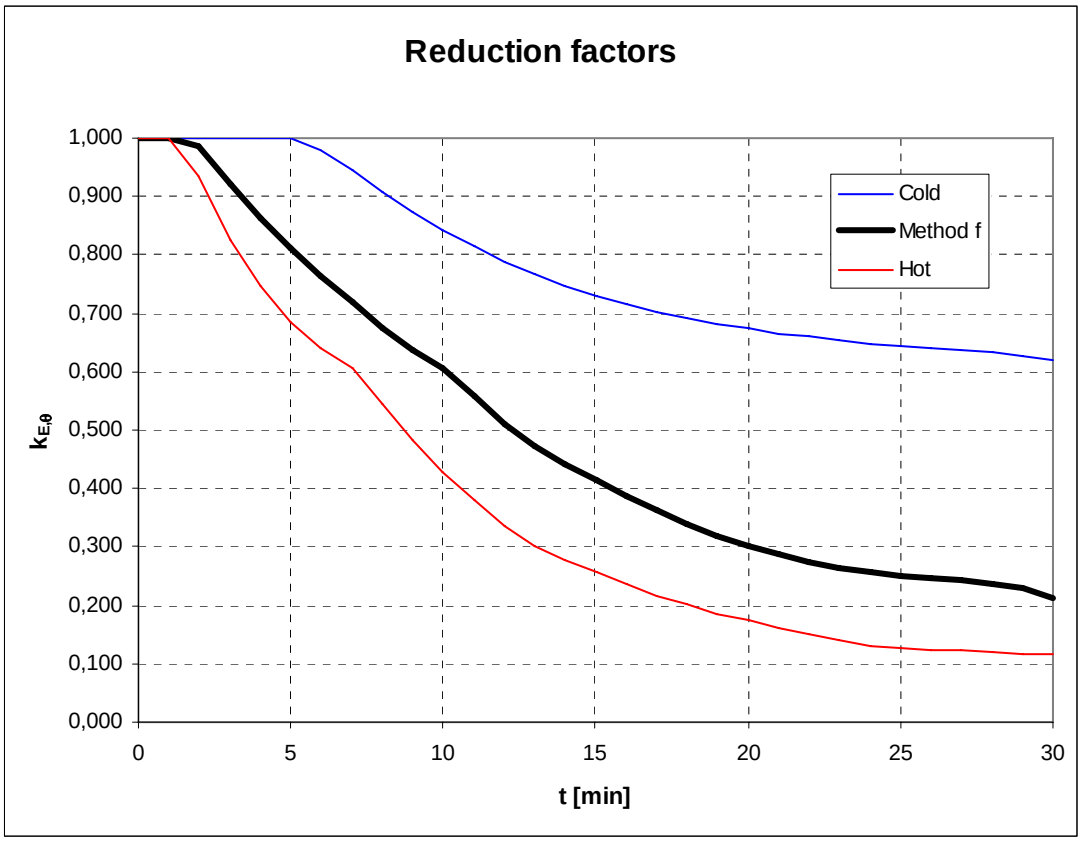

Figure 7.44. Reduction factors $k_{E,\theta,f}$, $k_{E,\theta}$ (T_{cold}) and $k_{E,\theta}$ (T_{hot}).

Figure 7.44 shows that the reduction factor from method f is clearly closer to the reduction factor corresponding to temperature T_{hot} than T_{cold}.

7.2.3. Comparison of the results

The critical shear forces at ambient and elevated temperatures from FEM analysis and hand-calculations with method f are shown in the following graphs. Figure 7.45 illustrates the case $a/h_w = 0,5$ and Figure 7.46 the case $a/h_w = 1$.

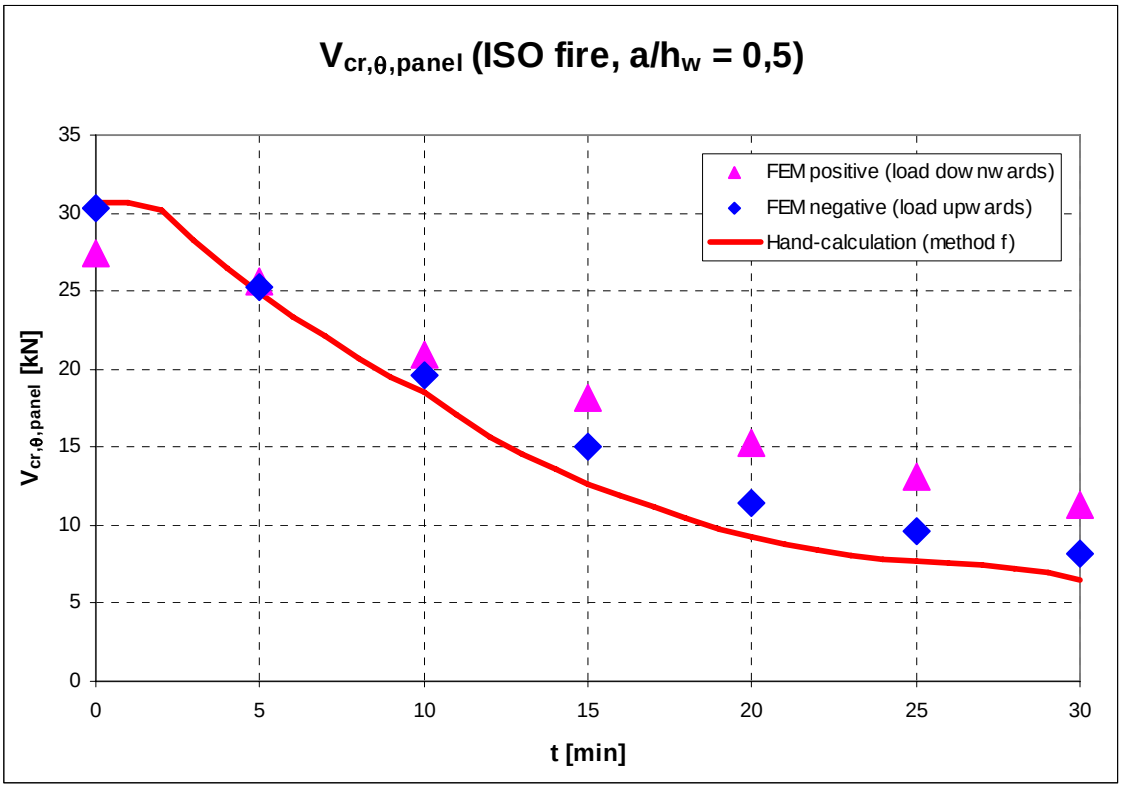

Figure 7.45. Critical shear forces for the case a/h_w = 0,5.

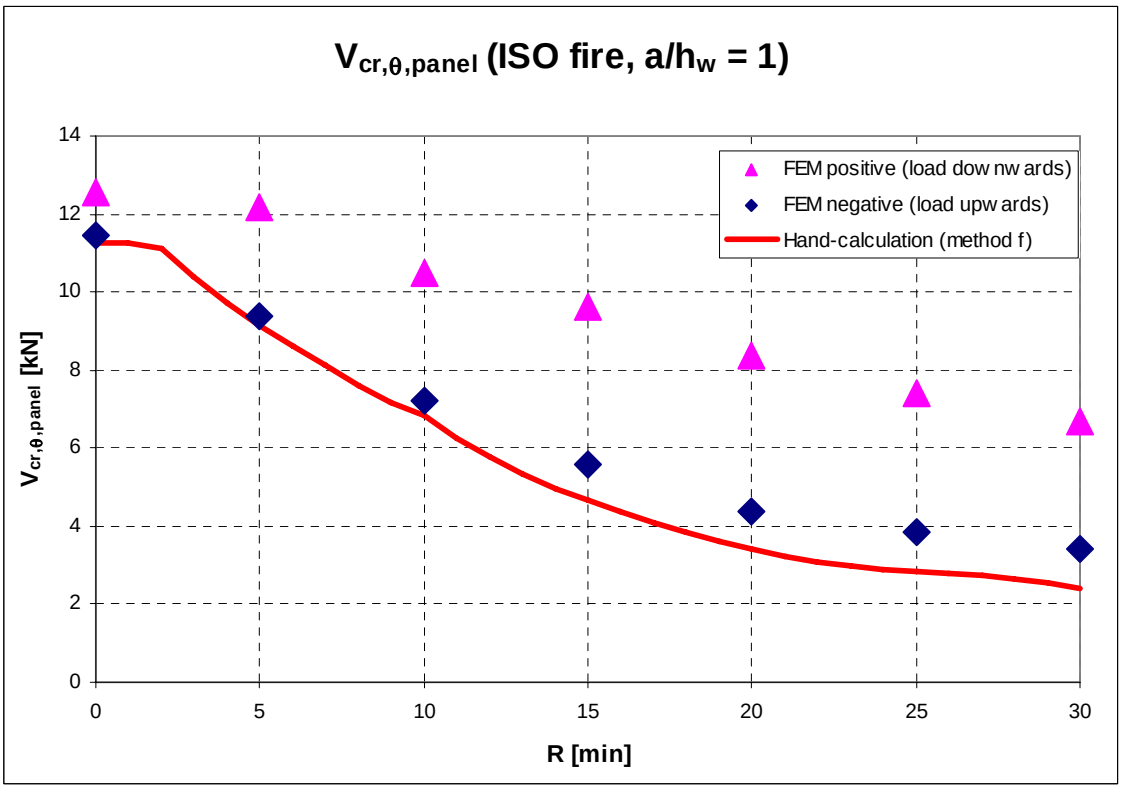

Figure 7.46. Critical shear forces for the case a/h_w = 1,0.

Figures 7.45 and 7.46 reveal that the differences between the positive and negative eigenvalues from FEM are clearly larger in the case $a/h_w = 1$. The results from the hand-calculations using the proposed method f are on the safe side at elevated temperatures in each case considered. Hand-calculations (Eqs. (7.17)-(7.20)) produced unsafe results only at ambient temperature in the case $a/h_w = 1$. Considering only the smallest absolute values for shear force, the results from FEM and hand calculations correlate quite well.

Figure 7.47 shows the minimum values for reduction factors from FEM and hand-calculations. The use of minimum values is justified, because the effect of the flanges was not taken into account in the hand-calculations.

EN 1990 [EN 1990, 2002] gives the recommended values for ψ_{fire}, which are used to reduce loads in a fire situation. The Finnish National Annex [Kansallinen liite standardiin SFS-EN 1990, 2008] defines the values for ψ in the typical cases considered in Table 7.4.

Table 7.4. Typical ψ-factors in a fire situation according to the Finnish National Annex.

Action	ψ_{fire}
Imposed loads on buildings:	
• Domestic, residential areas	0,3
• Office areas	0,3
• Congregation areas	0,3
Snow loads on buildings:	
• $s_k < 2{,}75$ kN/m^2	0,4
• $s_k \geq 2{,}75$ kN/m^2	0,5

Assuming that the entire load on the panel (Q_{amb}) is only one of the actions shown in Table 7.4 (meaning that we neglect e.g. the dead load), the load on the panel in a fire situation (Q_{fire}) can be calculated from the following:

$$Q_{fire} = \frac{\gamma_{fire}}{\gamma_{amb}} \cdot \psi_{fire} \cdot Q_{amb}, \tag{7.21}$$

where
- $\gamma_{fire} = 1{,}0$ (partial factor for actions in a fire situation),
- $\gamma_{amb} = 1{,}5$ (partial factor for live loads at ambient temperature).

Equation (7.21) shows that the resistance R_{fire} of all-metal sandwich panels in a fire situation should be at least $\psi_{fire}/1{,}5$ times the resistance R_{amb} at ambient temperature if the load from the panel is only an imposed or a snow load. For the loads considered in Table 7.4 it leads to following values:

$$\psi_{fire} = 0{,}3 \rightarrow R_{fire} = 0{,}20 \cdot R_{amb} \quad (7.22)$$

$$\psi_{fire} = 0{,}4 \rightarrow R_{fire} = 0{,}27 \cdot R_{amb} \quad (7.23)$$

$$\psi_{fire} = 0{,}5 \rightarrow R_{fire} = 0{,}33 \cdot R_{amb} \quad (7.24)$$

The required resistances at elevated temperatures ignoring the dead load of the panel (Equations (7.22)–(7.24)) are shown in Figure 7.47.

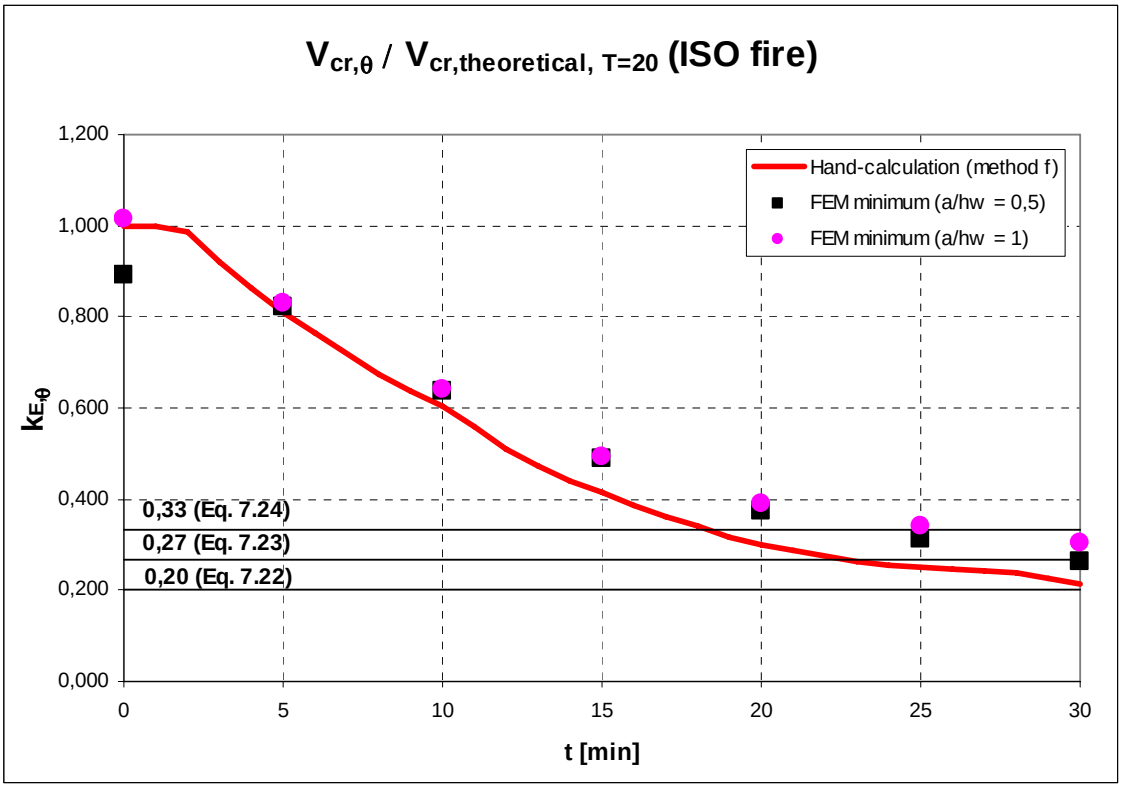

Figure 7.47. Reduction factors for the all-metal sandwich panel for imposed or snow loads only.

Figure 7.47 shows that the results of hand-calculation do not depend on the ratio a/h_w. It also reveals that the ratio $V_{cr,\theta} / V_{cr,theoretical,\ T=20}$ does not depend much on the length of the structure at elevated temperatures. At ambient temperature the result for the case $a/h_w = 0{,}5$ is unconservative.

Thus, it is obvious that the loads mentioned in Table 7.4 will not cause an all-metal sandwich panel of the examined type to shear buckle after 15 minutes' exposure to standard (ISO) fire, when dead loads are ignored. Resistance for 30 minutes can also be attained at least in the case of imposed loads on buildings ($\psi_{fire} = 0{,}3$) neglecting dead loads. If the dead load is considered, the ratio R_{amb}/R_{fire} becomes larger. In many cases the dead load of the panel is very small compared to the imposed and snow loads.

8. CONCLUSIONS

The goal of the study was to develop an analytical design method to predict the shear buckling resistance of thin metal plate at non-uniform elevated temperatures. The method was to give safe results for carbon steel, aluminium and stainless steel at different temperature distributions. Since no such test results were available, the validation of the proposed method was done by comparing its results to those of FEM calculations. The rectangular simply supported plate with different thermal boundary conditions was the basic subject of study.

Comparisons between FEM calculation and six different averaging schemata for elastic modulus showed that graphic method f gave accurate and safe results in the cases considered. It is the most accurate method for each material. The comparison involved a total of 54 cases. Only two of the results from method f were unconservative while three were more than 15 % on the safe side. On the other hand, method a, where the reduction factor for elastic modulus is taken from the middle of the height of the plate, gave only three conservative results. Direct comparison with the Eurocodes could not be done because their formulas are intended for determining ultimate shear resistance.

The proposed method f, which is presented in Chapter 5.3, is a graphic way to define the reduction of elastic modulus. The reduced elastic modulus is then applied to the whole plate, and the critical shear force is calculated using classical formulas. The method can also be presented analytically as a formula and it is easy to apply, for instance, in spreadsheet calculation.

The example calculation determined the temperatures and critical shear forces of one all-metal sandwich panel. The thermal analyses were performed using FEM and the comparison between FEM and test results showed that the calculation was reliable. Shear buckling loads of the panel in question were then defined at ambient and elevated temperatures while exposed for up to 30 minutes to standard (ISO) fire. The critical loads for two different lengths of structures were calculated by FEM and hand-calculation where the proposed method was applied. Both positive (load acting downwards) and negative (load acting upwards) eigenvalues were taken into account because the cross-section is not symmetric. The results from the example case show that the critical shear forces from the FEM calculation depend on the direction of the applied load in the case of a non-symmetric cross-section. The minimum absolute values from FEM analysis correlated quite well with the results from hand-calculations, which does

not take the effect of the flanges into account. According to FEM calculations, the flanges seem to have a significant effect on the results.

Shear buckling resistance is the first phase of the ultimate shear resistance of a thin plate. Tension field resistance and the effect of the flanges were ignored in this study, but their contribution to ultimate shear resistance is significant especially in the case of a slender plate.

Further research is needed to find a design method to predict the tension field resistance of a thin metal plate at non-uniform elevated temperatures. It means that yield strength reductions must also be known. The design method can be validated by using results calculated by commercial finite element software. Material and geometric non-linearity will be considered in this case. The buckling modes of the plates from this study can be used as imperfections in tension field FEM analysis.

The benchmark cases to validate the FEM models will be consist of the resistances of the plates at uniform elevated temperatures. The results will be compared to test results available in literature and Eurocode resistances. The kinds of plates and temperature distributions used in this study can also be used in that research.

REFERENCES

ABAQUS / Standard, User's Manual, Volume II, Version 6.2, Hibbitt, Karlsson & Sorensen, Inc. 2001

ABAQUS / Analysis User's Manual, Version 6.7, Dassault Systemes, 2007

ABAQUS / CAE User's Manual, Version 6.7, Dassault Systemes, 2007

AISC, Specification for the design, fabrication and erection of structural steel for building, New York (USA), American Institute of Steel Construction, 1963

Ala-Outinen T., Schaumann P., Kaitila O., Kettner F., Light weight structures exposed to fire: a stainless steel sandwich panel, Proceedings of the Fourth International Workshop: Structures in Fire, Aveiro, 2006, pp. 139-150

Alinia M.M., Gheitasi A., Erfani S., Plastic shear buckling of unstiffened stocky plates, Journal of Constructional Steel Research 65, 2009, pp. 1631-1643

Basler K., Thurlimann B., Plate girder research, In: Proceedings of AISC national engineering conference, 1959

Basler K., Strength of plate girder in shear, Journal of the Structural Division ASCE 1961; 87(ST7): 151-80

Basler K., Strength of plate girder under combined bending and shear, Journal of the Structural Division ASCE 1961;87(ST7): 181-97

Bryan G.H., On the stability of a plane plate under thrust in its own plane, with applications to the "buckling" of the sides of a ship, Proc. London Math. Society, Vol 22, 1891, pp. 54-67

BS 5950, Part I, Structural use of steelwork in building, In: Code of practice for design in simple and continous construction: Hot rolled sections, British Standards Institution, 1990

Colombi jr R.A., Ship Fires vs. Structure Fires: Differences and Preparation, Fire Engineering, November 2009, pp. 79-84

COMSOL Multiphysics User's Guide, Version 3.5a, COMSOL AB, 2008

COMSOL Heat Transfer Module User's Guide, Version 3,5a, COMSOL AB, 2008

Drysdale D., An Introduction to Fire Dynamics, John Wiley & Sons, 2004

Dubas P., Gehri E., (Eds.) Behaviour and Design of Steel Plated Structures, ECCS Technical Committee 8, Structural Stability, no 44, 1986

EN 1990, Eurocode – Basis of structural design, CEN, Bryssels, 2002

EN 1991-1-2, Eurocode 1: Actions on structures, Part 1-2: General actions – Actions on structures exposed to fire, CEN, Bryssels, 2002

EN 1993-1-1, Eurocode 3: Design of steel structures, Part 1-1: General rules and rules for buildings, CEN, Bryssels, 2005

EN 1993-1-2, Eurocode 3: Design of steel structures, Part 1-2: Structural fire design, CEN, Bryssels, 2005

EN 1993-1-4, Eurocode 3: Design of steel structures, Part 1-4: General rules, Supplementary rules for stainless steels, CEN, Bryssels, 2006

EN 1993-1-5, Eurocode 3: Design of steel structures, Part 1-5: Plated structural elements, CEN, Bryssels, 2005

EN 1999-1-1, Eurocode 9: Design of aluminium structures, Part 1-1: General structural rules, CEN, Bryssels, 2007

EN 1999-1-2, Eurocode 9: Design of aluminium structures, Part 1-2: Structural fire design, CEN, Bryssels, 2007

Feng M., Wang Y.C., Davies J.M, Axial strength of cold-formed thin-walled steel channels under non-uniform temperatures in fire, Fire Safety Journal 38, 2003, pp.679-707

Franssen J.M., Cooke G.M.E., Latham D.J., Numerical Simulation of a Full Scale Fire Test on a Loaded Steel Framework, Journal of Constructional Steel Research 35, 1995, pp. 377-408

Heinisuo M., Ylihärsilä H., All Metal Structures at Elevated Temperatures, Tampere University of Technology, Institute of Structural Engineering, Research Report 135, Tampere 2006

Höglund T., Design of thin plate I-girders in shear and bending with special reference to web buckling, Bull. 94, Division of Building Statics and Structural Engineering, Royal Institute of Technology, Stockholm, 1981

Höglund T., Shear Buckling Resistance of Steel and Aluminium Plate Girders, Thin-Walled Structures Vol. 29, Nos. 1-4, 1997, pp. 13-30

Johansson B., Maquoi R., Sedlacek G., New design rules for plated structures in Eurocode 3, Journal of Constructional Steel Research 57, 2001, pp. 279-311

Kaitila O., Finite element modeling of cold-formed steel members at high temperatures, Helsinki University of Technology, Laboratory of Steel Structures, Publications TKK-TER-24, Otamedia, Espoo, 2002

Kansallinen liite standardiin SFS-EN 1990 eurokoodi. Rakenteiden suunnitteluperusteet (In Finnish), Ympäristöministeriö, Helsinki, 2008

Kansallinen liite standardiin SFS-EN 1993-1-5 Eurokoodi 3: Teräsrakenteiden suunnittelu. Osa 1-5: Tasomaiset levyrakenteet (In Finnish), Ympäristöministeriö, Helsinki, 2008

Liang Q.Q., Uy B., Bradford M.A., Ronagh H.R., Ultimate strength of continous composite beams in combined bending and shear, Journal of Constructional Steel Research 60, 2004, pp. 1109-1128

Liu T.C.H., Chung K.F., Steel beams with large web openings of various shapes and sizes: finite element investigation, Journal of Constructional Steel Research 59, 2003, pp. 1159-1176

Lois P., Wang J., Wall A., Ruxton T., Formal safety assessment of cruise ships, Tourism Management 25, 2004, pp. 93-109

Rayleigh J.W., The theory of sound, First Edition in 1877

RakMK, C4, Lämmöneristys, Ohjeet 2003, Suomen rakentamismääräyskokoelma, Ympäristöministeriö, asunto- ja rakennusosasto, RT RakMK-21217, Helsinki, 2003

Rautaruukki Metform 2000, Rautaruukki's structural hollow section manual (in Finnish), Hämeenlinna.

Ritz W., Ueber eine neue Methode zur Lösung gewisser Variationsprobleme der mathematischen Physik, Journal fur reine und angewandte Mathematic, Bd. 135, 1908, pp. 1-61

Rockey K.C., Evans H.R., Porter D.M., Design method for predicting the collapse behaviour of plate girders, In: Proceedings of the institution of civil engineers, part 2, 1978, pp. 85-112

Rode H.H., Beitrag zur Theorie der Knickerscheinungen, Der Eisenbau, 1916, pp. 210-218

Roh J.S., Ryou H.S., Park W.H., Jang Y.J., CFD simulation and assessment of life safety in a subway train fire, Tunnelling and Underground Space Technology 24, 2009, pp. 447-453

Saint-Venant Barre de, p. 704 of his discussion of Clebsch's Theory of Elasticity of Solid Bodies, 1883

Salminen M., Heinisuo M., Aalto A., Shear Buckling of Steel Plates at Elevated Temperatures, 10th Finnish Mechanics Days, 3-4.12.2009, Jyväskylä

Tan K.H., Qian Z.H., Experimental behaviour of a thermally restrained plate girder loaded in shear at elevated temperature, Journal of Constructional Steel Research 64, 2008, pp. 596-606

Teräsnormikortti N:o 21/2009, WQ-palkin poikkileikkauksen mitoitus normaali- ja palotilanteessa (In Finnish), TRY, 2009

Timoshenko S.P., Bull. Polytech. Inst. Kiev, 1910; French translation in Ann. Ponts et Chaussees, Paris 1913, 2eme semester, pp. 374-412

Timoshenko S.P., Theory of Elastic Stability, McGraw-Hill Book Company, Inc., New York and London, 1936.

Vimonsatit V., Tan K.H., Qian Z.H., Testing of plate girder web panel loaded in shear, Journal of structural Engineering, ASCE, 2007

Vimonsatit V., Tan K.H., Ting S.K., Shear strength of plate girder web panel at elevated temperature, Journal of Constructional Steel Research 63, 2007, pp. 1442-1451

von Karman Th., Festigkeitsprobleme im Maschinenbau, Encyklopädie der matematischen Wissenschaften, Teilband IV.4, Teubner, Leipzig, 1910, pp. 348-350

von Karman, Th., Sechler E. E., Donnel, L. H., The strength of thin plates in compression, Trans. ASME, Appl. Mech., APM-54-5, 1932, pp. 53-57

Wagner H., Flat sheet metal girder with very thin metal web, National Advisory Committee for Aeronautics, 1931

Yin Y.Z., Wang Y.C., Numerical simulations of the effects of non-uniform temperature distributions on lateral torsional buckling resistance of steel I-beams, Journal of Constructional Steel Research 59, 2003, pp. 1009-1033

Yoo C.H., Lee S.C., Mechanics of Web Panel Postbuckling Behavior in Shear, Journal of Structural Engineering, October 2006, pp. 1580-1589

Zheng Y.Q., Han, L.H., Calculations on the fire resistance of steel reinforced concrete (SRC) columns, Advances in Steel Structures, Vol. II, 2005, pp. 1017-1022

APPENDIX A. TYPICAL KEYWORDS FOR *ABAQUS* / *CAE* PLATE CALCULATIONS

```
*Part, name=PL_1_POST_B
*End Part
**
**
** ASSEMBLY
**
*Assembly, name=Assembly
**
*Instance, name=PL_1_POST_B-3, part=PL_1_POST_B
*Element, type=S4R
** Section: PL_1_POST_B
*Shell Section, elset=_PickedSet2, material=POST_Steel
0.01, 5
*End Instance
**
*Nset, nset=Setti_2, instance=PL_1_POST_B-3, generate
*Elset, elset=Setti_2, instance=PL_1_POST_B-3, generate
*Surface, type=ELEMENT, name=_PickedSurf32, internal
*Surface, type=ELEMENT, name=_PickedSurf41, internal
*Surface, type=ELEMENT, name=_PickedSurf84, internal
*Surface, type=ELEMENT, name=_PickedSurf85, internal
*End Assembly
**
** MATERIALS
**
*Material, name=Aluminum
*Elastic
   7e+10, 0.3,  0.
   7e+10, 0.3, 20.
6.93e+10, 0.3, 50.
6.79e+10, 0.3,100.
6.51e+10, 0.3,150.
6.02e+10, 0.3,200.
5.46e+10, 0.3,250.
4.76e+10, 0.3,300.
3.78e+10, 0.3,350.
 2.8e+10, 0.3,400.
  0.001, 0.3,550.
```

```
*Material, name=POST_Steel
*Elastic
   2.1e+11,  0.3,   0.
   2.1e+11,  0.3, 100.
  1.89e+11,  0.3, 200.
  1.68e+11,  0.3, 300.
  1.47e+11,  0.3, 400.
  1.26e+11,  0.3, 500.
  6.51e+10,  0.3, 600.
  2.73e+10,  0.3, 700.
  1.89e+10,  0.3, 800.
1.4175e+10,  0.3, 900.
  9.45e+09,  0.3,1000.
 4.725e+09,  0.3,1100.
     0.001,  0.3,1200.
*Plastic
  3.55e+08,   0.,   0.
  3.55e+08,   0., 400.
 2.769e+08,   0., 500.
1.6685e+08,   0., 600.
 8.165e+07,   0., 700.
 3.905e+07,   0., 800.
  2.13e+07,   0., 900.
  1.42e+07,   0.,1000.
   7.1e+06,   0.,1100.
     0.001,   0.,1200.
*Material, name=Stainless_steel
*Elastic
   2e+11,  0.3,   0.
   2e+11,  0.3,  20.
1.92e+11,  0.3, 100.
1.84e+11,  0.3, 200.
1.76e+11,  0.3, 300.
1.68e+11,  0.3, 400.
 1.6e+11,  0.3, 500.
1.52e+11,  0.3, 600.
1.42e+11,  0.3, 700.
1.26e+11,  0.3, 800.
   9e+10,  0.3, 900.
   4e+10,  0.3,1000.
   2e+10,  0.3,1100.
   0.001,  0.3,1200.
```

```
**
**
** BOUNDARY CONDITIONS
**
** Name: A_Y Type: Displacement/Rotation
*Boundary
_PickedSet58, 3, 3
_PickedSet58, 5, 5
_PickedSet58, 6, 6
** Name: O_V Type: Displacement/Rotation
*Boundary
_PickedSet59, 3, 3
_PickedSet59, 4, 4
_PickedSet59, 6, 6
** Name: POST_muut_pisteet Type: Displacement/Rotation
*Boundary
_PickedSet36, 3, 3
_PickedSet36, 4, 4
_PickedSet36, 5, 5
_PickedSet36, 6, 6
** Name: POST_piste_A Type: Displacement/Rotation
*Boundary
_PickedSet35, 1, 1
_PickedSet35, 2, 2
_PickedSet35, 3, 3
_PickedSet35, 4, 4
_PickedSet35, 5, 5
_PickedSet35, 6, 6
**
** PREDEFINED FIELDS
**
** Name: Linear   Type: Temperature Using Field: Lin100-900
*Initial Conditions, type=TEMPERATURE
PL_1_POST_B-3.1, 900.
PL_1_POST_B-3.2, 900.
.
.
.
.
PL_1_POST_B-3.2600, 100.
PL_1_POST_B-3.2601, 100.
** ----------------------------------------------------------------
```

```
**
** STEP: BUCKLING
**
*Step, name=BUCKLING, perturbation
*Buckle
2, 2., 4, 30
**
** BOUNDARY CONDITIONS
**
** Name: A_Y Type: Displacement/Rotation
*Boundary, op=NEW, load case=1
_PickedSet58, 3, 3
_PickedSet58, 5, 5
_PickedSet58, 6, 6
*Boundary, op=NEW, load case=2
_PickedSet58, 3, 3
_PickedSet58, 5, 5
_PickedSet58, 6, 6
** Name: O_V Type: Displacement/Rotation
*Boundary, op=NEW, load case=1
_PickedSet59, 3, 3
_PickedSet59, 4, 4
_PickedSet59, 6, 6
*Boundary, op=NEW, load case=2
_PickedSet59, 3, 3
_PickedSet59, 4, 4
_PickedSet59, 6, 6
** Name: POST_muut_pisteet Type: Displacement/Rotation
*Boundary, op=NEW, load case=1
_PickedSet36, 3, 3
_PickedSet36, 4, 4
_PickedSet36, 5, 5
_PickedSet36, 6, 6
*Boundary, op=NEW, load case=2
_PickedSet36, 3, 3
_PickedSet36, 4, 4
_PickedSet36, 5, 5
_PickedSet36, 6, 6
** Name: POST_piste_A Type: Displacement/Rotation
*Boundary, op=NEW, load case=1
_PickedSet35, 1, 1
_PickedSet35, 2, 2
```

```
_PickedSet35, 3, 3
_PickedSet35, 4, 4
_PickedSet35, 5, 5
_PickedSet35, 6, 6
*Boundary, op=NEW, load case=2
_PickedSet35, 1, 1
_PickedSet35, 2, 2
_PickedSet35, 3, 3
_PickedSet35, 4, 4
_PickedSet35, 5, 5
_PickedSet35, 6, 6
**
** LOADS
**
** Name: BUCKLE_oikea_vasen   Type: Shell edge load
*Dsload
_PickedSurf84, EDSHR, -1000.
** Name: BUCKLE_yla_ala   Type: Shell edge load
*Dsload
_PickedSurf85, EDSHR, 1000.
**
** OUTPUT REQUESTS
**
*Restart, write, frequency=0
**
** FIELD OUTPUT: F-Output-2
**
*Output, field, variable=PRESELECT
*node file, nset=assembly.Setti_2,mode=1,last mode=1
u
*End Step
```

APPENDIX B. COMSOL MODEL REPORT OF PANEL

COMSOL Model Report

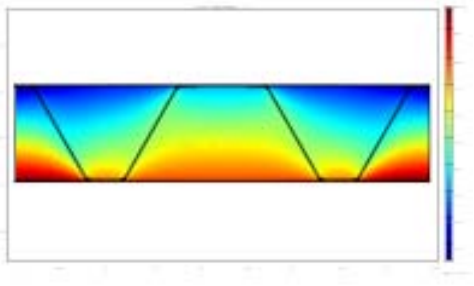

1. Table of Contents

2. Model Properties

Property	Value
Model name	
Author	
Company	
Department	
Reference	
URL	
Saved date	Jan 25, 2010 10:12:27 AM
Creation date	Aug 19, 2009 8:58:34 AM
COMSOL version	COMSOL 3.5.0.603

File name: E:\salmine0\Aktiiviset työtiedostot\Kuumat_Uumat\COMSOL\Panel_1-103_1\Valmiit_mallit\Panel_1-103_1_Testitulokset.mph

Application modes and modules used in this model:

- Geom1 (2D)
    - General Heat Transfer (Heat Transfer Module)

3. Constants

Name	Expression	Value	Description
p0	1[atm]		
rho0	1.205[kg/m^3]		

4. Geometry

Number of geometries: 1

4.1. Geom1

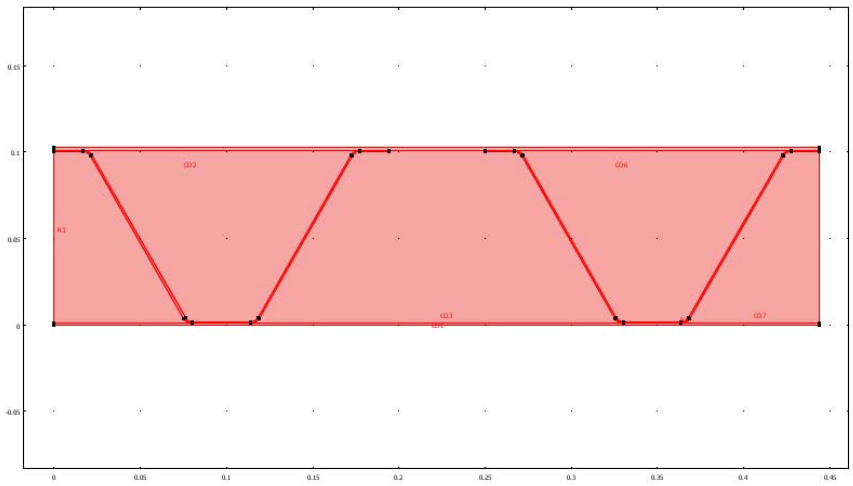

4.1.1. Point mode

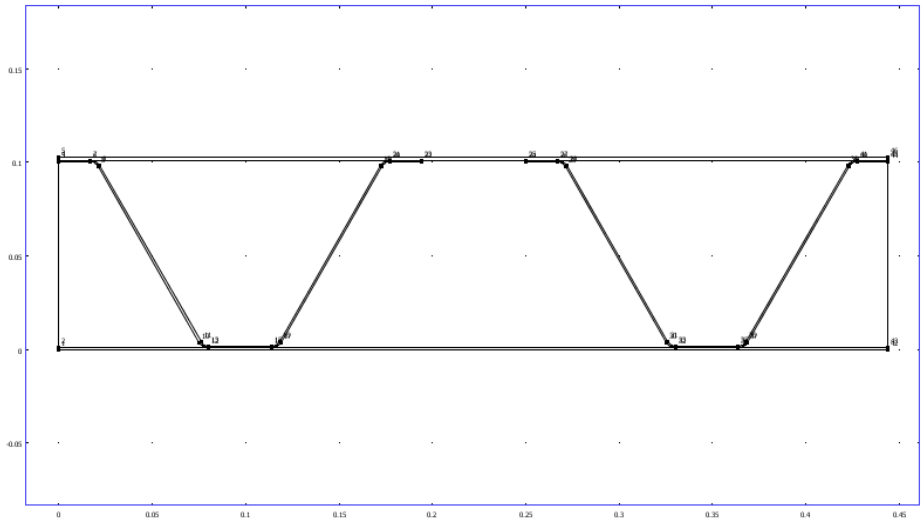

4.1.2. Boundary mode

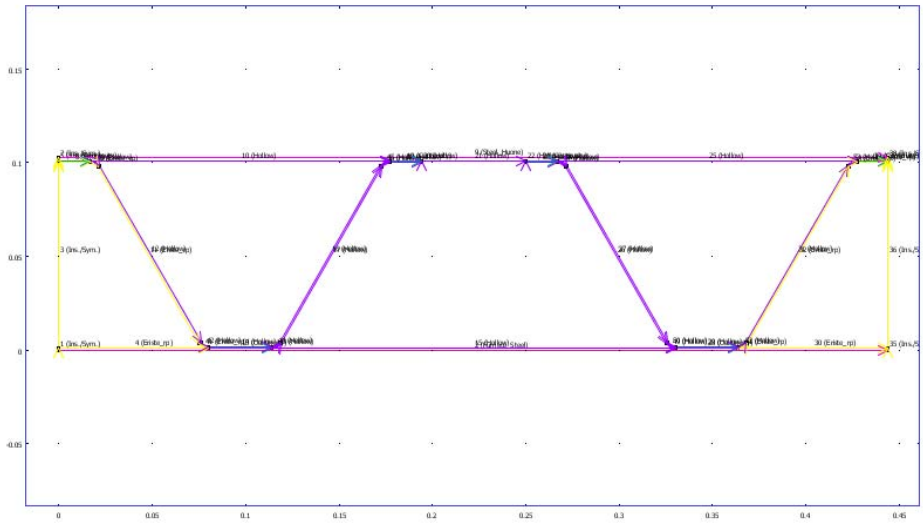

4.1.3. Subdomain mode

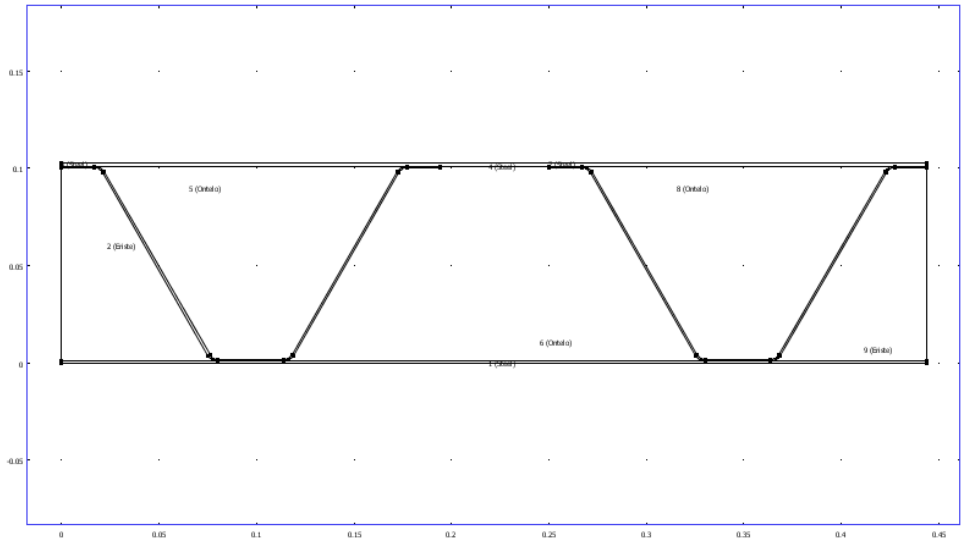

5. Geom1

Space dimensions: 2D

Independent variables: x, y, z

5.1. Mesh

5.1.1. Mesh Statistics

Number of degrees of freedom	24484
Number of mesh points	5972
Number of elements	11435
Triangular	11435
Quadrilateral	0
Number of boundary elements	2127
Number of vertex elements	46
Minimum element quality	0.148
Element area ratio	0

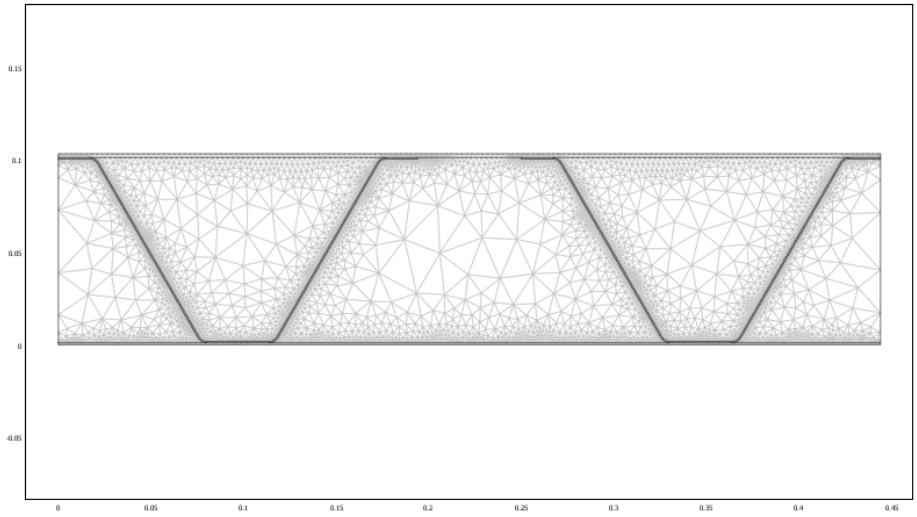

5.2. Application Mode: General Heat Transfer (htgh)

Application mode type: General Heat Transfer (Heat Transfer Module)

Application mode name: htgh

5.2.1. Scalar Variables

Name	Variable	Value	Unit	Description
sigma	sigma_htgh	5.67e-8	W/(m^2*K^4)	Stefan-Boltzmann constant
Rg	Rg_htgh	8.31451	J/(mol*K)	Universal gas constant

5.2.2. Application Mode Properties

Property	**Value**
Default element type	Lagrange - T_2 J_1
Analysis type	Transient
Out-of-plane heat transfer	Disabled
Surface-to-surface radiation method	Hemicube
Radiation integration order	4
Radiation resolution	256
Cache view factors	Auto
Turbulence model	None
Predefined multiphysics application	Off
Frame	Frame (ref)
Weak constraints	Off
Constraint type	Ideal

5.2.3. Variables

Dependent variables: T, J

Shape functions: shlag(1,'J'), shlag(2,'T')

Interior boundaries active

5.2.4. Boundary Settings

Boundary		1, 3, 5, 7, 35-38	2	4, 6, 11, 30, 32-33, 39, 41, 51, 54
Type		Insulation/Symmetry	Heat flux	Continuity
name		**Ins./Sym.**	**Furnace_Steel**	**Eriste_rp**
Shape functions (shape)		**shlag(1,'J') shlag(2,'T')**	**shlag(1,'J') shlag(2,'T')**	**shlag(1,'J') shlag(2,'T')**
Heat transfer coefficient (h)	$W/(m^2 \cdot K)$	**5.0[W/(m^2*K)]**	**25**	0
External temperature (Tinf)	K	**Tfire(t/60)[degC]**	**Ttest(t)[degC]**	**T**
Surface emissivity (epsilon)	1	**0.7**	**0.7**	**0.7**
Ambient temperature (Tamb)	K	**Tfire(t/60)[degC]**	**Ttest(t)[degC]**	**Tfire(t/60)[degC]**
Radiation type: (radType)		**Surface-to-ambient**	**Surface-to-ambient**	None
Layer thermal conductivity (ks)	$W/(m \cdot K)$	{400,0;0,400}	**{k(T[1/K])[W/(m*K)],0;0,k(T[1/K])[W/(m*K)]} (Air)**	{400,0;0,400}
Layer density (rhos)	kg/m^3	8700	**rho(p[1/Pa],T[1/K])[kg/m^3] (Air)**	8700
Layer heat capacity (Cs)	$J/(kg \cdot K)$	385	**Cp(T[1/K])[J/(kg*K)] (Air)**	385

Boundary		8, 13, 19, 24, 28, 34	9	10, 12, 14-18, 20-23, 25-27, 29, 31, 40, 42-50, 52-53
Type		Continuity	Heat flux	Heat source/sink
name		**Continuity**	**Steel_Huone**	**Hollow**
Shape functions (shape)		**shlag(1,'J') shlag(2,'T')**	**shlag(1,'J') shlag(2,'T')**	**shlag(1,'J') shlag(2,'T')**
Heat transfer coefficient (h)	$W/(m^2 \cdot K)$	**5.0[W/(m^2*K)]**	**7.7**	**25**
External temperature (Tinf)	K	**Tfire(t/60)[degC]**	**20[degC]**	**T**

Surface emissivity (epsilon)	1	**0.7**	**0.7**	**0.7**
Ambient temperature (Tamb)	K	**Tfire(t/60)[degC]**	**20[degC]**	**T**
Radiation type: (radType)		**Surface-to-ambient**	**Surface-to-ambient**	**Surface-to-surface**
Layer thermal conductivity (ks)	W/(m·K)	{400,0;0,400}	{400,0;0,400}	{400,0;0,400}
Layer density (rhos)	kg/m^3	8700	8700	8700
Layer heat capacity (Cs)	J/(kg·K)	385	385	385

5.2.5. Subdomain Settings

Subdomain		1, 3-4, 7	2, 9	5-6, 8
Shape functions (shape)		**shlag(1,'J') shlag(2,'T')**	**shlag(1,'J') shlag(2,'T')**	**shlag(1,'J') shlag(2,'T')**
name		**Steel**	**Eriste**	**Ontelo**
Opacity: (opacity)		Opaque	Opaque	**Transparent**
Thermal conductivity (k)	W/(m·K)	**{k(T[1/degC])[W/m/K],0;0,k(T[1/degC])[W/m/K]} (Miksa_Steel)**	**{H(T[1/degC]),0;0,H(T[1/degC])}**	**{k(T[1/K])[W/(m*K)],0;0,k(T[1/K])[W/(m*K)]} (Air)**
Density (rho)	kg/m^3	**7850[kg/m^3] (Miksa_Steel)**	**128**	**rho(p0[1/Pa],T[1/K])[kg/m^3] (Air)**
Heat capacity at constant pressure (C)	J/(kg·K)	**C(T[1/degC])[J/kg/K] (Miksa_Steel)**	**840**	**Cp(T[1/K])[J/(kg*K)] (Air)**
Ratio of specific heats (gamma)	1	1	**1.4**	**1.4 (Air)**
Dynamic viscosity (eta)	Pa·s	1	**eta(T[1/K])[Pa*s] (Air)**	**eta(T[1/K])[Pa*s] (Air)**
Streamline diffusion type (sdtype)		**Galerkin least-squares (GLS)**	**Galerkin least-squares (GLS)**	**Galerkin least-squares (GLS)**

Subdomain initial value		1, 3-4, 7	2, 9	5-6, 8
Temperature (T)	K	293.15	293.15	293.15

6. Materials/Coefficients Library

6.1. Miksa_Steel

Parameter	**Value**
Heat capacity at constant pressure (C)	C(T[1/degC])[J/kg/K]

Young's modulus (E)	200e9[Pa]
Yield stress level (Sys)	355[MPa]
Thermal expansion coeff. (alpha)	12.3e-6[1/K]
Relative permittivity (epsilonr)	1
Thermal conductivity (k)	k(T[1/degC])[W/m/K]
Relative permeability (mur)	1
Poisson's ratio (nu)	0.3
Density (rho)	7850[kg/m^3]
Electric conductivity (sigma)	4.032e6[S/m]

6.1.1. Piecewise Analytic Functions

6.1.1.1. Function: k(T)

Type: General

x_{start}	x_{end}	f(x)
20	800	54-3.33e-2*T
800	1200	27.3

6.1.1.2. Function: C(T)

Type: General

x_{start}	x_{end}	f(x)
20	600	425+7.73e-1*T-1.69e-3*T^2+2.22e-6*T^3
600	735	666+13002/(738-T)
735	900	545+17820/(T-731)
900	1200	650

6.2. Air

Parameter	Value
Heat capacity at constant pressure (C)	Cp(T[1/K])[J/(kg*K)]
Speed of sound (cs)	cs(T[1/K])[m/s]
Dynamic viscosity (eta)	eta(T[1/K])[Pa*s]
Ratio of specific heats (gamma)	1.4
Thermal conductivity (k)	k(T[1/K])[W/(m*K)]
Kinematic viscosity (nu0)	nu0(T[1/K])[m^2/s]
Density (rho)	rho(p[1/Pa],T[1/K])[kg/m^3]
Electric conductivity (sigma)	0[S/m]

6.2.1. Functions

Function	Expression	Derivatives	Complex output
cs(T)	sqrt(1.4*287*T)	d(sqrt(1.4*287*T),T)	false
rho(p,T)	p*0.02897/8.314/T	d(p*0.02897/8.314/T,p), d(p*0.02897/8.314/T,T)	false

6.2.2. Piecewise Analytic Functions

6.2.2.1. Function: Cp(T)

Type: Polynomial

x_{start}	x_{end}	f(x)

200	1600	0 1.04763657E+03 1 -3.72589265E-01 2 9.45304214E-04 3 -6.02409443E-07 4 1.28589610E-10

6.2.2.2. Function: eta(T)

Type: Polynomial

x_{start}	x_{end}	f(x)
200	1600	0 -8.38278000E-07 1 8.35717342E-08 2 -7.69429583E-11 3 4.64372660E-14 4 -1.06585607E-17

6.2.2.3. Function: nu0(T)

Type: Polynomial

x_{start}	x_{end}	f(x)
200	1600	0 -5.86912450E-06 1 5.01274491E-08 2 7.50108343E-11 3 1.80336823E-15 4 -2.91688030E-18

6.2.2.4. Function: k(T)

Type: Polynomial

x_{start}	x_{end}	f(x)
200	1600	0 -2.27583562E-03 1 1.15480022E-04 2 -7.90252856E-08 3 4.11702505E-11 4 -7.43864331E-15

6.3. Air_1

Parameter	Value
Heat capacity at constant pressure (C)	Cp(T[1/K])[J/(kg*K)]
Speed of sound (cs)	cs(T[1/K])[m/s]
Dynamic viscosity (eta)	eta(T[1/K])[Pa*s]
Ratio of specific heats (gamma)	1.4
Thermal conductivity (k)	k(T[1/K])[W/(m*K)]
Kinematic viscosity (nu0)	nu0(T[1/K])[m^2/s]
Density (rho)	rho(p[1/Pa],T[1/K])[kg/m^3]
Electric conductivity (sigma)	0[S/m]

6.3.1. Functions

Function	Expression	Derivatives	Complex output
cs(T)	sqrt(1.4*287*T)	d(sqrt(1.4*287*T),T)	false
rho(p,T)	p*0.02897/8.314/T	d(p*0.02897/8.314/T,p), d(p*0.02897/8.314/T,T)	false

6.3.2. Piecewise Analytic Functions

6.3.2.1. Function: Cp(T)

Type: Polynomial

x_{start}	x_{end}	f(x)
200	1600	0 1.04763657E+03 1 -3.72589265E-01 2 9.45304214E-04 3 -6.02409443E-07 4 1.28589610E-10

6.3.2.2. Function: eta(T)

Type: Polynomial

x_{start}	x_{end}	f(x)
200	1600	0 -8.38278000E-07 1 8.35717342E-08 2 -7.69429583E-11 3 4.64372660E-14 4 -1.06585607E-17

6.3.2.3. Function: nu0(T)

Type: Polynomial

x_{start}	x_{end}	f(x)
200	1600	0 -5.86912450E-06 1 5.01274491E-08 2 7.50108343E-11 3 1.80336823E-15 4 -2.91688030E-18

6.3.2.4. Function: k(T)

Type: Polynomial

x_{start}	x_{end}	f(x)
200	1600	0 -2.27583562E-03 1 1.15480022E-04 2 -7.90252856E-08 3 4.11702505E-11 4 -7.43864331E-15

7. Functions

Function	Expression	Derivatives	Complex output
Tstand(t)	20+345*log(8*(t/60)+1)	d(20+345*log(8*(t/60)+1),t)	false

8. Piecewise Analytic Functions

8.1. Function: k(T)

Type: General

x_{start}	x_{end}	f(x)
20	800	54-3.33e-2*T
800	1200	27.3

8.2. Function: C(T)

Type: General

x_{start}	x_{end}	f(x)
20	600	425+7.73e-1*T-1.69e-3*T^2+2.22e-6*T^3
600	735	666+13002/(738-T)
735	900	545+17820/(T-731)
900	1200	650

8.3. Function: Ttest(t)

Type: General

x_{start}	x_{end}	f(x)
0	135	-11.648*(t/60)^3+32.797*(t/60)^2+43.182*(t/60)+18.477
135	2085	-0.000446*(t/60)^4+0.044593*(t/60)^3-1.71588*(t/60)^2+35.9778946*(t/60)+78.481642

2085	12000	0.0000000001081*(t/60)^6-0.00000008278*(t/60)^5+0.00002510087*(t/60)^4-0.003785924*(t/60)^3+0.28302190196*(t/60)^2-6.24420633481*(t/60)+482.1987
12000	14040	0.0006231*(t/60)^3-0.4078553*(t/60)^2+89.9162199*(t/60)-5795.86

8.4. Function: H(T)

Type: General

x_{start}	x_{end}	f(x)
0	200	0.066
200	1000	0.000255*T+0.015

9. Solver Settings

Solve using a script: off

Analysis type	Transient
Auto select solver	On
Solver	Time dependent
Solution form	Automatic
Symmetric	auto
Adaptive mesh refinement	Off
Optimization/Sensitivity	Off
Plot while solving	On

9.1. Direct (UMFPACK)

Solver type: Linear system solver

Parameter	Value
Pivot threshold	0.1
Memory allocation factor	0.7

9.2. Time Stepping

Parameter	Value
Times	range(60,60,14040)
Relative tolerance	0.01
Absolute tolerance	0.0010
Times to store in output	Specified times
Time steps taken by solver	Free
Maximum BDF order	5
Singular mass matrix	Maybe
Consistent initialization of DAE systems	Backward Euler
Error estimation strategy	Exclude algebraic
Allow complex numbers	Off

9.3. Advanced

Parameter	Value
Constraint handling method	Elimination
Null-space function	Automatic
Automatic assembly block size	On
Assembly block size	1000

Use Hermitian transpose of constraint matrix and in symmetry detection	Off
Use complex functions with real input	Off
Stop if error due to undefined operation	On
Store solution on file	Off
Type of scaling	Automatic
Manual scaling	
Row equilibration	On
Manual control of reassembly	Off
Load constant	On
Constraint constant	On
Mass constant	On
Damping (mass) constant	On
Jacobian constant	On
Constraint Jacobian constant	On

10. Postprocessing

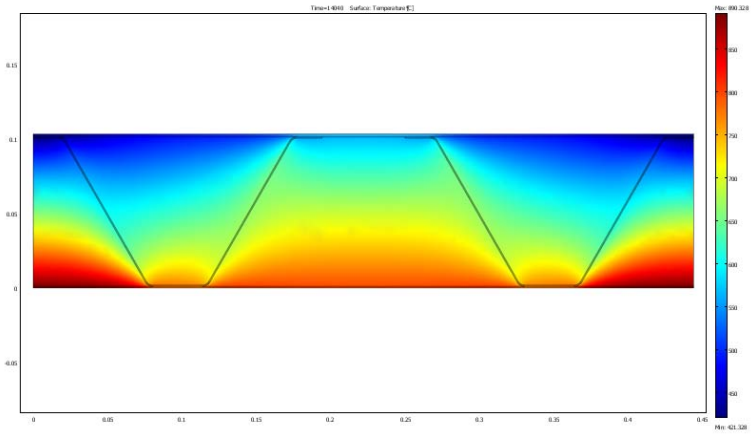

11. Variables

11.1. Boundary

11.1.1. Boundary 1, 3-8, 11, 13, 19, 24, 28, 30, 32-39, 41, 51, 54

Name	Description	Unit	Expression
ndflux_htgh	Normal conductive heat flux	W/m^2	nx_htgh * dflux_x_htgh+ny_htgh * dflux_y_htgh
ncflux_htgh	Normal convective heat flux	W/m^2	rho_htgh * C_htgh * T * (nx_htgh * u_htgh+ny_htgh * v_htgh)
ntflux_htgh	Normal total heat flux	W/m^2	ndflux_htgh+ncflux_htgh
J0_htgh	Surface radiosity expression	W/m^2	
G_htgh	Surface irradiation	W/m^2	
rflux_htgh	Radiative flux	W/m^2	
U_htgh	Convection fluid velocity for h	m/s	
L_htgh	Convection length scale for h	m	

s_htgh	Convection local coordinate for h	m	
dVolbnd_htgh	Volume integration contribution	1	1

11.1.2. Boundary 2, 9

Name	Description	Unit	Expression
ndflux_htgh	Normal conductive heat flux	W/m^2	nx_htgh * dflux_x_htgh+ny_htgh * dflux_y_htgh
ncflux_htgh	Normal convective heat flux	W/m^2	rho_htgh * C_htgh * T * (nx_htgh * u_htgh+ny_htgh * v_htgh)
ntflux_htgh	Normal total heat flux	W/m^2	ndflux_htgh+ncflux_htgh
J0_htgh	Surface radiosity expression	W/m^2	epsilon_htgh * sigma_htgh * T^4
G_htgh	Surface irradiation	W/m^2	
rflux_htgh	Radiative flux	W/m^2	epsilon_htgh * sigma_htgh * (T^4-Tamb_htgh^4)
U_htgh	Convection fluid velocity for h	m/s	1
L_htgh	Convection length scale for h	m	1
s_htgh	Convection local coordinate for h	m	s
dVolbnd_htgh	Volume integration contribution	1	1

11.1.3. Boundary 10, 12, 14-18, 20-23, 25-27, 29, 31, 40, 42-50, 52-53

Name	Description	Unit	Expression
ndflux_htgh	Normal conductive heat flux	W/m^2	nx_htgh * dflux_x_htgh+ny_htgh * dflux_y_htgh
ncflux_htgh	Normal convective heat flux	W/m^2	rho_htgh * C_htgh * T * (nx_htgh * u_htgh+ny_htgh * v_htgh)
ntflux_htgh	Normal total heat flux	W/m^2	ndflux_htgh+ncflux_htgh
J0_htgh	Surface radiosity expression	W/m^2	J
G_htgh	Surface irradiation	W/m^2	Gm_htgh+Famb_htgh * sigma_htgh * Tamb_htgh^4
rflux_htgh	Radiative flux	W/m^2	J-Gm_htgh-Famb_htgh * sigma_htgh * Tamb_htgh^4
U_htgh	Convection fluid velocity for h	m/s	1
L_htgh	Convection length scale for h	m	1
s_htgh	Convection local coordinate for h	m	s
dVolbnd_htgh	Volume integration contribution	1	1

11.2. Subdomain

Name	Description	Unit	Expression

gradT_htgh	Temperature gradient	K/m	sqrt(abs(Tx)^2+abs(Ty)^2)
k_htgh	Thermal conductivity	W/(m*K)	kxx_htgh
kmean_htgh	Mean effective thermal conductivity	W/(m*K)	k_htgh
da_htgh	Total time scale factor	J/(m^3*K)	rho_htgh * C_htgh
cflux_x_htgh	Convective heat flux, x component	W/m^2	0
beta_x_htgh	Convective field, x component	W/(m^2*K)	0
dflux_x_htgh	Conductive heat flux, x component	W/m^2	-kxx_htgh * TSx_htgh-kxy_htgh * TSy_htgh
tflux_x_htgh	Total heat flux, x component	W/m^2	dflux_x_htgh+cflux_x_htgh
cflux_y_htgh	Convective heat flux, y component	W/m^2	0
beta_y_htgh	Convective field, y component	W/(m^2*K)	0
dflux_y_htgh	Conductive heat flux, y component	W/m^2	-kyx_htgh * TSx_htgh-kyy_htgh * TSy_htgh
tflux_y_htgh	Total heat flux, y component	W/m^2	dflux_y_htgh+cflux_y_htgh
dflux_htgh	Conductive heat flux	W/m^2	sqrt(dflux_x_htgh^2+dflux_y_htgh^2)
cflux_htgh	Convective heat flux	W/m^2	sqrt(cflux_x_htgh^2+cflux_y_htgh^2)
tflux_htgh	Total heat flux	W/m^2	sqrt(tflux_x_htgh^2+tflux_y_htgh^2)
Dm_htgh	Mean diffusion coefficient	W/(m*K)	(kxx_htgh * beta_x_htgh^2+kxy_htgh * beta_x_htgh * beta_y_htgh+kyx_htgh * beta_y_htgh * beta_x_htgh+kyy_htgh * beta_y_htgh^2)/(beta_x_htgh^2+beta_y_htgh^2+eps)
cellPe_htgh	Cell Peclet number	1	0.5 * h * sqrt(beta_x_htgh^2+beta_y_htgh^2)/(Dm_htgh+eps)
Qs_htgh	Production/absorption	W/m^3	qs_htgh * T
helem_htgh	Element size	m	h
dr_guess_htgh	Width in radial direction default guess	m	0
R0_guess_htgh	Inner radius default guess	m	0
Sx_htgh	Infinite element x coordinate	m	x
S0x_guess_htgh	Inner x coordinate default guess	m	0
Sdx_guess_htgh	Width in x direction default guess	m	0
Sy_htgh	Infinite element y coordinate	m	y
S0y_guess_htgh	Inner y coordinate default guess	m	0
Sdy_guess_htgh	Width in y direction default guess	m	0
dVol_htgh	Volume integration contribution	1	detJ_htgh
TSx_htgh	Scaled temperature	K/m	Tx

	gradient, x component		
TSy_htgh	Scaled temperature gradient, y component	K/m	Ty

APPENDIX C. TYPICAL KEYWORDS FOR *ABAQUS / CAE* KEYWORDS PANEL CALCULATION

```
**
** PARTS
**
*Part, name=Alalaippa
*Element, type=C3D8R
** Section: Alalaippa
*Solid Section, elset=_PickedSet42, material=Steel
,
*End Part
**
*Part, name=Alalaippa_2
*Element, type=C3D8R
** Section: Alalaippa
*Solid Section, elset=_PickedSet42, material=Steel
,
*End Part
**
*Part, name=Paatylevy_1
*Element, type=C3D8R
** Section: Paatylevy_1
*Solid Section, elset=_PickedSet2, material=Steel
,
*End Part
**
*Part, name=Paatylevy_2
*Element, type=C3D8R
** Section: Paatylevy_2
*Solid Section, elset=_PickedSet3, material=Steel
,
*End Part
**
*Part, name=Uuma
*Element, type=C3D8R
** Section: Uuma
```

```
*Solid Section, elset=_PickedSet16, material=Steel
,
*End Part
**
*Part, name=Uuma_2
*Element, type=C3D8R
** Section: Uuma
*Solid Section, elset=_PickedSet16, material=Steel
,
*End Part
**
*Part, name=Valilevy
*Element, type=C3D8R
** Section: Paatylevy_1
*Solid Section, elset=_PickedSet2, material=Steel
,
*End Part
**
*Part, name=Ylalaippa
*Element, type=C3D8R
** Section: Ylalaippa
*Solid Section, elset=_PickedSet22, material=Steel
,
*End Part
**
*Part, name=Ylalaippa_2
*Element, type=C3D8R
** Section: Ylalaippa
*Solid Section, elset=_PickedSet22, material=Steel
,

*End Part
**
**
** ASSEMBLY
**
*Assembly, name=Assembly
**
*Instance, name=Alalaippa-1, part=Alalaippa
*End Instance
**
*Instance, name=Uuma-1, part=Uuma
```

```
*End Instance
**
*Instance, name=Ylalaippa-1, part=Ylalaippa
*End Instance
**
*Instance, name=Paatylevy_1-1, part=Paatylevy_1
*End Instance
**
*Instance, name=Paatylevy_2-1, part=Paatylevy_2
*End Instance
**
*Instance, name=Alalaippa_2-2, part=Alalaippa_2
*End Instance
**
*Instance, name=Uuma_2-3, part=Uuma_2
*End Instance
**
*Instance, name=Ylalaippa_2-1, part=Ylalaippa_2
*End Instance
**
*Instance, name=Valilevy-1, part=Valilevy
*End Instance
**
*Surface, type=ELEMENT, name=_PickedSurf133, internal
*Surface, type=ELEMENT, name=_PickedSurf138, internal
*Surface, type=ELEMENT, name=_PickedSurf139, internal
*Surface, type=ELEMENT, name=_PickedSurf140, internal
*Surface, type=ELEMENT, name=_PickedSurf141, internal
*Surface, type=ELEMENT, name=_PickedSurf142, internal
*Surface, type=ELEMENT, name=_PickedSurf143, internal
*Surface, type=ELEMENT, name=_PickedSurf144, internal
*Surface, type=ELEMENT, name=_PickedSurf145, internal
*Surface, type=ELEMENT, name=_PickedSurf146, internal
*Surface, type=ELEMENT, name=_PickedSurf147, internal
*Surface, type=ELEMENT, name=_PickedSurf148, internal
*Surface, type=ELEMENT, name=_PickedSurf149, internal
*Surface, type=ELEMENT, name=_PickedSurf150, internal
*Surface, type=ELEMENT, name=_PickedSurf151, internal
*Surface, type=ELEMENT, name=_PickedSurf152, internal
*Surface, type=ELEMENT, name=_PickedSurf153, internal
*Surface, type=ELEMENT, name=_PickedSurf166, internal
** Constraint: Oikea_paatylevy
```

```
*Tie, name=Oikea_paatylevy, adjust=yes
_PickedSurf141, _PickedSurf140
** Constraint: Oikea_uuma_ala
*Tie, name=Oikea_uuma_ala, adjust=yes
_PickedSurf151, _PickedSurf150
** Constraint: Oikea_uuma_yla
*Tie, name=Oikea_uuma_yla, adjust=yes
_PickedSurf153, _PickedSurf152
** Constraint: Valilevy_oikea
*Tie, name=Valilevy_oikea, adjust=yes
_PickedSurf145, _PickedSurf144
** Constraint: Valilevy_vasen
*Tie, name=Valilevy_vasen, adjust=yes
_PickedSurf143, _PickedSurf142
** Constraint: Vasen_paatylevy
*Tie, name=Vasen_paatylevy, adjust=yes
_PickedSurf139, _PickedSurf138
** Constraint: Vasen_uuma_ala
*Tie, name=Vasen_uuma_ala, adjust=yes
_PickedSurf147, _PickedSurf146
** Constraint: Vasen_uuma_yla
*Tie, name=Vasen_uuma_yla, adjust=yes
_PickedSurf149, _PickedSurf148
*End Assembly
**
** MATERIALS
**
*Material, name=Steel
*Elastic
   2.1e+11,   0.3,-1000.
   2.1e+11,   0.3,  100.
  1.89e+11,   0.3,  200.
  1.68e+11,   0.3,  300.
  1.47e+11,   0.3,  400.
  1.26e+11,   0.3,  500.
  6.51e+10,   0.3,  600.
  2.73e+10,   0.3,  700.
  1.89e+10,   0.3,  800.
 1.4175e+10,   0.3,  900.
  9.45e+09,   0.3, 1000.
 4.725e+09,   0.3, 1100.
       0.1,   0.3, 1200.
```

```
*Expansion
  1.22e-05,  30.
 1.504e-05, 740.
  1.31e-05, 860.
 1.509e-05,1200.
*Plastic
   3.55e+08,   0.,   0.
   3.55e+08,   0., 400.
  2.769e+08,   0., 500.
 1.6685e+08,   0., 600.
  8.165e+07,   0., 700.
  3.905e+07,   0., 800.
   2.13e+07,   0., 900.
   1.42e+07,   0.,1000.
    7.1e+06,   0.,1100.
         1.,   0.,1200.
*Material, name=Steel_laipat
*Elastic
 2.1e+22, 0.3
*Material, name=Steel_paatylevyt
*Elastic
 2.1e+22, 0.3
**
** PREDEFINED FIELDS
**
** Name: R30_alalaippa   Type: Temperature
*Initial Conditions, type=TEMPERATURE
_PickedSet161, 779.
** Name: R30_uuma   Type: Temperature Using Field: R30
*Initial Conditions, type=TEMPERATURE
Uuma-1.1, 493.932
Uuma-1.2, 487.924
.
.
.
Paatylevy_2-1.2243, 700.881
Paatylevy_2-1.2244, 726.543
** Name: R30_ylalaippa   Type: Temperature
*Initial Conditions, type=TEMPERATURE
_PickedSet162, 477.
** ----------------------------------------------------------------
**
```

```
** STEP: Buckle
**
*Step, name=Buckle, perturbation
*Buckle
1, 2., 2, 300
**
** BOUNDARY CONDITIONS
**
** Name: Keskituki Type: Displacement/Rotation
*Boundary, op=NEW, load case=1
_PickedSet154, 3, 3
*Boundary, op=NEW, load case=2
_PickedSet154, 3, 3
** Name: Sivutuet_nivel_tapaus_1 Type: Displacement/Rotation
*Boundary, op=NEW, load case=1
_PickedSet167, 2, 2
*Boundary, op=NEW, load case=2
_PickedSet167, 2, 2
** Name: Symmetry Type: Symmetry/Antisymmetry/Encastre
*Boundary, op=NEW, load case=1
_PickedSet155, XSYMM
*Boundary, op=NEW, load case=2
_PickedSet155, XSYMM
**
** LOADS
**
** Name: Buckle_paine   Type: Pressure
*Dsload
_PickedSurf133, P, 1.6e+06
**
** OUTPUT REQUESTS
**
*Restart, write, frequency=0
**
** FIELD OUTPUT: F-Output-1
**
*Output, field
*Node Output
CF, RF, RM, RT, TF, U, VF
*Element Output, directions=YES
ESF1, NFORC, S, SF
*End Step
```